EXPERIMENTAL AND NUMERICAL ANALYSIS OF FOAM-FILLED COMPOSITE STRUCTURES SUBJECTED TO AXIAL CRUSHING

by
Serdar Demir
B.S., Mechanical Engineering, Yıldız Technical University, 2020

Submitted to the Institute for Graduate Studies in
Science and Engineering in partial fulfillment of
the requirements for the degree of
Master of Science

Graduate Program in Mechanical Engineering
Boğaziçi University
2022

ACKNOWLEDGEMENTS

First of all, I would like to present my sincere thanks and appreciation to my supervisor Prof. Nuri Ersoy for his great support, patience and guidance through my study.

I also would like to thank to my committee members, Assoc. Prof. Sami And Kılıç and Assist. Prof. Hatice Sinem Şaş for their comments and critics.

I also thank to Assoc. Prof. Kenan Çınar for his helps and advices during my thesis study.

I am also thankful to my friend and colleague Mehmet Can Engül for his help and assistance through the study.

I present my thanks to Hakan Moldur and Selamet Çevik for their help during the manufacturing of specimens and moulds.

Finally, I am grateful to my family for their never ending support and love.

ABSTRACT

EXPERIMENTAL AND NUMERICAL ANALYSIS OF FOAM-FILLED COMPOSITE STRUCTURES SUBJECTED TO AXIAL CRUSHING

Crash components in transport vehicles are significant structures for the application of the composite materials due to their high energy absorption capacities. Even better energy absorption values can be achieved by foam filled crash components due to the interaction effect between foam core and structure wall. In this thesis study, axial crushing behavior of composite circular tube structures and foam filled composite circular tube structures were examined experimentally and numerically. Experimental tests on crash specimens were performed as quasi-static axial crushing tests. Numerical analyses carried out in ABAQUS/Explicit Finite Element Analysis software. Main goals of the study are to investigate composite tubular structures and foam filled structures axial crushing behavior by energy absorption and specific energy absorption and to simulate the axial crushing behavior of the specimens accurately. Empty composite tube specimens used in the study were manufactured from plain weave fabric carbon fiber composite with three different diameters of Ø30mm, Ø40mm and Ø50mm. Empty tubes as well as polyurethane (PU) foam filled and syntactic foam filled composite tubes were tested experimentally. Effect of the crushing by using external crush plugs on axial crushing characteristics of empty tubes were also investigated in this study. Crushing characteristics, energy absorption values and specific energy absorption values of various specimens were discussed. Experimental tests were simulated in ABAQUS finite element software by modelling composite materials by using built-in VUMAT subroutine “ABQ_PLY_FABRIC” for intra-laminar damage, and cohesive surface method for inter-laminar damage. Built-in *CRUSHABLE FOAM material model was used to model PU foams. Experimental test results and numerical simulation results were evaluated with load displacement curves and specific energy absorption (SEA) displacement curves. At the end of the study, numerical simulations exhibited coherent results to experimental studies and it is found out that specific energy absorption of the foam filled tubes is lower than empty tubes even the absorbed energy is higher.

ÖZET

EKSENEL EZİLMEYE MARUZ KALAN KÖPÜK DOLGULU KOMPOZİT YAPILARIN DENEYSEL VE NUMERİK ANALİZİ

Taşıt araçlarındaki ezilme komponentleri, yüksek enerji soğurma kapasiteleri nedeniyle kompozit malzeme uygulamaları için önemli yapılardır. Köpük dolgu ve yapı duvarı arasındaki etkileşim etkisi nedeniyle, köpük dolgulu çarpışma komponentleri ile daha da iyi enerji soğurma değerleri elde edilebilir. Bu tez çalışmasında, dairesel yapılı kompozit tüplerin ve dairesel yapılı köpük dolgulu kompozit tüplerin eksenel ezilme davranışları deneysel ve nümerik olarak incelenmiştir. Ezilme numunelerine uygulanan deneysel testler yarı statik eksenel ezilme testleri olarak gerçekleştirilmiştir. Nümerik analizler ABAQUS/Explicit Sonlu Elemanlar Analizi programında yürütülmüştür. Çalışmanın temel hedefleri, kompozit boru yapılarının ve köpük dolgulu yapıların eksenel ezilme davranışlarının enerji ve spesifik enerji soğurma değerleri açısından incelenmesi ve numunelerin eksenel ezilme davranışını doğru bir şekilde simüle edilmesidir. Çalışmada kullanılan boş kompozit tüp numuneleri Ø30mm, Ø40mm ve Ø50mm olmak üzere üç farklı çapta düz dokuma kumaş karbon fiber kompozitten üretilmiştir. Boş tüplerle birlikte poliüretan (PU) köpük dolgulu ve sentaktik köpük dolgulu kompozit tüpler de deneysel olarak test edilmiştir. Bu çalışmada ayrıca ezilme kapakları kullanılarak yapılan testlerde kapakların boş tüplerin eksenel ezilme özelliklerine etkisi de incelenmiştir. İncelenen numunelerin ezilme özellikleri, enerji soğurma değerleri ve spesifik enerji soğurma değerleri karşılaştırılmıştır. Gerçekleştirilen deneysel testler, lamina içi hasar, ABAQUS içinde hazır bir VUMAT altyönergesi olan ABQ_PLY_FABRIC VUMAT ile ve laminalar arası hasar ise koheziv yüzeyler metodu ile modellenerek ABAQUS sonlu elemanlar yazılımı kullanılarak simule edilmiştir. PU köpükleri modellemek için ABAQUS programındaki dahili *CRUSHABLE FOAM malzeme modeli kullanılmıştır. Deneysel test sonuçları ve sayısal simülasyon sonuçları, yük deplasman eğrileri ve spesifik enerji absorpsiyon (SEA) deplasman eğrileri açısından değerlendirilmiştir.

TABLE OF CONTENTS

LIST OF FIGURES

LIST OF TABLES

LIST OF SYMBOLS

A	Cross-sectional area
Al	Aluminium
C	Hardening equation coefficient
C	Carbon
cm^3	Cubic centimeter
°C	Celcius degree
D	Damage variable
d_{1+}	Tensile damage along fiber direction 1
d_{1-}	Compressive damage along fiber direction 1
d_{2+}	Tensile damage along fiber direction 2
d_{2-}	Compressive damage along fiber direction 2
d_{12}	Shear damage
d_{max}	Max value of damage variable
d_{12}^{max}	Max shear damage
E_1	Elasticity Modulus along fiber direction 1
E_2	Elasticity Modulus along fiber direction 2
E_3	Elasticity modulus through-the-thickness
F	Force
G	Fracture energy
GPa	Gigapascal
G_{12}	Shear Modulus
G_f^{1+}	Tensile fracture energy per unit area along fiber direction 1
G_f^{1-}	Compressive fracture energy per unit area along fiber direction 1
G_f^{2+}	Tensile fracture energy per unit area along fiber direction 2
G_f^{2-}	Compressive fracture energy per unit area along fiber direction 1
G_n^c	Fracture energy per unit area for normal traction
G_s^c	Fracture energy per unit area for first shear traction
G_t^c	Fracture energy per unit area for second shear traction

g	Gram
kg	Kilogram
kJ	Kilojoule
km	Kilometer
kN	Kilo-Newton
K^0	Interface stiffness
L_c	Characteristic length
m	Mass
mm	Milimeter
mm^3	Cubic milimeter
MPa	Megapascal
N	Newton
P	Load
P_{max}	Maximum load
$\overline{P}$	Mean crushing load
p	Hardening equation power term
r_{1+}	Tensile damage threshold along fiber direction 1
r_{1-}	Compressive damage threshold along fiber direction 1
r_{2+}	Tensile damage threshold along fiber direction 2
r_{2-}	Compressive damage threshold along fiber direction 2
r_{12}	Shear damage threshold
s	Second
S	Displacement
S	Shear Stress at the initiation of shear damage
S_i	Initial distance
S_b	Final distance
S^0	Shear strenght
t	Thickness
t_n^0	Damage initiation stress for normal traction
t_s^0	Damage initiation stress for first shear traction
t_t^0	Damage initiation stress for second shear traction
W	Energy

X_{α}	Strength in relative direction
X_{1+}	Tensile Strength along fiber direction 1
X_{1-}	Compressive Strength along fiber direction 1
X_{2+}	Tensile Strength along fiber direction 2
X_{2-}	Compressive Strength along fiber direction 2
α_{12}	Shear damage equation parameter
δ	Separation
δ_0	Damage initiation separation
δ_{cr}	Critical damage separation
ε	Strain
$\tilde{\varepsilon}^{pl}$	Equivalent plastic strain
ε_{11}^{el}	Elastic strain component 11
ε_{22}^{el}	Elastic strain component 22
ε_{12}^{el}	Elastic strain component 12
η	Benzeggagh-Kane cohesive property
θ	Angle
v_{12}	Principal Poisson Ratio
ρ	Density
$\bar{\sigma}$	Mean stres
$\tilde{\sigma}_{y0}$	Initial effective shear yield stress
ϕ_{α}	Damage initiation criterion symbol
%	Percent
◦	Degree
Ø	Diameter symbol
µ	Micro sign

LIST OF ACRONYMS / ABBREVIATIONS

1DelFlag	Element deletion flag
2D	Two dimension
3D	Three dimension
CFRP	Carbon Fibre Reinforced Plastics
CODAM	(Composite Damage)
CO_2	Carbon dioxide
CPS	Plane stress elements
D/t	Diameter to thickness
EA	Energy absorption
EU	European Union
EVs	Electric Vehicles
FE	Finite element
FEA	Finite Element Analysis
FIA	Federation Internationale de l'Automobile
FRP	Fiber-reinforced polymer
GFRP	Glass Fibre Reinforced Plastics
H:A	Hoop-to-axial
HGMS	Hollow glass micro spheres
MpStatus	Material point status
PA	Polyamide
PEEK	Polyether etherkethone
PET	Polyethylene terephthalate
PP	Polypropylene
PU	Polyurethane foam
PVC	Polyvinyl chloride
RIMP	Rear impact structure
SEA	Specific energy absorption
SDV	Solution dependent output variables
UD	Unidirectional

VCCT Virtual Crack Closure Technique

1. INTRODUCTION

The utilization of new materials is an important matter of technological advancement in engineering. In many applications, materials with better performance are demanded regarding to the changing and increasing needs of the developing industry. Crashworthiness is a property that is very important for transport industries because of the safety and efficiency matters. Improving crashworthiness of transporting vehicles and application of novel crashworthy materials is an important subject for technological development.

Recently, driving factor of design in automotive, aerospace and railway transporting sectors is to use lightweight products to reduce fuel consumption and carbon emissions. Since the decrease of fuel resources and the increase of CO_2 emissions in atmosphere are global problems, governments and communities such as European Union (EU) take measures against these problems. According to regulation EU 2019/631, it is aimed to achieve the target of 95g of CO_2/km in passenger cars in 2020-2024 period, decreasing the emission limit by 12% from the previous regulation. In 2025-2030 period, another 15% decrease is targeted in emission limits [1].

Due to the environmental friendly and energy saving policies followed by governments and political communities through the past years, in search of better performance, vehicle manufacturers are motivated to do researches to use new materials and manufacture lightweight components. As a result of these researches, application of composite materials and hybrid materials become frequent over the last decades. Especially, Carbon Fibre Reinforced Plastics (CFRP) and Glass Fibre Reinforced Plastics (GFRP) are composites used in transportation vehicles as a replacement of traditional metallic materials since they are light in weight, efficient, strong and stiff.

Through the development in manufacturing technologies over the past years, load-critical components such as chassis, suspension rods and body panels can be manufactured from CFRP today [2]. In many of today's sports cars and luxury cars, body and chassis components made from CFRP exists [2, 3]. Yet, high prices and the complex behavior of composite materials restricts the manufacturers to produce most of the components from composite or hybrid materials in many passenger cars. Components that can make significant advantage have priority when using CFRP material for automotive components. Crash components in automobiles are examples to components with high performance conditions that make a good cause to use composites.

Car crash is an incident that occurs very often in traffic. The increase in the number of vehicles in circulation induced the increase in accidents in recent years. Every year, millions of people in the world have minor or major traffic accidents. During 2020, 983,808 traffic accidents occurred in the road network of Turkey. 833,533 of these accidents were with material loss and 150,275 were with death or injury. Road traffic accident statistics are illustrated in Figure 1.1 [4].

Year	Total number of accidents	Number of accidents involving death or injury	Number of accidents involving material loss only	Number of persons killed			Number of persons injured
				Total	At accident scene	Accident follow-up(1)	
2009	1 053 346	111 121	942 225	4 324	4 324	-	201 380
2010	1 106 201	116 804	989 397	4 045	4 045	-	211 496
2011	1 228 928	131 845	1 097 083	3 835	3 835	-	238 074
2012	1 296 634	153 552	1 143 082	3 750	3 750	-	268 079
2013	1 207 354	161 306	1 046 048	3 685	3 685	-	274 829
2014	1 199 010	168 512	1 030 498	3 524	3 524	-	285 059
2015	1 313 359	183 011	1 130 348	7 530	3 831	3 699	304 421
2016	1 182 491	185 128	997 363	7 300	3 493	3 807	303 812
2017	1 202 716	182 669	1 020 047	7 427	3 534	3 893	300 383
2018	1 229 364	186 532	1 042 832	6 675	3 368	3 307	307 071
2019	1 168 144	174 896	993 248	5 473	2 524	2 949	283 234
2020	983 808	150 275	833 533	4 866	2 197	2 669	226 266

(1) Includes the deaths within 30 days after the traffic accidents due to related accident and its impacts for people who were injured and sent to health facilities.

- Denotes magnitude null.

Figure 1.1. Road traffic accident statistics in Turkey roads, 2009-2020 [4].

Car crashes have drawn attention to the importance of vehicle safety and reliability over the years. As they threatens passenger safety, they cause severe economic problems because of the damage to the vehicle itself and its repair costs. To reduce the impact of these accidents, vehicle crashworthiness has a critical role.

Crashworthy structures improves the crashworthiness of vehicles. In all of the transporting and motorsport vehicles, crashworthy components are placed with the purpose of absorbing the impact energy during the crash to reduce the outcomes. Crash boxes are examples to the crashworthy structures in passenger automobiles. Crash boxes are placed into the back of rear and front bumpers to reduce the effect of impact from front and rear. Examples of crash box placed behind bumper structure is illustrated in Figure 1.2 [5].

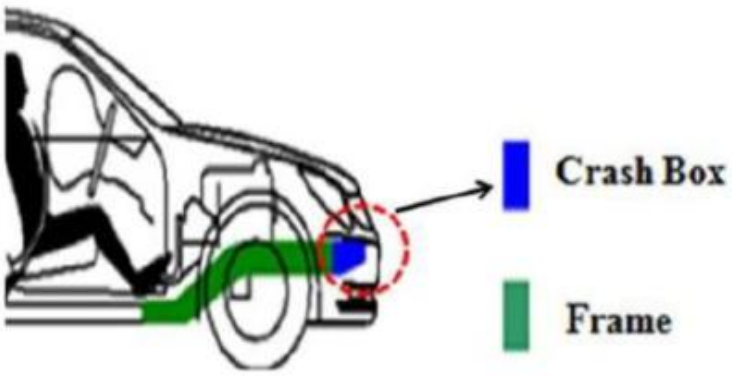

Figure 1.2. Crash box structures [5].

Crash components in vehicles absorbs the impact energy during the crash by failing mechanically and deforming. Absorption of the impact energy results the decrease of velocity of the vehicle since the impact energy is the kinetic energy of the high-speed object at crash incident. During a frontal impact, crash box components subjected to axial crush. Crushed crash box components reduces damage on engine and other critical parts and prevents intrusion to the occupant cabin.

Traditional materials used for crash components are metallic materials such as aluminum and steel. Metallic materials have been used in crash components for a long time and they have become benchmark materials through these years. Some of the experimental studies on crushing response of composite and hybrid materials showed that properly designed composite structures have higher specific energy absorption capacity, higher stiffness-weight ratio and higher corrosion resistance than their traditional metal counterparts. Thermoplastic carbon fibre structures such as Carbon/PEEK material has specific energy absorption capacity of approximately 200-250 kJ/kg. Specific energy absorption capacity values of aluminum and steel are approximately 25-50 kJ/kg [6]. Specific energy absorption capacity values for most convenient materials are shown in Figure 1.3 [6].

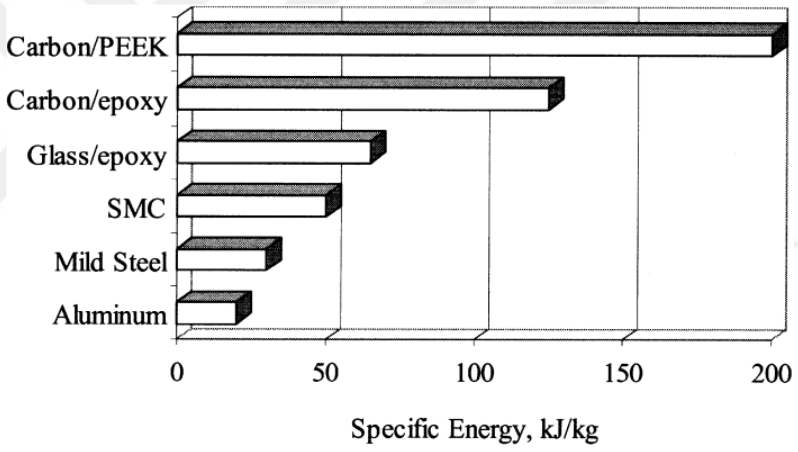

Figure 1.3. Specific energy absorption capacities for different materials [6].

Even higher energy absorption capacity values than carbon composite components can be achieved by using sandwich design on components. Sandwich components generally consist of two face sheet section and a core section. Materials used in typical sandwich crash components are traditional metallic materials or composite materials for face sheets and honeycomb or foam type materials for the core. Experimental studies have shown that foam-filled crash components has significant positive effect on the axial crush characteristics [7, 8, 9]. Crush behavior of face sheets becomes more stable and resistant to the impact in sandwich design components.

In foam-filled components, the energy absorption capacity of the foam-filled component itself generally higher than the linear sum of the face sheet and foam core capacities during axial crush [7, 8, 9]. This positive improvement is based on the interaction effect between foam core and face sheet [9]. Foam filling can change the crushing mode of the component, thus crushing characteristics. For instance, a thin-walled aluminum crash box which shows plastic folding behavior on axial crushing may have more folding lobes when it is subjected to axial crushing when its interior filled with foam. Also, the diamond folds occurred in empty crash box may be replaced with concertina folds. Increasing of the folds and reduced buckling length increase the stability of the crushing behavior [9]. An example of foam effect in aluminum thin-walled square crash box has been illustrated in Figure 1.4 [9].

Figure 1.4. Empty and foam-filled aluminum square crash box [9].

The most basic must-have feature for a crash component is to show progressive failure behavior [10]. During axial crushing, metallic components show progressive plastic folding behavior generally. However, components made from brittle materials, such as CFRP, may fail catastrophically which will result the initial force to get high, and then extreme drops causes an unstable crushing process so puts up lower resistance. This type of failure must be avoided since small amount energy will be absorbed and most of the component will stay undamaged in this case. First mode Euler buckling of a CFRP component is an example of catastrophic crushing behavior.

Preventing catastrophic behavior and inducing progressive crushing mode in CFRP crash boxes are achieved by using trigger mechanisms [10, 11]. By initiating the crushing at the tip, trigger mechanism prevents the possible stress concentration at crash box points. Thus, progressive crushing obtained instead of catastrophic crushing. Triggering can be done by either forming the desired shape to the crushing end of the component or using an external crush cap [12]. Many different types of trigger mechanism that may provide different crush characteristics is possible. 45° bevel, tulip, saw tooth, steeple etc. are examples to the trigger mechanisms generated by forming the tip of the component. Inwards-crushing or outwards-crushing crush plugs are examples to the triggers generated by using external crush caps. Schematics of various trigger mechanisms has shown in Figure 1.5 [13].

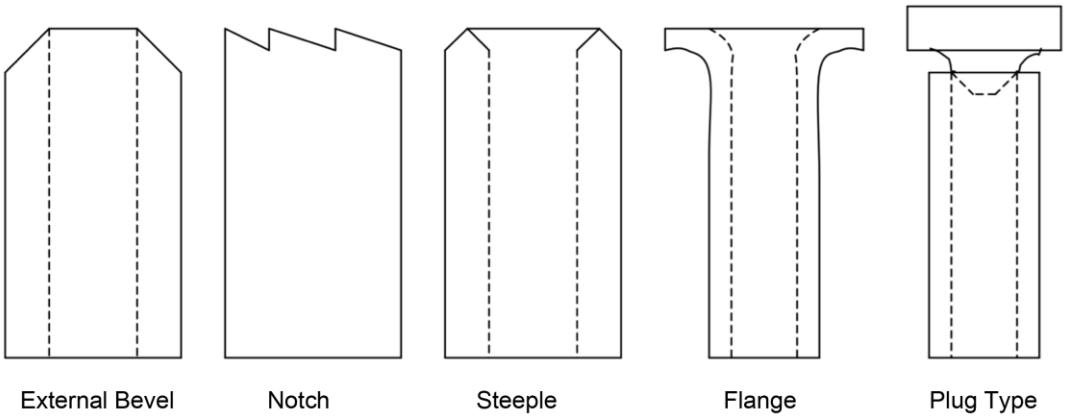

Figure 1.5. Various types of trigger mechanisms [13].

Metallic materials absorbs the energy by plastic deformation. CFRP materials absorbs the impact energy through fibre tensile and compressive failure, matrix tensile and compressive failure and delamination failure modes. Due to the complexity of failure mechanisms in CFRP composites, it is quite hard to guess crush characteristics or to design crashworthy structures made from CFRP composites and sandwich structures made of CFRPs.

Conventionally, designing of crash components is based on experimental testing. Crush characteristics of the designed components can be examined by quasi-static or dynamic crushing tests on coupon specimens or the component itself [14]. Due to the high prices of composite materials, experimental testing is quite expensive. Yet, it is important to gain information about crush characteristics of composite structures. This is also necessary for satisfying safety regulations during the design process.

Another way of gaining information about the crushing behavior of a component is Finite Element Analysis (FEA) method. FEA is an important asset on designing crash components. FEA has brought some solutions about the problems of designing composite crash components. It suggests an alternative solution to experimental testing by examining the components crush behavior on a virtual environment. Using FEA has advantages in terms of several trial-and-error iterations and enables performing fewer and less expensive tests and getting faster results. Since experimental tests during the first design stages is not very practical, the ability to simulate crashing event is quite important and shorten the time required for design process. There are three main modelling method using FEA to simulate crushing behavior of composite crashworthy structures. These are micro-scale (fiber level), meso-scale (ply level) and macro-scale (laminate-level) modelling. Macro-scale modelling methods is the general type modelling method for crash components [15, 16, 17]. Apart from the benefits that is provided by FEA, there are still some improvements needed for modelling methods to improve the reliability.

Because of the price fact and reliability questions caused by the lack of confidence to explain complex composite crush behavior completely under dynamic load cases, automotive industry was quite reluctant to apply composites to the crash structures before the last two decades. Designing an efficient crash component from CFRP, still is a challenging task. Because of the uncertain matters about composites, using metallic crash structures was a simpler solution. However, with the introduction of Electric Vehicles (EVs) automotive industry requires better and lighter crash structures in today’s conditions. Composite and hybrid materials is quite important for safety and efficiency for transporting industry. Therefore, understanding the response of the novel materials and designs is critical.

1.1. Literature Review

Various researches about crash boxes subjected to axial crushing, examining the behaviors and the effects of materials and design, exists in the literature. Many researchers studied the crushing behaviors of crash components experimentally to get a better understanding. Also, there are considerable amount of numerical studies about axial crushing and how to model composite crash components for axial crushing efficiently. In this section, important studies about the axial crushing of CFRP materials, foam-filled design and numerical modelling are reviewed and summary of the theoretical information about these subjects are given in this order.

1.1.1. Evaluation of Crushing Characteristics

Crash components are used in vehicles to absorb kinetic energy of the vehicle during impact to slow down the vehicle and prevent damage on other critical components and intrusion on occupant cabin. During impact, crash components works as a column that shows resistance against impactor and deforms as it dissipates impact energy. Energy absorption capability of a component is measured by energy absorption (EA) and specific energy absorption (SEA) value which is the energy absorbed per unit mass [10, 11].

Energy absorption and specific energy absorption capacities of a crash box subjected to axial crushing is obtained from load-displacement curves of the component. Load-displacement curves are used to examine the crushing behavior of the component. Load values on the curve are the values of resistance force of component against axial crushing. A typical load-displacement curve of a metallic component that shows progressive folding is illustrated in Figure 1.6 [10].

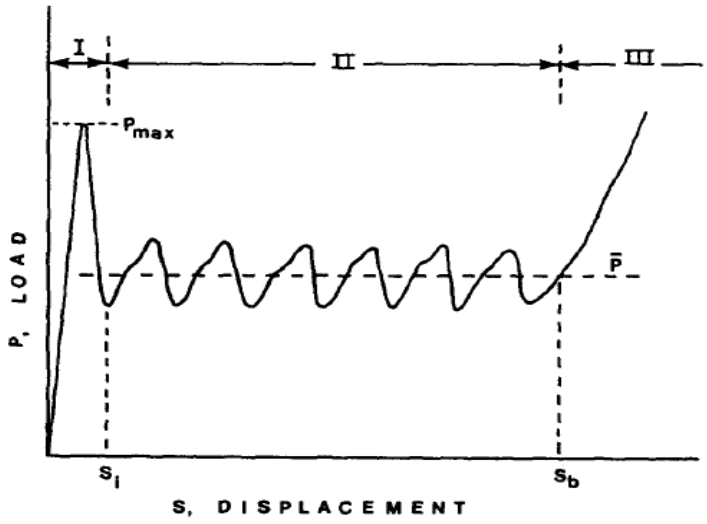

Figure 1.6. Load-displacement curve of a metallic components progressive folding [10].

Total energy absorbed by composite structure during crash is the area under the load displacement curve. The energy mathematically defined as

$$W = \int_0^S PdS\,, \tag{1.1}$$

where the energy is noted as W, the load is noted as P and the folding distance is S. Referring to Figure 1.6, the load-displacement curve is divided into three zones: elastic deformation period (I), the progressive folding period (II) the post folding period (III). The energy absorbed in progressive crushing zone can be defined mathematically as

$$W = \int_{S_i}^{S_b} PdS = \overline{P}(S_b - S_i), \tag{1.2}$$

where $\overline{P}$ is the mean crushing load, S_i is the distance progressive folding begins and S_b is the distance it ends. Specific energy absorption is obtained by dividing the absorbed energy W, by the mass of the structure. The equation of SEA can be written as

$$SEA = \frac{W}{m} = \frac{\overline{P}(S_b - S_i)}{\rho AL} = \frac{\bar{\sigma}(S_b - S_i)}{\rho L}, \tag{1.3}$$

where $\bar{\sigma}$ is the mean folding stress, A is cross-sectional area and ρ is density.

In the load-displacement curve, peak force P_{max} is higher than $\overline{P}$ mean folding force. In general, peak force is higher than mean force, since there are no failure started before failure initiation at the start of period II. High peak force is undesired due to its effects on components and occupants.

1.1.2 Testing Methods of Crush Components

There is not a standardized test method for measuring the SEA capacities of crashworthy structures. In general, specimens are tested by using flat material coupons or using the structure itself. Flat material coupon tests are usually performed to examine the effects of different parameters such as material effects. They are mostly used for composite materials. Testing flat coupons requires fixtures since flat coupons are not self-supporting specimens. Feraboli et al. [14], compared the crushing behavior of self-supporting composite structures and flat coupons. They developed a fixture to test flat coupon composites, which is shown in Figure 1.7a. Crash structures that self-supporting themselves do not need fixtures for testing. Most of the studies in the literature are based on tubular or corrugated specimens that self-supporting. Effects of different geometrical and material parameters are examined with self-supporting specimen testing. Manufacturing a flat coupon specimen is much easier than tubular specimen but self-supporting feature of tubular specimen makes them preferred. A square tube specimen that self-supporting has been illustrated in Figure 1.7b [14].

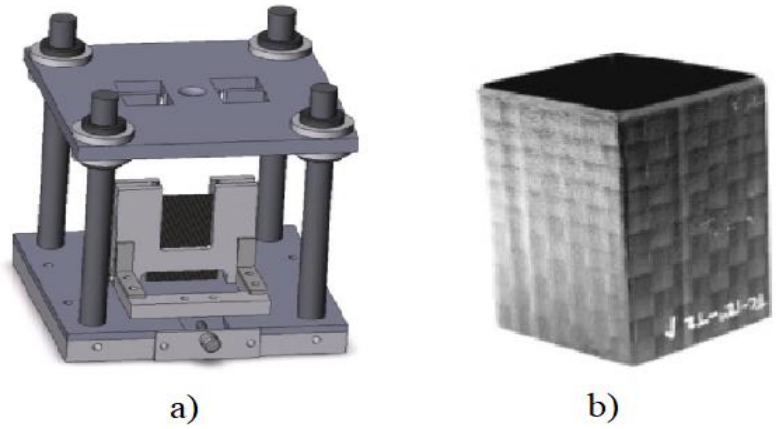

Figure 1.7. Crushing test setups, a) Test fixture for testing flat coupon specimens b) Self-supporting, square tube crush specimen [14].

The experimental tests on crash components subjected to axial crushing can be done by two main methods, which are quasi-static and dynamic testing methods. Quasi-static tests are being done by crushing the specimen at a steady rate by using conventional tension testing machines [18]. Drawback of this type of testing that it does not form a sufficiently accurate model of the true crash behavior, since they do not reflect the loading rate effects on the material behavior. Yet it is simpler than impact tests and easier to control. Also they cost less than impact tests. A quasi-static test setup to crush tubular specimen is illustrated in Figure 1.8.

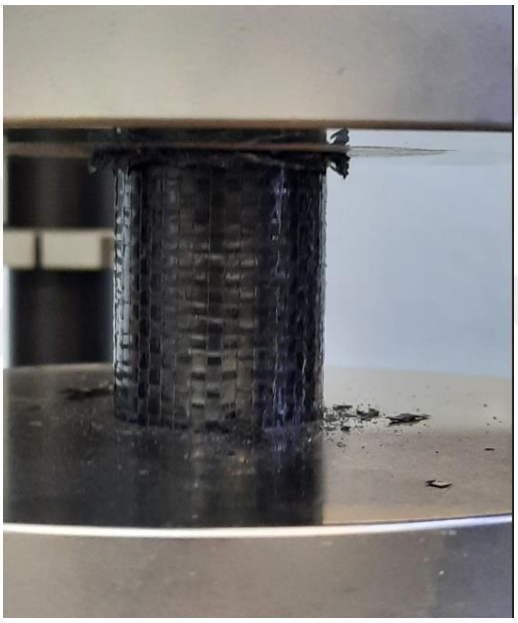

Figure 1.8. Quasi-static test setup to crush tubular CFRP composite specimen.

Dynamic tests are the true simulation of crash incident as specimen subjected to an impact load that generates a suddenly increasing crushing rate. Crash conditions can be generated accurately with a dynamic test. However, special equipment is required to achieve data from the test since it occurs rapidly [18]. The cost of the test mechanism is high as a consequence of need to use very sensitive devices. Dynamic tests are generally being done by dropping a large mass impactor from a certain height. Thus the effect of gravity acceleration will be considered. Zarei et al. [19], in 2006, published a study where they investigated crashworthiness of thermoplastic composite crash boxes experimentally and numerically. They performed dynamic tests using an impact tower rig which is schematically shown in Figure 1.9 [19].

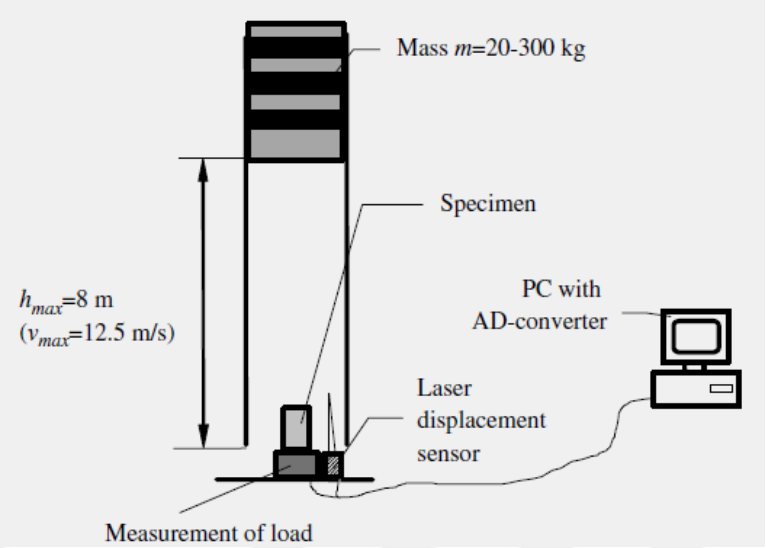

Figure 1.9. Dynamic test setup for axial crushing [19].

Also, it must be indicated that in some dynamic test setups, the component linked to a test wagon with speed being crushed to a wall for axial crushing testing. These kind of test setup would give information at higher acceleration conditions. An example of a rear impact structure (RIMP) of a F1 car subjected to crash testing with this kind of test setup is shown in Figure 1.10 [20].

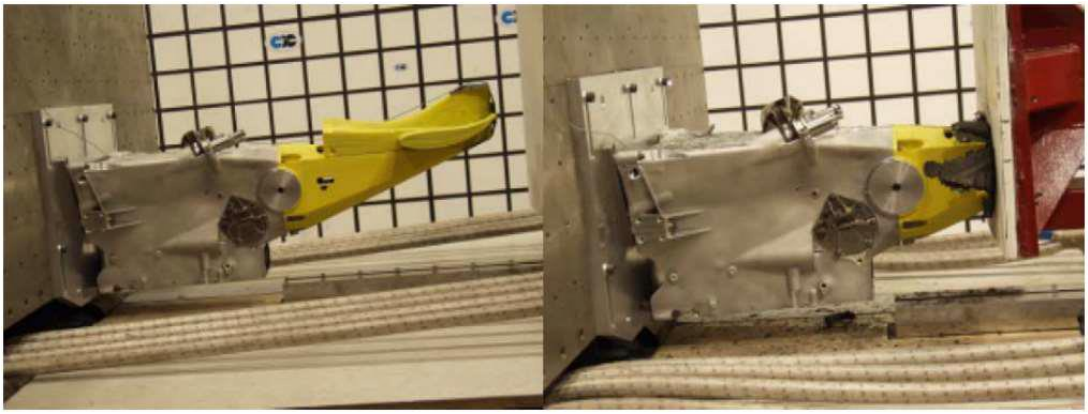

Figure 1.10. Official FIA F1 RIMP test [20].

1.1.3. FRP Composite Materials

Composite materials are made of two or more materials combined together in a form that each material maintains its integrity. In general, composite material consists two materials named as matrix material and reinforcement material. Matrix material surrounds the reinforcement and holds them together. It is possible to categorize composite materials in many classes according to shape, type and behavior of matrix and reinforcement materials. Fiber-reinforced polymer composites are the type of composites that consists polymer material as matrix material and fibers as reinforcement material.

Fiber-reinforced composites can be classified into many categories. Polymer matrix may be a thermosetting resin or thermoplastic resin. Some of the thermosetting resins are epoxy, polyester and vinylester. Polypropylene (PP), Polyether ether kethone (PEEK) and Polyamide (PA) are examples to the thermoplastic resins. Fiber materials may be in form of short fibers or continuous fibers. In general, continuous fibers are used in FRP composites. Carbon fibers, glass fibers and aramid fibers are common fiber materials used in FRP composites.

Fiber-reinforced composites can be classified into three categories according to commercial types. These are unidirectional (UD), 2D woven and 3D woven fiber-reinforced composites. UD composites are the basic type of FRP composites, which fibers are aligned in the same direction in a single ply. In woven composites, fibers have two or more directions because of the woven structure. FRP composites may be in a form of single layer or multi layers stacked together. Multi-layered composites are made of UD and 2D woven layers stacked in an orientation in different directions. Orientation changes the laminates mechanical properties such as strength and stiffness.

2D woven fabrics can be classified in terms of their architectures according to weaving pattern used in prepreg. Plain weaves, twill weaves and satin weaves are the main weaving patterns in woven composites. Weaving patterns are shown in Figure 1.11 [21].

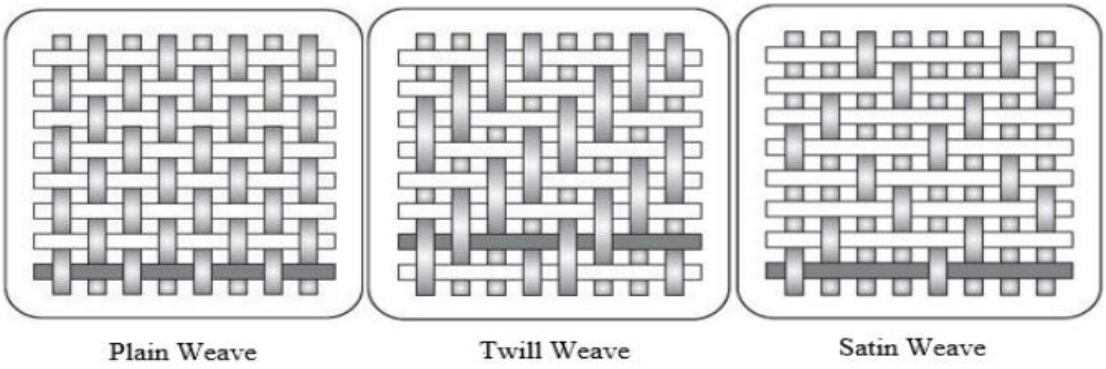

Figure 1.11. 2D Woven fabric weaving patterns [21].

3D woven composites are the most recent type of the FRP composites. In 3D composites warp and weft yarns are woven in three orthogonal directions. So, 3D woven laminates are made of one thick woven ply. Although it is suggested that 3D composites could be efficient in many applications, 2D woven and UD composites are used because of the extreme costs of 3D composites.

Failure of the structures manufactured from FRP composites are related to the failure of the layers in composite laminate. Main failure types of FRP composite plies are matrix failure, fiber failure and delamination. In a composite subjected to loading, many of these failure types may occur in the structure. FRP composites are anisotropic materials which their mechanical properties differ in different directions. So, failure of the composites will differ in different directions too. In brittle composites, failure of the plies leads to fracture under tension, compression and shear stresses. Fractures modes of a unidirectional fiber composite lamina are shown in Figure 1.12 [10].

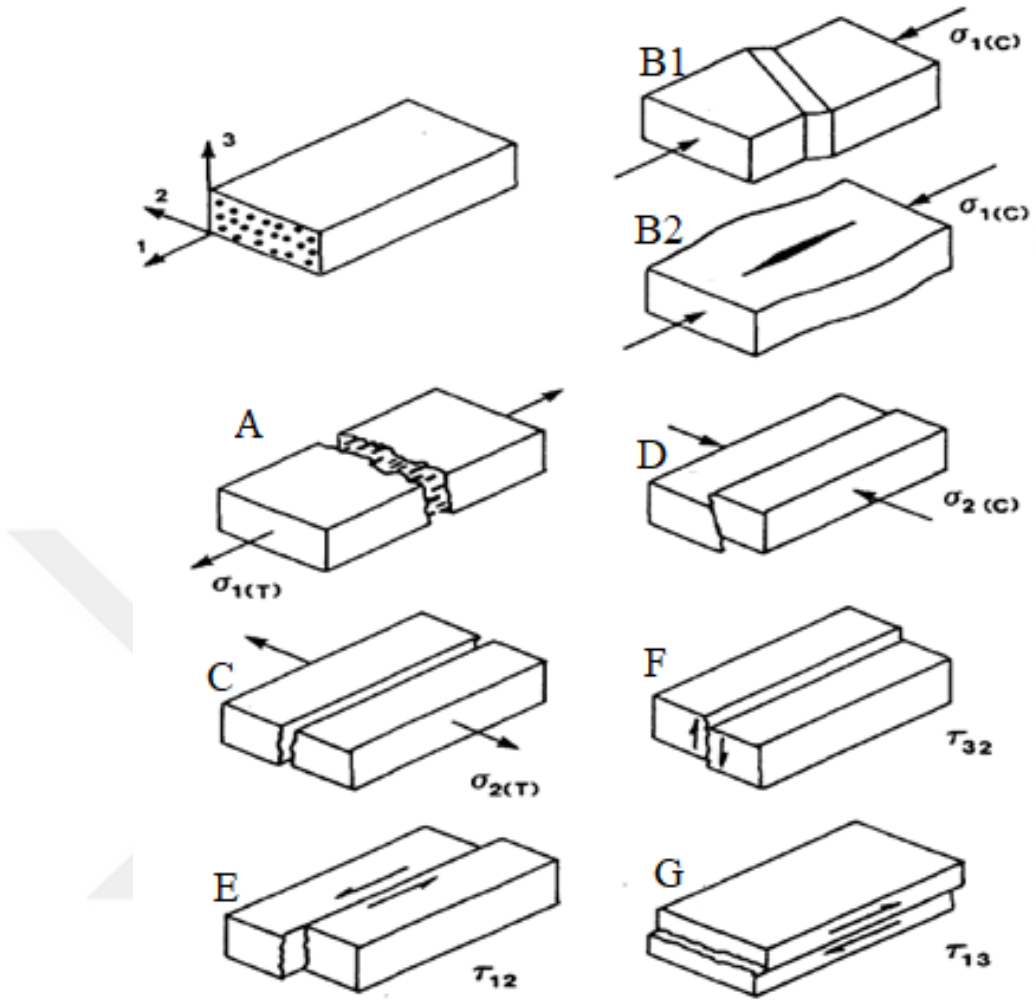

Figure 1.12. Fracture modes of a unidirectional lamina [10].

If a composite material subjected to tensile load in fiber direction, tensile fracture of fibers and matrix can be observed in ply (see Figure 1.12 A). Under compressive loads, ply may exhibit shear fracture of fiber and matrix materials (see Figure 1.12 B1) or fibers may exhibit micro buckling which will form kinks in the ply (see Figure 1.12 B2). Tensile loads in matrix direction will result in matrix fracture and fibers will stay integrated to the fractured parts (see Figure 1.12 C). Compressive loads in matrix direction will result shear matrix fracture in ply (see Figure 1.12 D). Shear loads may effect both matrix and fibers. However, due to the lower strength of matrix, shear loads leads matrix cracks in ply dependent to the plane that shear load subjected (see Figure 1.12 E, F and G) [10].

The fracture modes occurs in a ply subjected to loading are intra-laminar fracture modes. Since FRP composite structures are generally made of laminated layers stacked together, it is expected to these layers to split from each other when subjected to loading. This type of failure between layers is called as inter-laminar failure or delamination. Delamination crack is generally initiated by an intra-laminar crack that extend to the interface between plies. In Figure 1.13, delamination is shown alongside matrix crack and fiber fracture in a CFRP laminate [22].

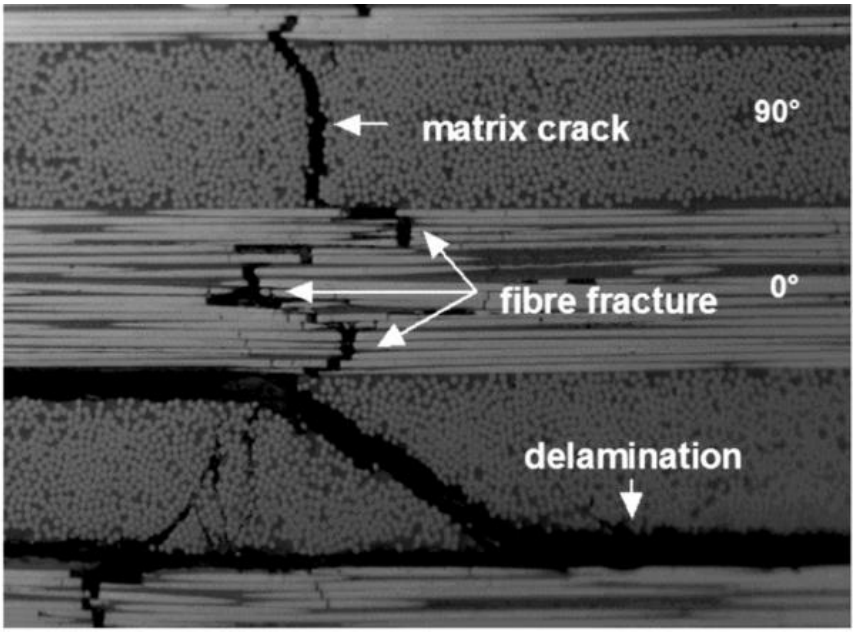

Figure 1.13. Delamination, fiber fracture and matrix fracture in a CFRP laminate [22].

1.1.4. Crushing Behavior of FRP Composite Tubes

Material type of the crash box is one of the main factors that effects the crushing behavior of crash box. As it was stated before, traditional materials used for crash boxes in automobiles are metallic materials such as aluminum and steel. Metallic materials are ductile materials which have high failure strain rate. Metallic crash boxes fails by plastically folding or buckling when they subjected to impact. Folding occurs progressively like an accordion that make it possible to absorb certain values of energy. Typical progressive folding of a tubular metallic crash box and its load-displacement curve are illustrated in Figure 1.14 [10].

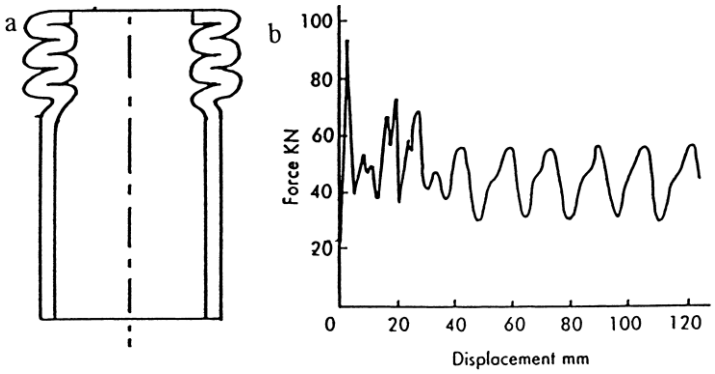

Figure 1.14. Crushing behavior of metallic tubes a) Progressive folding when subjected to axial impact load b) Load-displacement curve [10].

Folding behavior makes the progressive zone wavy in load-displacement curve. This can be attributed to the high resistance before a fold starts and decrease in the resistance as fold completes.

Unlike traditional metallic materials, crash boxes made from fiber reinforced composite materials, progressive failure mechanism is usually progressive fracturing rather than folding. Most of the FRP composites are made of brittle fibres embedded in a ductile polymer matrix. They show brittle fracturing characteristics when they subjected to impact loads. Folding is possible for continuous carbon and glass fibre materials [11]. But the desired crush behavior in composite tubes is progressive fracturing, since smaller load oscillation is observed. A schematic representation of progressive crushing of a carbon composite tube is shown in Figure 1.15 [10].

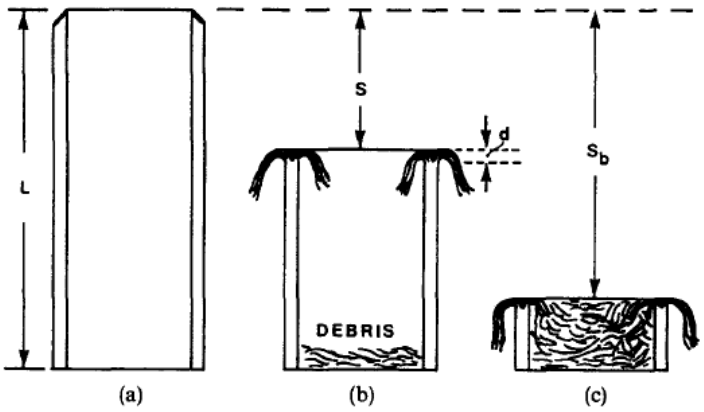

Figure 1.15. Schematic representation of progressive crushing, a) Initial shape b) Half-crashed tube c) Fully crashed tube [10].

Typical force-displacement curve achieved from a FRP composite tube is shown in Figure 1.16 [10].

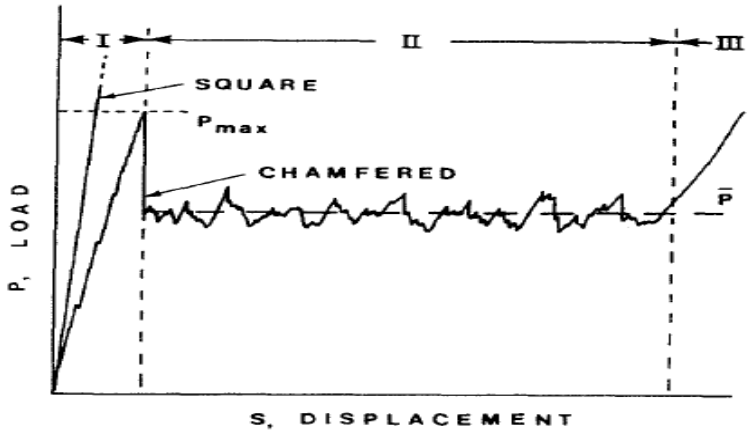

Figure 1.16. Typical force-displacement curve of a CFRP tube subjected to axial impact loading [10]: I, Crush zone formation; II, Progressive crushing, III, Debris compaction.

Crushing behavior of a crash structure is classified into two main categories as progressive crushing and catastrophic crushing. Progressive crushing shows a stable behavior and good energy absorption characteristics. However catastrophic crushing is unstable and undesired. Load-displacement curve of a catastrophic failure draws a curve that consists a suddenly increased peak load and it is followed by a post failure mode.

Structures that show catastrophic crush behavior have very low energy dissipation capability. So structures that show catastrophic crush behavior are not able to prevent damage to the passengers in the vehicle. Therefore, catastrophic crush behavior is not a desired failure mode. Long tubes with thin walls commonly show catastrophic behavior due to their columnar instability. Catastrophic crush metallic materials is generally in the form of Euler buckling. For the composite materials, it is generally cracking from middle. A typical load-displacement curve of a composite structure shows catastrophic crush behavior and its crush mode are shown in Figure 1.17 [10, 13].

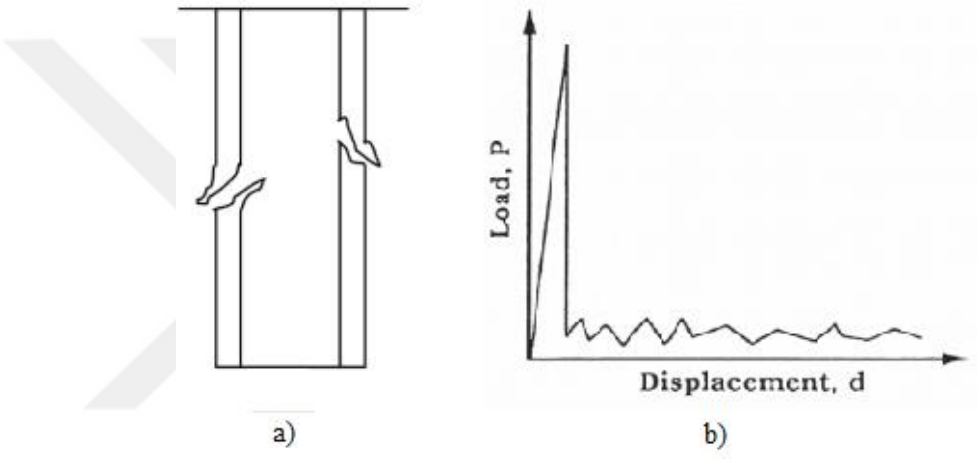

Figure 1.17. Catastrophic crushing behavior a) Crushing mode illustration [13] b) Typical load displacement curve [10].

1.1.5. Progressive Crushing Modes of FRP Composite Tubes

Progressive crushing is the desired crushing behavior for a CFRP tubular crash box since it absorbs high energy values in a controlled manner. Progressive crushing of a composite tube may occur in different forms depending on the arrangement of fibers, materials used and crush zone morphology. Hull [10] and Farley and Jones, [11] classified the progressive crushing modes of composites. Hull identified the progressive crushing two extreme modes: splaying and fragmentation modes [10]. Local buckling (Progressive Folding) mode that can be observed in aramid material composites and metallic structures was examined separately by Hull.

In Hull's study, splaying mode was described through the experimental tests on a [0/90/90/0] glass fibre-polyester resin tube and the fragmentation mode described through woven glass cloth-epoxy tubes [10].

Illustration of a crush zone a [0/90/90/0] glass fibre-polyester composite tube that shows splaying mode is given in Figure 1.18 [10]. When the tube is subjected to axial compression, the load is carried by axial fibers majorly due to the high elasticity modulus in axial layers. Layers that provides hoop fibers support the axial layers and prevents the premature buckling modes. Thus compressive strength of the tube is directly related to the strength of axial layers [10]. During axial compression, splaying mode occurs with the formation of fronds as tube progressively crushed. Axial fibers splays in a series of fronds towards outside and inside of the tube wall as a crack forms along the center of the tube wall. In tubes that shows splaying crush mode, generally a debris of crushed fibers and resin separates the two fronds that moves towards inside and outside the tube. Debris at the crush zone acts as a wedge that separates the two fronds of the tube wall. In addition, axial splits occurs in fronds as crushing progresses in many composite materials.

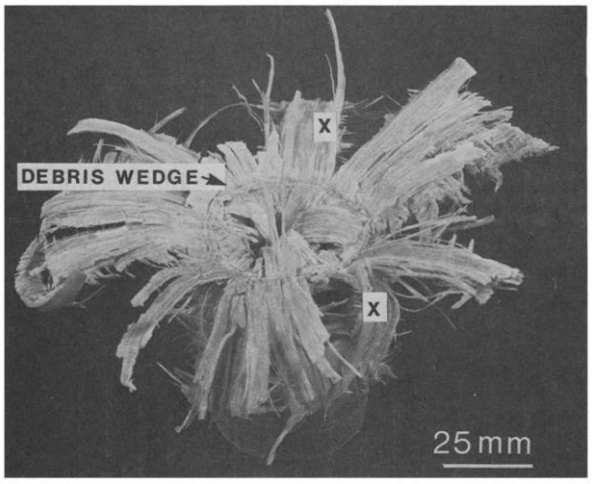

Figure 1.18. Crush zone of a [0/90/90/0] glass fibre-polyester resin tube [10].

Developing a detailed understanding about micro-fracture events inside the tube wall is possible by examining the crushed wall section view. Stable crush zone formation process of $\theta = 30°$ chamfered [0/90/90/0] glass fibre-polyester resin tube from section view is illustrated in Figure 1.19 [10].

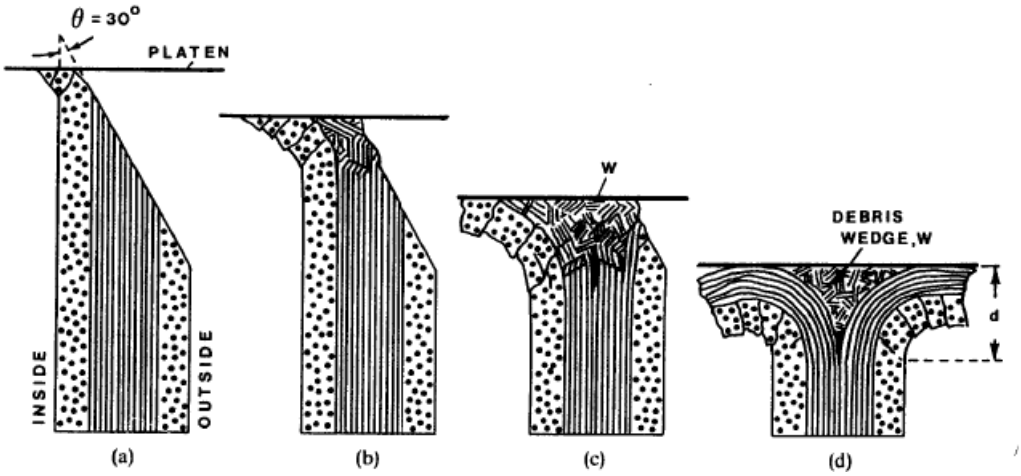

Figure 1.19. Schematic representation of formation of a splaying mode crush zone [10].

Splaying crushing mode is quite complex since various failure modes take place in the layers. A debris wedge is formed by transverse shearing failure in the center layers. Intra-laminar shear occurs in the axial layers generating axial cracks parallel to fibers. A center-line crack is generated due to the delamination caused by debris wedge. Axial splits in tube wall formed due to the transverse shear and tensile failure in hoop layers.

Fragmentation mode is the other progressive crushing mode of the described modes by Hull. Fragmentation mode was examined through the tubes made from woven E-glass cloth. Fragmentation mode involves the formation of fragments in the crush zone during axial compression. Fragments are forced to move towards inside and outside as they separated from the tube wall. Fragments have a characteristic shape dependent on the material and test conditions. Crush zone of a woven glass cloth tube showing fragmentation mode is illustrated in Figure 1.20 [10].

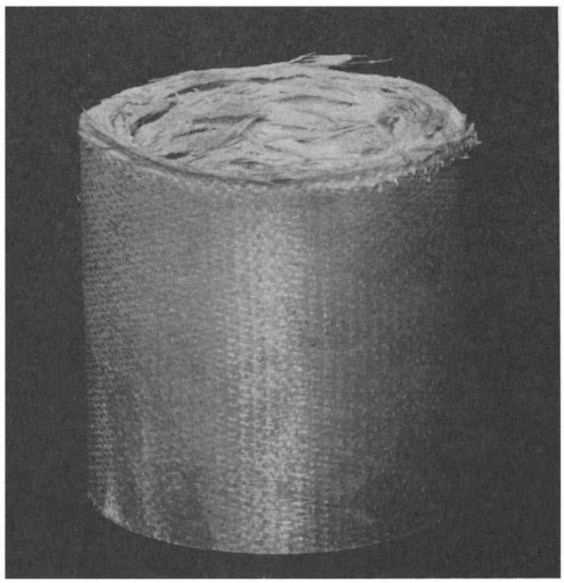

Figure 1.20. Crush zone of a woven glass cloth tube showing fragmentation mode [10].

In fragmentation mode, compressive load generates shear failure in the layers of the tube wall. Fragments forms and forced outwards from the wall as the crushing platen progresses. Shear failure in layers involves the fiber fracture, buckling and delamination failures. Section view of the tube wall that show fragmentation mode is illustrated in Figure 1.21 [10].

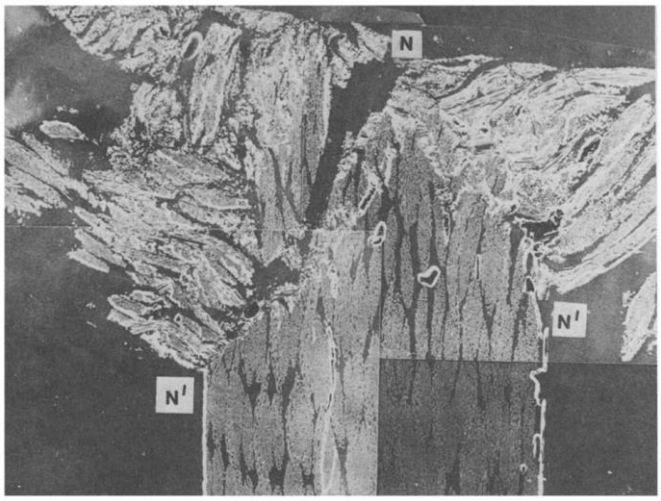

Figure 1.21. Cross-section through crush zone of a woven glass cloth-epoxy resin tube that shows fragmentation [10].

Shear failures are visible along N-N’ line in Figure 1.22. As with the splaying mode, crush zone is quite complex since different failure types take place during crushing. Main force in the crush zone is the compressive load against tube in fragmentation mode. With the rapid fracture and bending of the fragments, load is consequently relaxed during crushing. This leads to the serrated form of load-displacement curve. The nature of fragmentation mode and its differences from splaying mode can be examined in the schematic representation of formation of a fragmentation mode in cross section view in Figure 1.22 [10].

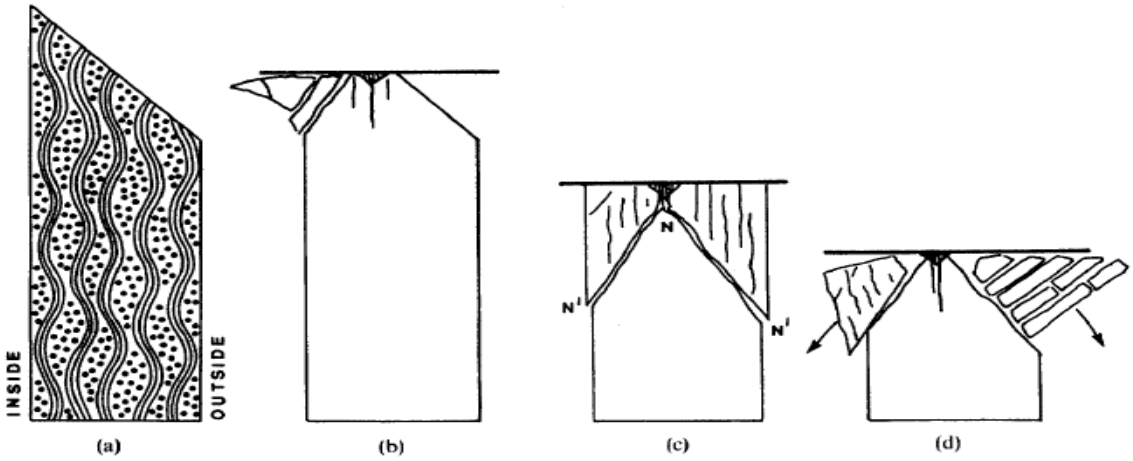

Figure 1.22. Schematic representation of formation of a fragmentation mode in cross section view [10].

Comparison between the splaying and fragmentation modes indicates that the microfracture mechanisms determines the crush mode. The results suggested that if splaying does not occur in crushing, tube will be crushed until it reaches critical value for shear fracture and will show fragmentation.

Farley and Jones described the progressive crushing modes of composite tubes in four categories. These are transverse shearing, lamina bending, brittle fracturing and local buckling modes. Farley and Jones stated that most tubular specimens shows a combination of these crushing modes and mechanical properties of the tube materials and the structure determines the crushing mode [11].

Transverse shearing mode shows the same essential features with the fragmentation mode identified by Hull. Transverse shearing mode can be recognized by wedge shaped cross section of the laminate and short inter-laminar and longitudinal cracks which forms fragmented parts of the lamina bundle [11]. Lamina bending mode is essentially same with the splaying crushing mode. Recognized features of the lamina bending modes are long inter-laminar, intra-laminar and parallel to fiber cracks and lamina bundles that splays during crushing [11]. Third main mode identified by Farley is brittle fracturing mode. Brittle fracturing mode is considered as a combination of transverse shearing mode and lamina bending mode. Inter-laminar cracks and longitudinal cracks in brittle fracturing mode are shorter than the cracks in the lamina bending mode and longer than the cracks in the transverse shearing mode. As a result of this case, energy absorption mechanism of brittle fracturing mode is a combination of these two failure mechanisms [11].

Final crushing mode identified by Farley and Jones is local buckling mode. Local buckling occurs by plastic deformation of the specimen in the form of local buckles as specimen progressively compressed. Local buckling is the same with the progressive folding of ductile materials under progressive compression [11]. Crushing modes identified by Farley and Jones are illustrated in Figure 1.23 [11].

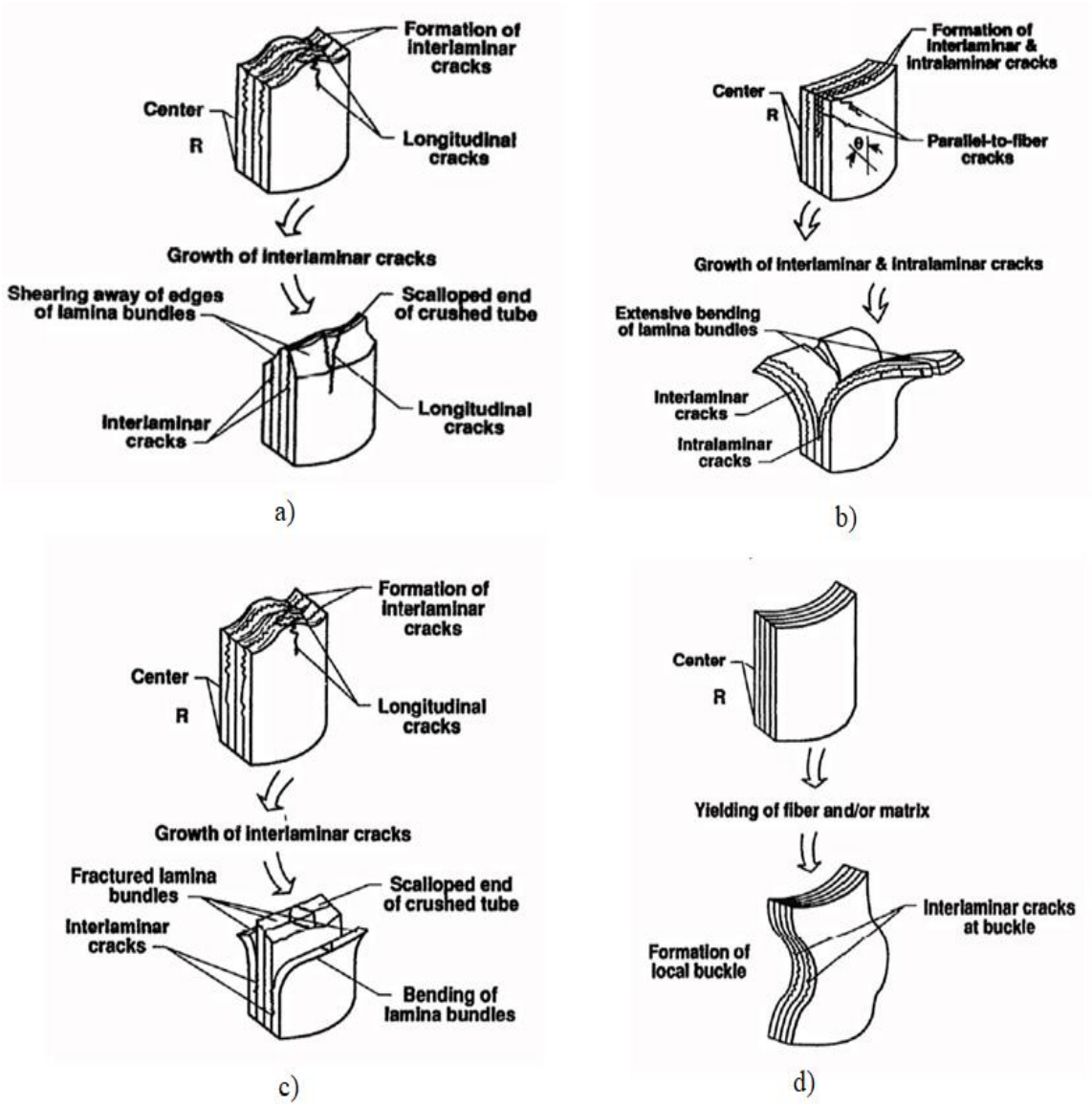

Figure 1.23. Crushing modes identified by Farley and Jones, a) Transverse shearing, b) Lamina bending, c) Brittle fracturing, d) Local buckling [11].

1.1.6 Factors Affect Crushing of CFRP Tubes

Energy absorbing characteristics and crushing behavior of a FRP tubular crash component depends on various parameters such as material type of the constituent matrix and fibers, content ratio of fibers, architecture of the composite, manufacturing conditions, geometry of the tube and testing conditions. Selection of the parameters during the designing process of a CFRP crash tube is critical for providing high energy absorption to the tube.

Summary of the factors that effects crushing characteristics of a CFRP crash tube is categorized in the schematic at Figure 1.24 [6].

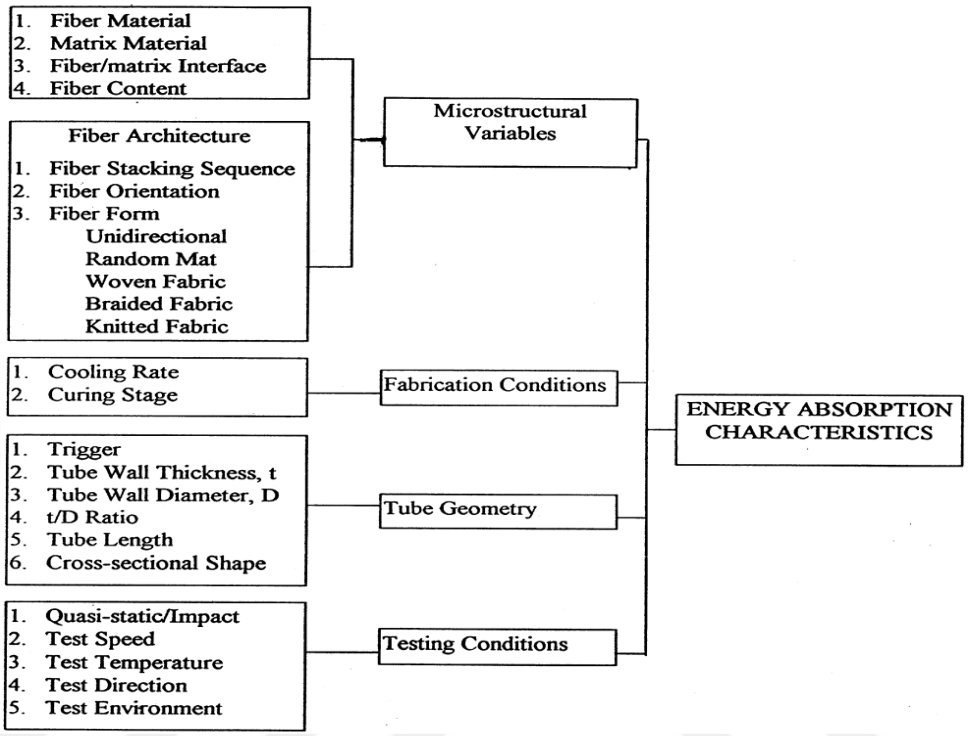

Figure 1.24. General parameters that effects the energy absorption characteristics of a composite tube [6].

Vast majority of the studies on the effect of materials on composite crushing is based on the individual effects of fiber and matrix materials. Thornton [23], Schmuesser and Wickliffe [24] and Farley and Jones [11], individually stated that carbon-epoxy tubes absorbs more energy than glass-epoxy or aramid-epoxy components. In Schmuesser and Wickliffe's study, crush tests on graphite-epoxy and Kevlar-epoxy specimens were conducted and it is observed that graphite-epoxy specimen show brittle fracture behavior and Kevlar-epoxy specimen showed folding behavior like an accordion. This difference can be explained on the basis of the failure strains of two different types of the fibers. Aramid fiber fails about %8 strain whereas carbon fiber fails about %1 strain rate. Ductile fibers like aramid will show plastic deformation rather than brittle fracture. However, composites that has brittle fibers may show progressive folding if matrix material strain rate is very high according to Farley and Jones's study [11].

Farley [25] also suggested that to obtain maximum crushing performance from a fiber, the matrix material must have a greater failure strain than fiber material. If matrix material has higher failure strain, then crack growth of inter-laminar cracks will be slowed, thus this will increase the energy absorption capacity. Yet, too much restriction of inter-laminar cracks will lead to local buckling modes or catastrophic failure mode.

Hamada et al. [26], worked on crushing of carbon composite tubes that consists of carbon fiber and thermoplastic Polyether Ether Ketone (CF/PEEK) as matrix material and carbon/epoxy tubes. PEEK offers high resistance to inter-laminar crack growth. This can be attributable to the higher energy absorption capacity of the thermoplastic PEEK material. It is stated that CF/PEEK composites can reach specific energy absorption capacity values of 180 kJ/kg.

Hamada et al. [27], investigated carbon fiber/PEEK and glass fiber/PEEK tubes axial crushing. They used AS4 and IM7 carbon fiber/PEEK specimens and S2 glass fiber/PEEK specimens. They found out AS4/PEEK and IM7/PEEK displays similar specific energy absorption values and they reach higher values than S2/PEEK specimens do although their mean crush forces are comparable. This difference simply arises from the density differences between carbon fibers and glass fibers. Due to their low density, specific energy absorption is higher in carbon/PEEK specimens.

Fiber architecture is a critical variable among microstructural variables. Direction of fibers and their design pattern is highly effective on mechanical properties of the composite structure. So, fiber architecture effects crushing behavior, thus energy absorption characteristics of the composite structure. Berry's study proposes a good example on how fiber architecture can effect crushing characteristics of a composite tubes [10, 28]. Berry examined the crushing behavior of woven glass-cloth polyester tubes with different hoop-to-axial fiber ratios. Seven different hoop-to-axial fiber ratios, which are 8.5:1, 7:1, 4:1, 1:1, 1:4, 1:7 and 1:8.5, used in the study. Schematic representation of different hoop-to-axial fiber ratios is given in Figure 1.25 [10].

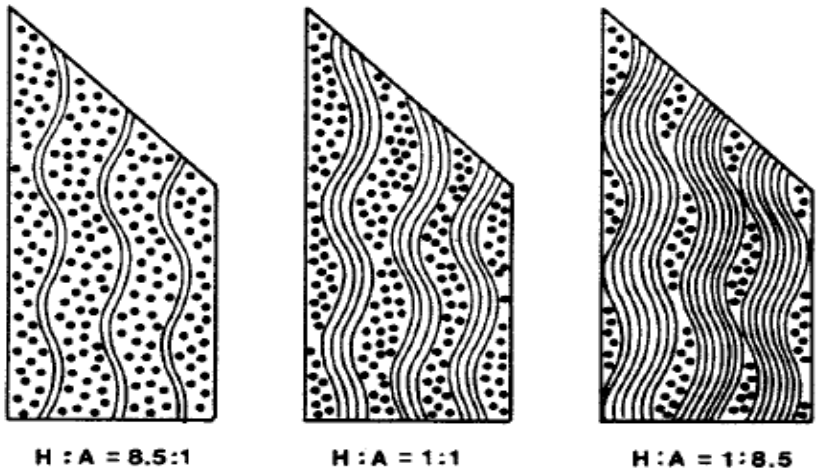

Figure 1.25. Schematic representation of section views of composite tubes with different hoop-to-axial fiber ratios [10].

Fibers in axial direction provides high stiffness and strength to the tubes in compression. Fracturing of fibers is quite harder in compression loading than it is in tension loading. Thus, axial fibers in tubes tends to buckle, kink and splay during crushing. Hoop fibers, on the other hand, encircle the tube and holds the tube together and tries to prevent the splaying fronds during crushing. So they face tensile and shear loads that they may show fracture eventually. Schematics of the crush zones of the tubes examined by Berry are given in Figure 1.26 [10]. As it can be observed in the schematics, the tubes tends to splay as axial fiber content is increased and tends to fragmentation as hoop fiber content is increased.

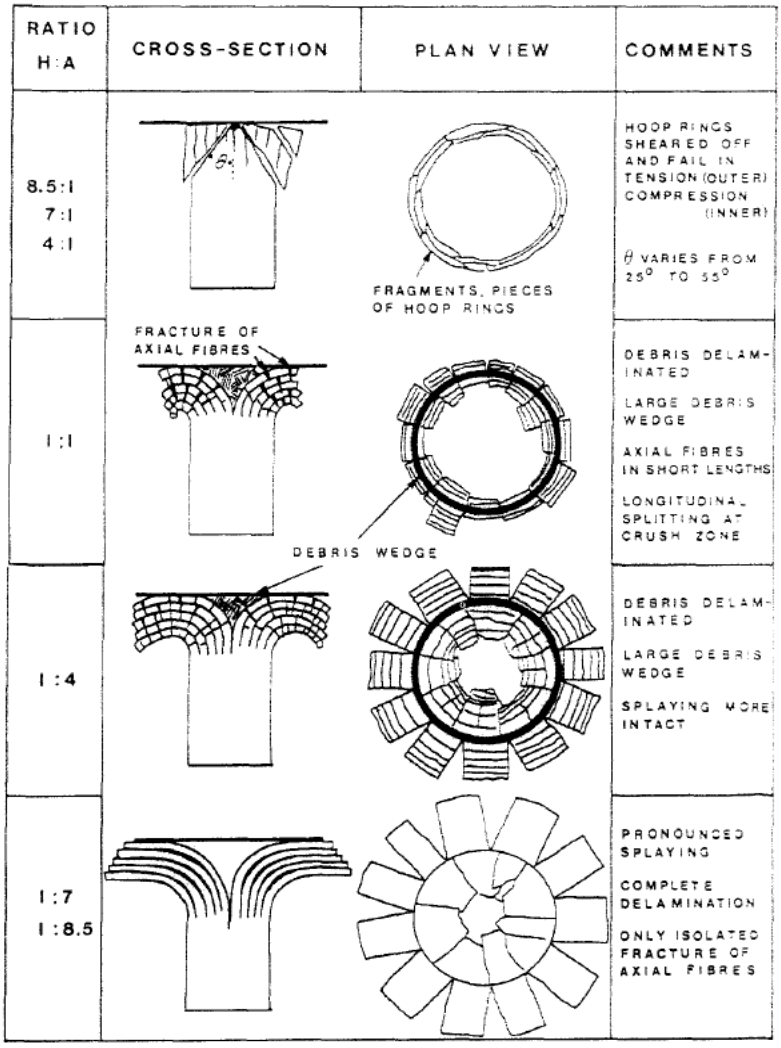

Figure 1.26. Crush zones of different hoop-to-axial fibers ratio of composite tubes [10].

Energy absorption characteristics is directly related to crushing behavior of the tube. It is stated that axial fibers provide high stiffness and strength to the tubes in axial direction. This will result high peak load in load displacement curves of the crushed tube. However, as the content of axial fibers increases the tube tends to pronounced splaying. Only inter-laminar failure take place during progressive crushing and tube wall acts as column, will form fronds that act as rigid beams. Thus, load bearing ability of the tube wall will be decreased and the tube will have a low value of progressive crushing load. Tubes with high content of hoop fibers tends to fragmentation so splaying mode does not occur in these tubes. Yet, the less number of axial fibers will result lower loads on load-displacement curves and lower energy absorption capacity. Load-displacement curves of the examined tubes are given in Figure 1.27 [10].

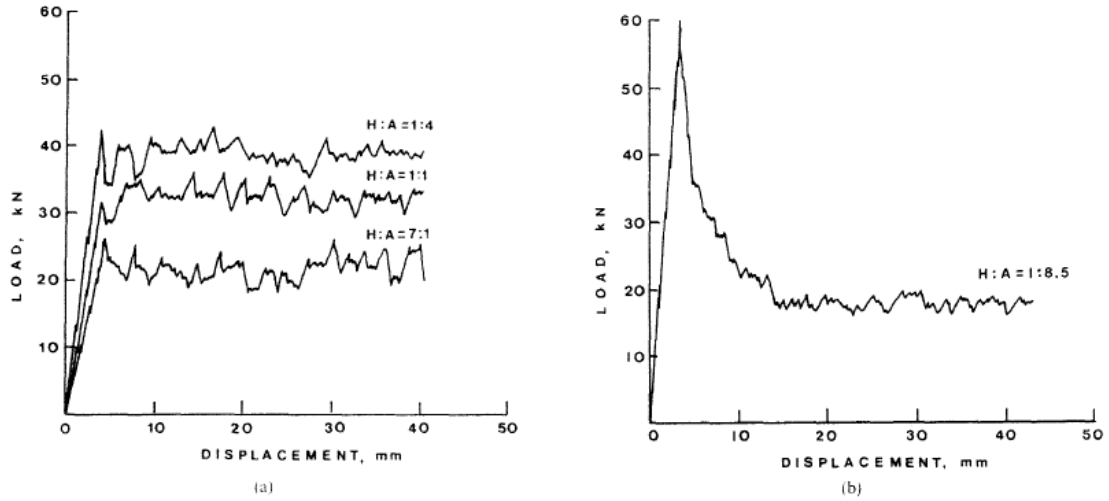

Figure 1.27. Load-displacement curves of examined tubes with different hoop-to-axial fiber ratio crushed at 4mm/s, a) H:A between 7:1 and 1:4 b) H:A=1:8.5 [10].

Both axial and hoop fibers are very important to design an efficient composite crash box tube. Hoop fibers provides circular constraints to the tube which induces the tubes crushing mode closer to the fragmentation, which is efficient than splaying. Axial fibers provides higher crushing loads but they induces the tubes crushing mode towards splaying, and not to reach its full potential. Same situation goes for UD laminate composites as well [6]. A design of fiber architecture that provides strength on both hoop and axial direction will result with an efficient crash structure.

Structural geometry has significant effect on crushing behavior of composite tubes as well. Geometry is the second main topic of designing process after microstructural variables. Effect of the geometry is investigated on wall thickness, axial length, cross-sectional shape, mean diameter or circumference, conic angle in case of conic tubes and trigger mechanism parameters [29].

Many researchers investigated these parameters and reported their effects. Study of Thornton and Edwards [30] stated that circular tubes has higher energy absorption capacity than square or rectangular cross-section tubes in their study. This is because the corners of square and rectangular tubes makes stress concentration points leads to splitting cracks that results low energy absorption.

Findings of Thornton and Edwards are also supported by studies of Kindervater [31] and Mamalis et al., [29]. Farley and Jones found out that as tubes energy absorption capacity increases as tubes become more elliptical [11].

Thickness and mean diameter of the tubes has effects on crushing characteristics as much as cross-section of tubes. Farley and Jones reported that energy absorption capacity is a non-linear function of diameter to thickness, D/t [11]. Energy absorption tends to decrease as D/t increases. The energy absorption capacity increases as both diameter and thickness variables increases. This is because of the increasing cross sectional area of the tube wall. Also, Farley and Jones found out that tubes energy absorption capacity increases as tubes become more elliptical [11].

Mamalis et al., indicated that axial length of the tubes has no significant effect on energy absorbing characteristics of the tube [29]. However, very long tubes have the risk of exhibiting Euler buckling. Mamalis et al., also reported that as the conical angle decreases on a conical tube the energy absorption increases, which is very logical and again related to the fiber directions. The effective feature of the conical parts is that they do not require collapse trigger mechanism to avoid catastrophic failure behavior [29].

1.1.7 Effect of the Foam Filled Design

Foam materials are extensively used in automobile and aerospace industries as core materials for sandwich components due to their lightweight feature and stable deformation behavior. Most of the foams are cellular materials that exhibits deformation close to the perfectly plastic behavior when crushed, which is excellent for axial crushing. However foam material strength values are relatively low so they are generally used as a support material for crushing components. Foam materials has influence on the crash behavior of the components they applied to. Some of the studies exists in the literature about foam filled tubular crash components are discussed in this section.

Hanssen et al. [9], worked on aluminum foam-filled metallic crash boxes and they showed that the crushing behavior is effected by the foam applied. It is stated that as the density of foam inside tube increases it changes the folding number of the crushed metallic tube in this study. An illustration of this phenomenon is given in Figure 1.28 [9].

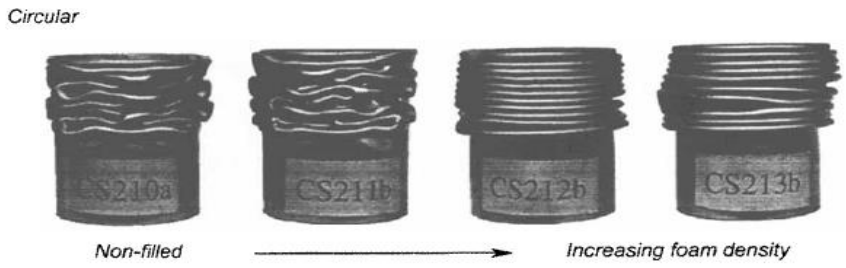

Figure 1.28. Foam filled metallic tube folding subjected to axial crushing as foam density increases [9].

It is observed in the study of Hannsen et al., foam filling cause a positive interaction effect and energy absorption capacity of foam filled component becomes higher than linear sum of the foams and tubes capacity [9]. This increase in energy absorption capacity caused by an interaction effect. The interaction effect on load displacement curve is shown in Figure 1.29 [9].

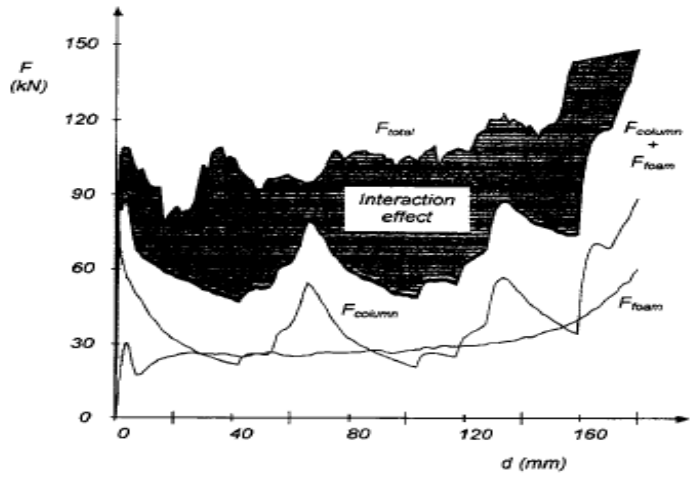

Figure 1.29. Interaction effect on a load displacement curve of a foam filled metallic tube [9].

Main purpose of foam filling the crushing tubes is to restrict the deformation towards inside of the tube. In metallic tubes, foam core minimize the buckle length and increases the number of folds on the tube wall. In composite tubes foam core constraints inwards fronds and results the crushing mode with outwards fronds and debris wedge between foam and tube wall. So, foam core causes more failure of the material during crushing by supporting the tube wall and positioning it perpendicularly to the impact object. This interaction effect leads to high resistance loads during crushing.

Sun et al., [8] investigated tubular sandwich components made of aluminum tubes and CFRP tubes used as face materials and aluminum foam used as core materials. Positive increase in the absorbed energy caused by interaction effect is seen in the studies of Sun et al.

Yao et al., [32] investigated tubular sandwich components made of aluminum tubes and CFRP tubes. Polyurethane foam core is used in their study. Increase of the absorbed energy in the sandwich components caused by interaction effect is observed in their study. Crushing modes observed in the Yao et al., study is shown in Figure 1.30 [32]. Interaction effect on the composite sandwich curves are shown in Figure 1.31 [32]. Red lines indicates linear sum of the load displacement curves that forms the sandwich component and black lines indicates the load displacement curve of the sandwich component itself in Figure 1.31.

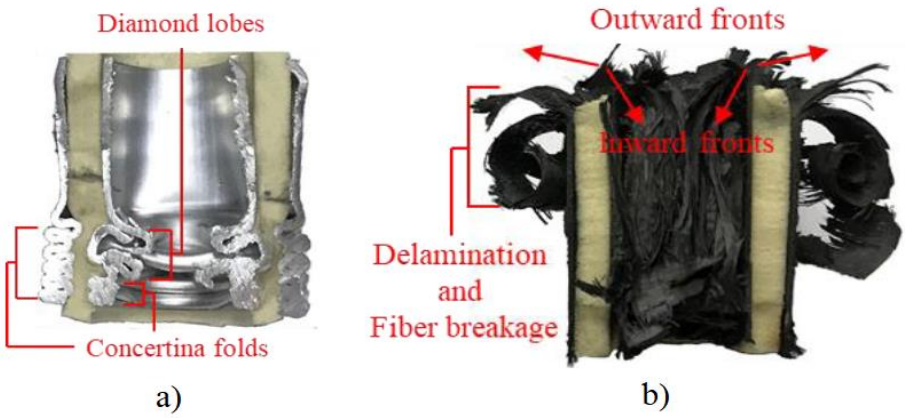

Figure 1.30. Crushing modes of the tubular sandwich components investigated by Yao et al., a) Al-PU-Al sandwich tube, b) CFRP-PU-CFRP sandwich tube [32].

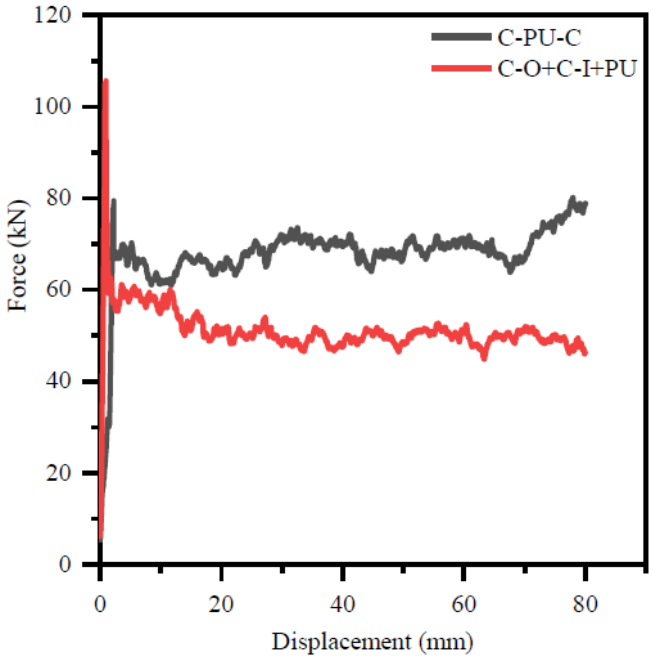

Figure 1.31. Load displacement curves of the C-PU-C sandwich components in Yao et al.'s study [32].

Wang et al. [7] investigated the crushing of CFRP braided textile tubes filled with PU foam. Braided composite tube specimens investigated in this study are manufactured with different fiber angles (θ) of 30°, 45° and 60°. Specimens show the behavior of local buckling in Wang et al.'s study. Specimens filled with PU foams has more folds in the tube wall and their energy absorption value is increased.

Mostly used foam cores in the literature includes polyurethane foam, aluminum foam, polyvinyl chloride (PVC) foam and polyethylene terephthalate (PET) foam. Some of the studies exists in the literature focused on modifying the foam core materials. Costas et al. [33] studied aluminum tubes filled with PET foams supported with GFRP reinforced polyamide skeleton. They found out that energy absorption capacity of the aluminum tube extrusion filled with modified core is higher than tubes filled with only PET foam or GFRP skeleton. Geometry and crushing mode of the tube with modified core is illustrated in Figure 1.32 [33]. Load displacement curve of the aluminum tube filled with modified core compared to the curves of empty aluminum tube, only PET foam filled aluminum tube and only GFRP filled aluminum tube is given in Figure 1.33 [33].

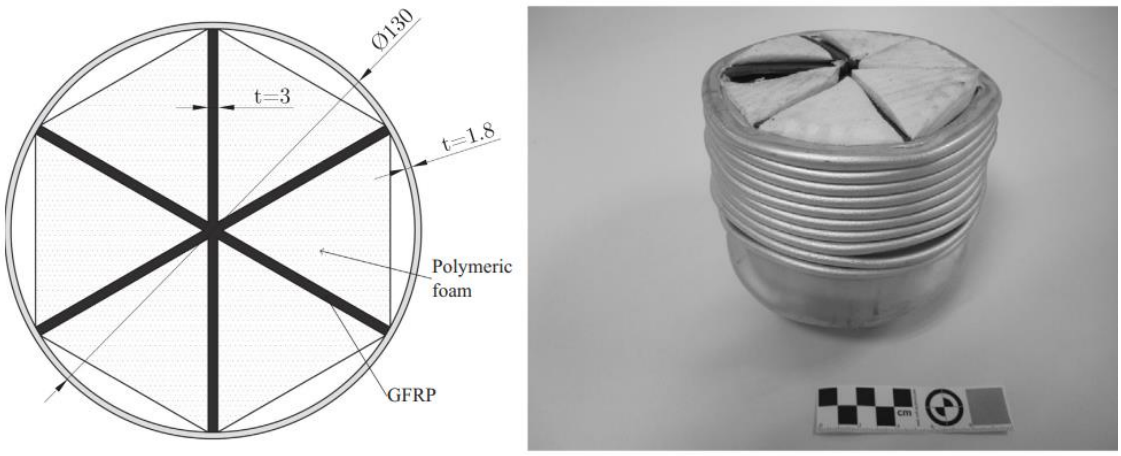

Figure 1.32. Aluminum tube filled with PET foam supported with GFRP skeleton in Costas et al.'s study, a) Schematic of the geometry b) Crushing mode [33].

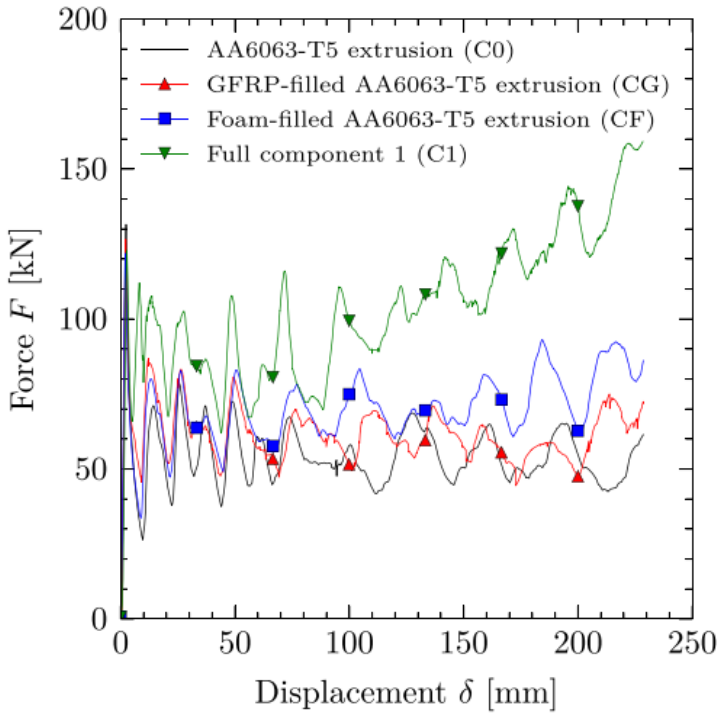

Figure 1.33. Load displacement curve of full component of aluminum tube filled with modified core compared to the curves of empty tube, only GFRP skeleton filled tube and only PET foam filled tube [33].

Pietras et al. [34] published a study about out of plane crushing of aluminum honeycomb components filled with graphene reinforced PU foams. Filling the honeycomb structure with PU foam doubles the stress values in stress strain curves of the component.

Zhou et al. [35] studied crushing behavior of a PVC foam panel where composite tubes embedded inside the foam. Composite tubes surrounded by the foam in the panel while inside of the tube remains empty. Energy absorption characteristics is increased by surrounding the tube from outside.

1.1.8 Finite Element Modelling of the Axial Crushing of Foam-Filled Composite Structures

Modelling composite structures are much more demanding than modelling traditional metallic materials due to their complexity and different failure modes involved in fracturing. Complexity of the composites cause difficulties since they require more degree of freedom to model that results in high computational costs. Getting accurate results and simulating the axial crush efficiently are the main goals of the modelling studies.

Modelling composite structures can be classified into three categories: macro-scale modelling, micro-scale modelling and meso-scale modelling. Macro-scale modelling adopt a method of modelling the composite structure by using homogeneous anisotropic finite elements of 2D shells or 3D solids. Entire laminate or plies modelled with anisotropic finite elements in macro-scale modelling approach. Micro-scale approach adopts modelling the material in laminate microstructure level which comprise modelling fibers and matrix materials individually with 3D solid finite elements. Meso-scale modelling adopts the approach of modelling structure in ply level. Schematics of levels of modelling of layered fiber reinforced composites illustrated in Figure 1.34 [36].

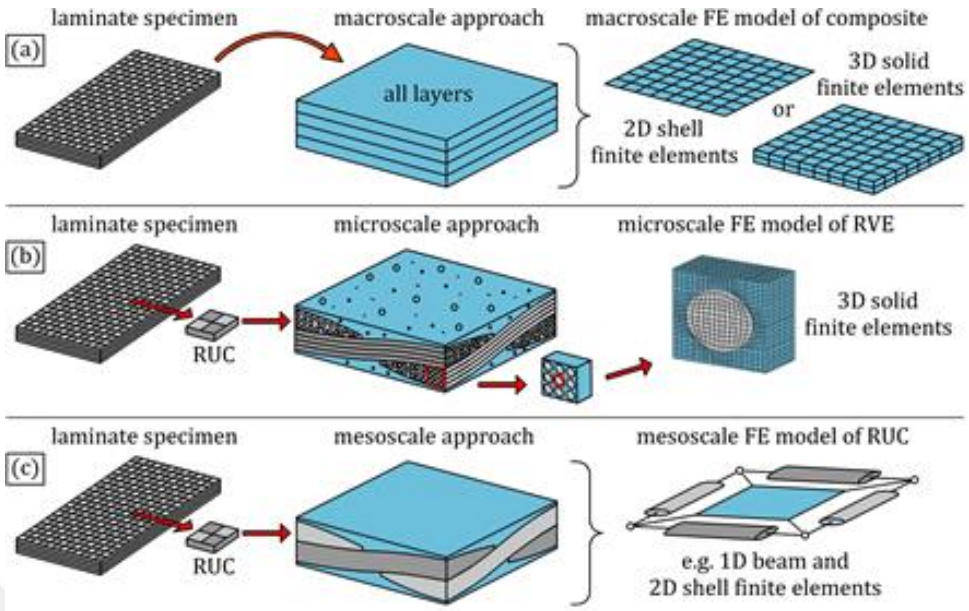

Figure 1.34. Modelling approaches of layered fiber-reinforced composites; a) Macro-scale level, b) Micro-scale level, c) Meso-scale level. [36].

Macro-mechanical modelling approach is more effective computationally and it is more suitable to model axial crushing. Micro-scale and meso-scale models are often used to model the micro mechanical behavior. The computational cost would be very high in micro-scale and meso-scale approach to model a complete composite structure crushing behavior. [36, 37].

Macro-mechanical modelling mainly divide into two methods. These are single shell layer method and the stacked shell method. Single shell layer modelling method is modelling the whole composite part by using a single layer of shell elements. No inter-laminar behavior defined in this method. Stacked shell model approach is the most popular method to simulate composite crush structures. Each ply in laminate is modelled separately using shell elements and linked together with contact constituents such as tie contact models, cohesive interface models or fracture mechanics models [37]. A schematic illustration of stacked shell modelling is given in Figure 1.35.

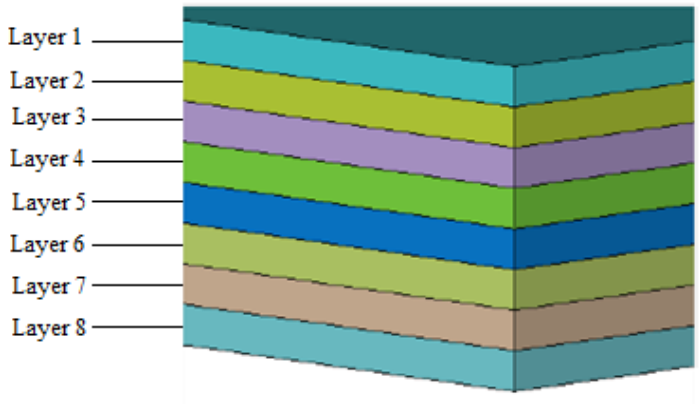

Figure 1.35. Model set of stacked shell modelling.

Most of the studies in the literature adopted intra-laminar composite damage models included in commercially available FEA software, such as MAT54, MAT55, MAT58 in LS-DYNA, Hashin progressive damage model and ABQ_PLY_FABRIC VUMAT in ABAQUS and ply type 7 model of PAM-CRASH [16]. ABAQUS also has a special add-on which is CZone used to model the behavior of the elements in the crash-end of the composite structure during crushing. Some of the studies use a in-house damage models developed by writing a VUMAT code in ABAQUS.

Inter-laminar damage of composite structures generally modelled by defining cohesive behavior or using fracture mechanics damage model in interfaces between plies. In ABAQUS software, cohesive behavior can be modelled by generating cohesive elements between ply surfaces tied to the plies surface nodes or by generating cohesive surfaces on plies interface region. Virtual Crack Closure Technique (VCCT) is another method for modeling inter-laminar damage that is based on fracture mechanics damage. Cohesive surface behavior is the method mostly used since it is simpler to apply than cohesive element method and can model crack initiation which is not possible in VCCT [17].

Various studies exists in the literature about numerical modelling of composite structures axial crushing. Mamalis et al. [38], in 2002, used LS-DYNA for simulating the crash response of square CFRP tubes and verified the simulations with the results they got in experimental tests.

Sokolinsky et al. [15], in 2010, simulated the crush response of a corrugated, sine wave beam manufactured from carbon/epoxy fabric in stacked shell modelling. Continuum shells are used to model plies and cohesive zone modelling is used to simulate delamination failures.

Zhou et al. [39], in 2017, modelled the axial quasi-static crush of square CFRP tubes with stacked shell method using cohesive zone modelling for inter-laminar failure and continuum damage based user interface model for intra-laminar failure. Constitutive equations of the material model used for intra-laminar behavior is given in detail in the study. Modelled square tube in stacked shell method is illustrated in Figure 1.36 [39].

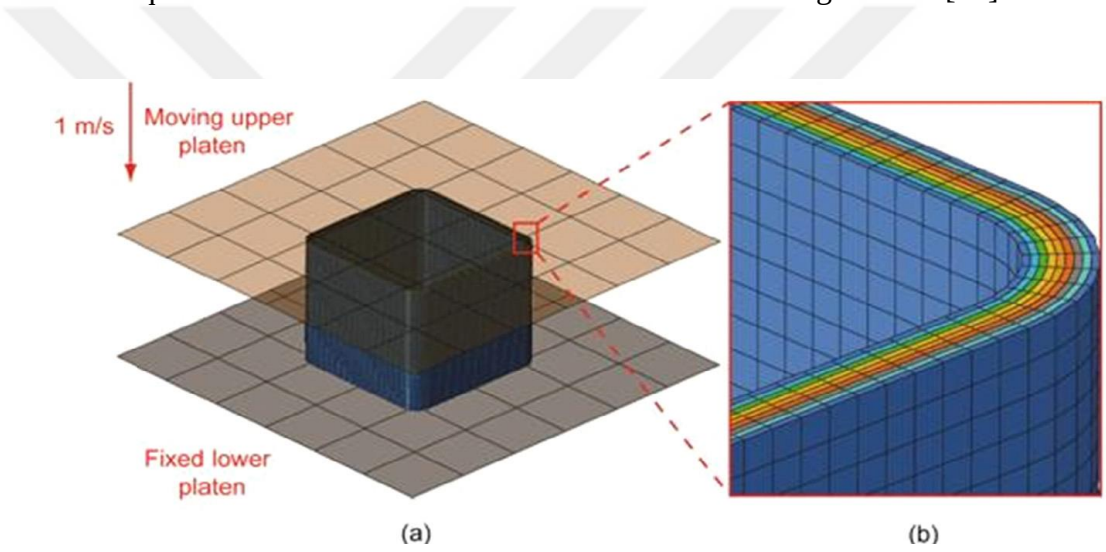

Figure 1.36. Stacked shell model of a square CFRP tube a) Assembly model b) Detailed view of the tube [39].

Lombarkia et al. [40], in 2020, simulated the axial crush of hat shape open section woven composites in ABAQUS. They used continuum shells with ABQ_PLY_FABRIC user interface to model plies and cohesive zones to simulate delamination.

Sun et al., in 2018, published a study about numerically modelling the axial crushing of aluminum foam filled composite and aluminum tubes in ABAQUS [8]. In their study, the material model of the study of Zhou et al. [39] is used to model composite tubes and built-in *CRUSHABLE FOAM material model used for modelling aluminum foam and isotropic plastic material model used to model aluminum tubes.

Polymeric foam core materials that fills the tube shows plastic deformation. Crushable foam plasticity models are used define constitutive equations of foam core materials. *CRUSHABLE FOAM material model with conjunction of *CRUSHABLE FOAM HARDENING option are selected in material property module to define the properties of foam material. Mechanical properties that require to define behavior are Young's modulus, density, plastic Poisson's ratio, nonlinear true stress-true strain curve of foam [41].

McGregor et al. [42], in 2010, simulated the progressive axial crushing of braided composite tubes in LS-DYNA. They used CODAM (Composite Damage) material model and conventional shell elements to model composite tubes. In this study, the tubes subjected to crushing by a plug external trigger and also a virtual debris wedge generated in the impact planes to model splaying mode. Achieved numerical results are very close to the experimental results in the study. Modelling approach of virtual debris used by McGregor et al. is illustrated in Figure 1.37 [42].

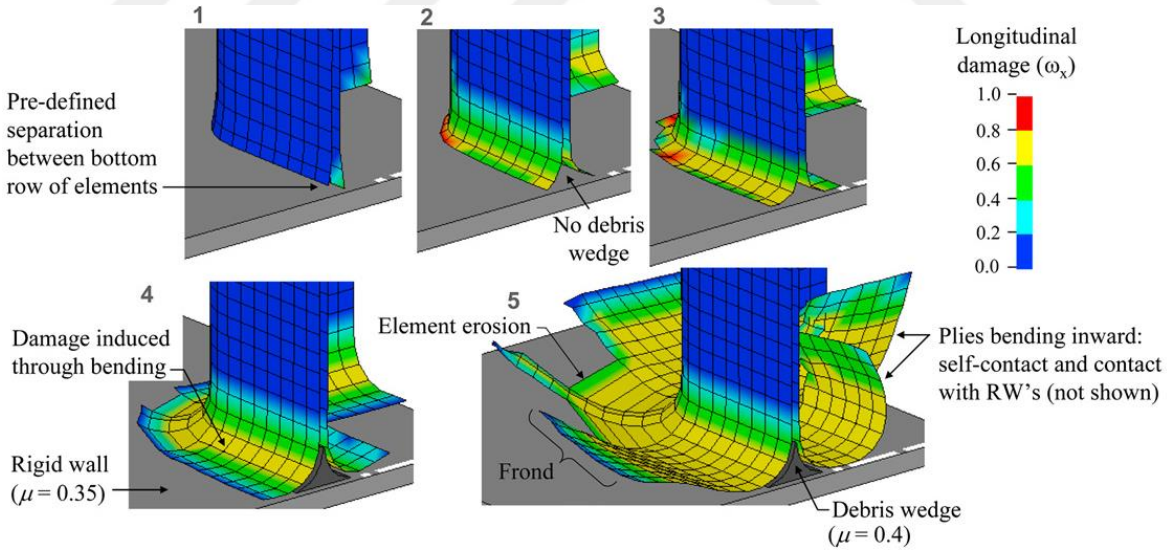

Figure 1.37. Virtual debris wedge modelling approach [42].

1.2. Problem Statement, Thesis Overview and Objectives

Crash components are very important for automobile safety and reliability. They are one of the most critical parts in transport vehicles. Most distinctive example of crash components in an automobile is crash box component placed into the back of the bumpers. A crash box is expected to absorb high values of impact energy and to be light in weight. Especially with due to increased concerns about safety and environmental impact, automotive manufacturers are motivated to use composite materials. Foam filled design of composite materials increases the absorption performance of crash box with almost no increase in weight.

Design of composite crash components is based on experimental testing. Using Finite Element Analysis is a useful method for designing crash components since it gives information about crash characteristic without doing many high priced experimental tests and shortens the design procedure. Three main methods of simulating crash events on composite crash components are micro-scale, meso-scale modelling and macro-scale modelling. Simulation of composites crash behaviour is a topic that still needs developing and there is still work to be done to do simulations more efficiently.

Modelling axial crush of composite crash box tubes is quite demanding and according to the crushing mode of the tube, simulations may not correspond to the results that are obtained experimentally. There are not so many studies in the literature that involves the effect of the debris generated in crushing while simulating the axial crush. Also, effects of using a different core material in foam-filled tubes is not a subject that is investigated in detail. Modelling foam-filled composite structures is also a subject that must be worked on.

In this thesis study, it is intended to examine axial crushing behaviour of sole composite and foam filled composite crash boxes both experimentally and numerically. Since the most dangerous crashing event is the frontal accident, the axial crushing of components is the main subject. For numerical analysis ABAQUS/Explicit software was used.

To model composite structures material model the built in ABQ_PLY_FABRIC VUMAT code was used to define intra-laminar damage and cohesive zone model was used to define inter-laminar damage. For the foams used as core material in foam filled structure, built-in *CRUSHABLE FOAM material model was used.

Trigger mechanisms are also important for the crush characteristics of composite structures. Axial crush of composite structures can be manipulated by bevel, saw teeth or tulip type triggers on the structure or using crush caps and plugs. Design of the crush plugs have significant influence of structure crush characteristics and stability. The crush characteristics of composite tubular structures by using inwards and outwards crushing crush caps were examined both numerically and experimentally.

Three different circular crash box tubes with the diameters of Ø30, Ø40 and Ø50mm were examined in this study. Effect of the foam-filled composites is examined both experimentally and numerically with a high density PU foam filled Ø50mm diameter specimen. Apart from the high density PU foam, syntactic foams made of epoxy resin and hollow glass microballoons and syntactic foam filled tubes were examined experimentally.

Experimental crushing tests on tubular specimens in this study were carried out as quasi-static tests. Quasi-static tests are preferred rather than dynamic tests because crushing rate dependency is not effective on crushing characteristics of the composite materials as it is in metals. Farley [43] examined the effects of the crushing rate in the range of 0.01 m/s to 12 m/s. It is observed that crushing mode doesn’t differ dependent to the crushing rate. Generally there is a slight difference in energy absorption dependent on the ply orientation of the composite. Jackson et al. [44] also published a study where a semi-circular composite structure quasi-static and dynamic crushing behavior are investigated. Crushing modes remains the same in quasi-static and dynamic crushing and there is an acceptable difference in the load displacement curves.

To prevent misunderstandings, difference between crash and crush is also must be noted. Crash is the collision incident of vehicles where crush is the incident of a component subjected to progressive compression caused from collision and be damaged. Crash structures are generally subjected to crushing, so they can be called as crushing structures as well.

In the upcoming sections, first manufacturing of composites tubes and test methods are discussed in experimental work section. Then, theoretical information about numerical intra-laminar and inter-laminar damage models of composites used in the study and detailed information about construction of numerical modelling of crash box components are summarized. Next, the results will be presented in detail with a discussion on their implications, finally future work and possible improvements are discussed.

2. EXPERIMENTAL STUDY

In this section, experimental part of the study is explained. Quasi-static compression test method was used for testing the crush specimens. Main goal of the experimental work is to observe crushing characteristics and obtain load displacement curves of sole CFRP tubes, PU foam filled CFRP tubes and syntactic foam filled CFRP tubes. Manufacturing of the crash tube specimens and quasi-static compression test procedure are discussed in detail.

2.1. Manufacturing of Specimens

CFRP tubes of crush specimens were manufactured from KordSA KOM10T HSCF 3KD PL200 prepregs which consists of plain weave fabric woven from 200K high strength carbon fiber tows and epoxy matrix. Roll wrap method was used to manufacture circular tube specimens. Three sets of specimens with different diameters of Ø30mm, Ø40mm and Ø50mm were manufactured with roll wrapping method by first wrapping the prepreg to a mandrel firmly, then wrapping with shrink tape and then curing in an oven. During rolling, exerting a compressive force to compact plies is important. Mandrels used in roll wrapping must have a high thermal expansion coefficient so that after prepregs cured, they can be separated from the mandrel easily. Aluminum is the common material used for mandrel in roll wrapping. A schematic illustration of roll wrapping carbon prepregs to aluminum mandrel is given in Figure 2.1 [45].

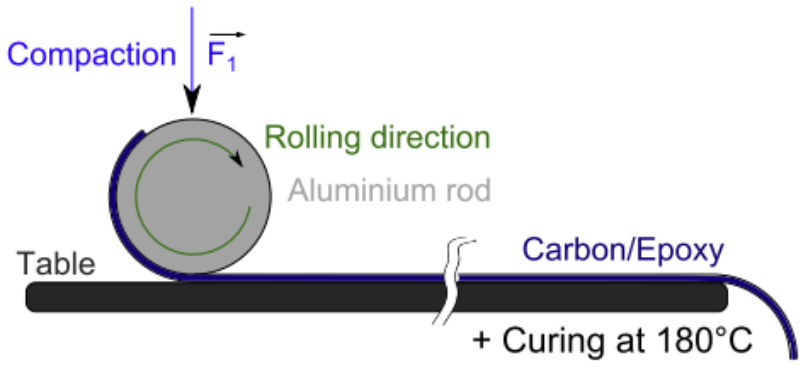

Figure 2.1. Roll wrapping carbon tubes [45].

Aluminum mandrels were also used in this study to manufacture composite tubes. Mandrels surfaces were machined to prevent any defects on tubes and remove possible obstacles while separating the cured tubes. Release agent was applied to surface of the mandrel before roll wrapping to eliminate difficulties during separating cured tubes.

CFRP tubes used in this study have six plies. Long prepreg fabrics were wrapped for six turns on the aluminum mandrels. After the prepregs were wrapped to the mandrel, heat shrink tape was applied to the surface of the carbon fiber prepreg to constrict and squeeze the wrapped structure when heated. Compressive forces generated by heat shrink tape consolidates the plies of material in curing process. Shrink tape can be used as an alternative method to vacuum bagging or autoclaving composite parts, and it can also be used together with these methods [46]. Heat shrink tapes are able to withstand high temperatures up to 165 °C. Manufactured roll wrapped tubes with heat shrink tape applied is shown in Figure 2.2.

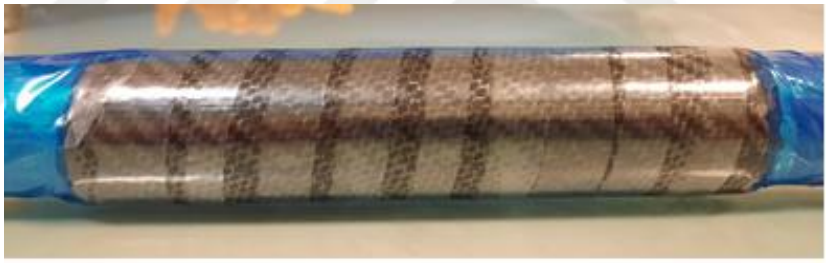

Figure 2.2. Roll wrapped CFRP tube with heat shrink tape applied.

The resin system of the prepreg used to manufacture crush tubes is named as OM10. According to recommended curing cycle by manufacturer, CFRP tubes were cured at 130 °C for 100±5 minutes. Recommended curing cycle involves manufacturing parts by using autoclave. Thus, it involves guidance about applying pressure. In this study, composite tubes were manufactured in a vacuum oven. Heat shrink tapes put adequate pressure to consolidate plies when heated. Also manufacturing decent circular tubes is quite harder in autoclave because of the pressure levels in autoclave may easily forms wrinkles in tubes which affects their crush characteristics. Recommended curing cycle by manufacturer for the used KordSA KOM10T HSCF 3KD PL200 plain weave woven fabric prepreg is given in Figure 2.3 [47].

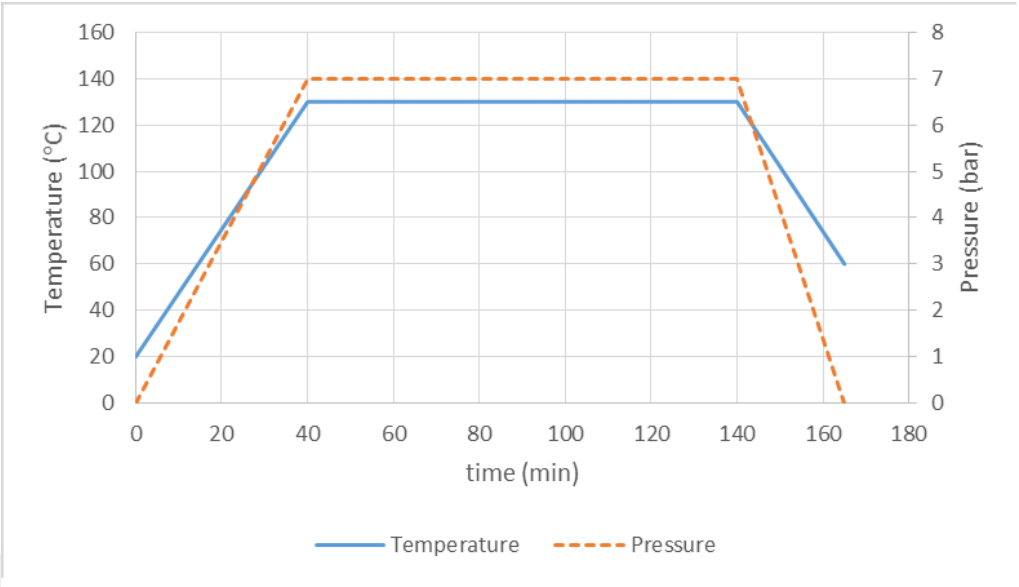

Figure 2.3. Recommended curing cycle for KordSA KOM10T HSCF 3KD PL200 plain weave woven fabric prepreg [47].

CFRP tubes were manufactured with a length close to 200 mm in first place. After curing is complete, heat shrink tape was removed and tubes were separated from mandrels. Then tube specimens were cut to smaller specimens with the length of 40 mm. In the last step of the manufacturing sole tubes, specimens chamfered in a lathe to form bevel trigger mechanism. Manufactured sole tube specimens are illustrated in Figure 2.4.

Figure 2.4. Manufactured tube specimens; Ø50 mm, Ø40 mm, Ø30 mm from left to right.

Crushing behavior of foam filled tubes were examined by using two different foam core materials, which are Polyurethane foam (PU) and HGMS/epoxy resin syntactic foam. Polyurethane foam used in this study has a density of 0.158 g/cm³. Syntactic foam used in this study is a composite material itself which is made of KP25 hollow glass microspheres and epoxy resin hardener mix. Polyurethane filled specimens were manufactured by cutting polyurethane in desired cylinder shape and then stuffing the foam to the manufactured sole tube. Syntactic foams were prepared by using epoxy resin, MGS LR285 epoxy resin mixed with MGS LH287-5 hardener and KP25 hollow glass microspheres (HGMS). The epoxy resin MGS LR285 and hardener MGS LH287-5 are manufactured by HEXION. Density of the neat resin-hardener mix after cure is around 1.20 g/cm³, modulus of elasticity is around 3 GPa and compressive strength is around 130 MPa [48]. Mechanical properties enhances as reinforced with HGMS particles. KP25 HGMS particles manufactured by Zhengzhou Hollowlite Materials company is used as reinforce particles. Bulk density of HGMS is 0.15 g/cm³ and particle size is around 96 μm [49]. During preparation, ingredient materials mixed with the ratio of 64.3% epoxy resin, 25.7% hardener and 10% HGMS by weight. To be more specific, for 100 g epoxy resin, 40 g hardener and 15.4 g HGMS is used to produce syntactic foam. Ingredients were mixed and stirred for 3 hours then mixture was poured into composite tubes and waited to cure. Curing process time is 24 hours at 23 °C [48]. Polyurethane filled specimen and syntactic foam filled specimen are shown in Figure 2.5.

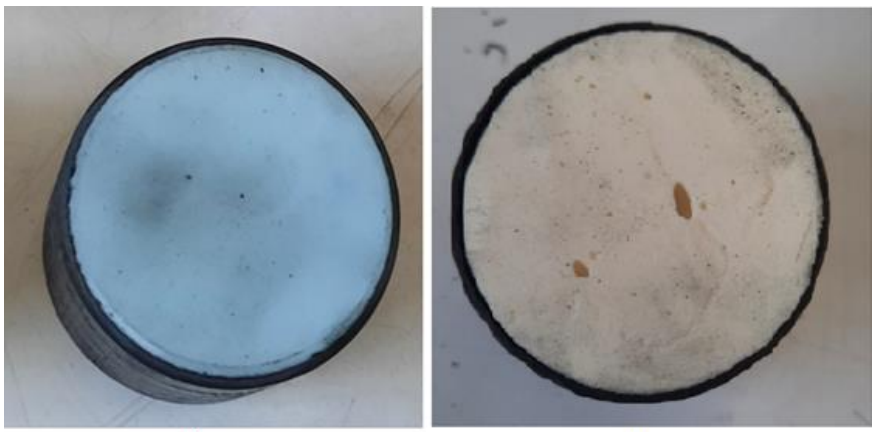

Figure 2.5. Foam filled specimens; a) HGMS/epoxy syntactic foam filled, b) PU foam filled.

2.2. Crush Plugs Used in Testing

Crushing behaviors of sole tubes crushed with external crush plugs were also examined in this study. Inwards-crushing crush plug and outwards-folding crush plugs were used to examine behavior of crushing response to external triggering. Both type of crush plugs were designed for three different diameters. Designed crush plugs restrict the movement of the crushed tube fronds in one direction and guides tube wall to fracture in a controlled way. Crushing zone radius was set as 2 mm in the designed crush plugs. Crush plugs used in the study are shown in Figure 2.6.

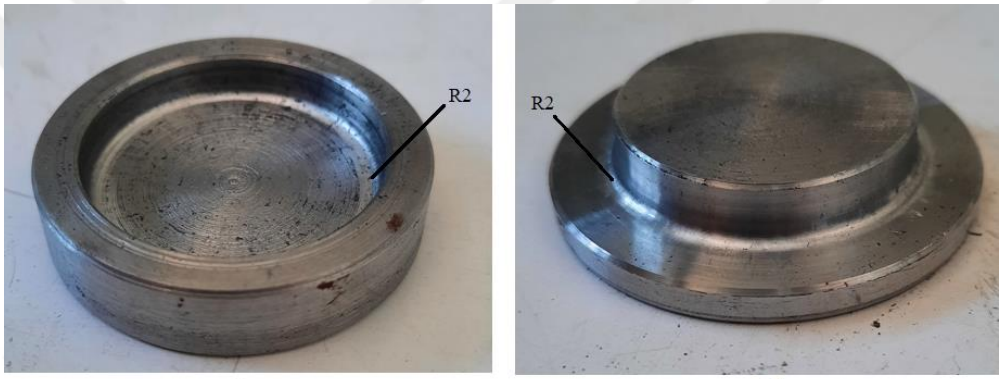

Figure 2.6. Crush plugs for Ø30mm tubes crushing, a) Inwards-crushing b) Outwards-crushing.

2.3. Testing Process

Quasi-static experimental tests were performed by using Zwick Roell Z/100 Universal Testing Machine. No test fixtures or supports were used because all specimens are self-supporting. Specimens were placed on bottom rig with flat end of the tubes faces the plate and triggered end facing up. Test setup for quasi-static tests are shown in Figure 2.7.

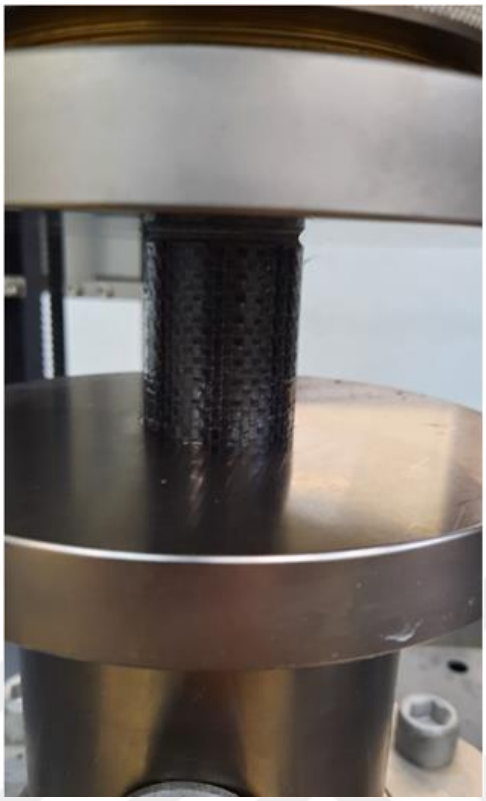

Figure 2.7. Test setup for quasi-static crushing.

Three different diameter tubes and foam filled tubes were tested by crushing between flat plates of bottom and top rigs. Crush plugs are only used in three different diameter sole tubes. They were tested after crush plugs positioned to the top end of the tube. Upper rigs crushing speed was set to 2 mm/min and crushing displacement was set to 20 mm during quasi-static tests.

3. NUMERICAL STUDY

In the numerical part of the study, experimental quasi-static compression tests were simulated on ABAQUS/Explicit finite element software. First step of the numerical study is modelling material properties of composite tubes, polyurethane foams. Built-in ABQ_PLY_FABRIC material model is used to define intra-laminar failure of composite tubes and Cohesive Surface Model is used to define inter-laminar (delamination) failure. Polyurethane foams were modelled by *CRUSHABLE FOAM material model of ABAQUS.

After material models defined in ABAQUS, tube specimen models were created with stacked shell method. Modelled specimens crushed between two rigid plates representing the rigs of universal test machine and crush plugs. In this section, material damage models for composites are discussed first, then construction of the models used to simulate axial crushing are introduced.

3.1. Intra-laminar Damage Modelling with ABQ_PLY_FABRIC VUMAT

ABQ_PLY_FABRIC VUMAT is a built-in VUMAT user subroutine material model for fabric reinforced composite damage in ABAQUS. This VUMAT subroutine can be accessed by creating a material property with a material name typed that begins with ABQ_PLY_FABRIC string in property module of ABAQUS, e.g. ABQ_PLY_FABRIC_1 [51].

ABQ_PLY_FABRIC material model is based on continuum damage mechanics. Model is supported for plane-stress elements which includes shell elements (S4R, S3R), continuum shell elements (SC6R, SC8R), plane stress elements (CPS) and membrane elements (M3D). Fabric-reinforced ply is modeled as a homogeneous orthotropic elastic material that exhibits linear elastic behavior up to the failure point in longitudinal and transverse fiber directions. Shear response is dominated by the non-linear plastic behavior of matrix [17, 50].

Constitutive equations of the model are created in a local Cartesian coordinate system which its base vectors are aligned with fiber directions. Schematic of a plain weave fabric on a local coordinate system has shown in Figure 3.1.

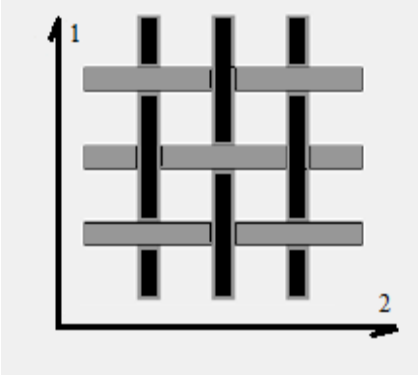

Figure 3.1. Schematic of a plain weave fabric composite on a local coordinate system.

3.1.1 Elastic Stress-Strain Relations

Orthotropic damaged elasticity is used to model elastic stress-strain relations in material model. Elastic stress-strain relations are based on a local coordinate system as it is shown in Figure 3.1, can be defined as

$$\begin{pmatrix} \varepsilon_{11} \\ \varepsilon_{22} \\ \varepsilon_{12}^{el} \end{pmatrix} = \begin{pmatrix} \frac{1}{(1-d_1)E_1} & \frac{-v_{12}}{E_1} & 0 \\ \frac{-v_{21}}{E_2} & \frac{1}{(1-d_2)E_2} & 0 \\ 0 & 0 & \frac{1}{(1-d_{12})2G_{12}} \end{pmatrix} \begin{pmatrix} \sigma_{11} \\ \sigma_{22} \\ \sigma_{12} \end{pmatrix}, \tag{3.1}$$

where variables d_1 and d_2 indicates the damage variables related to fiber fracture along 1 and 2 local directions. Variable d_{12} is the damage variable related to matrix micro-cracking due to shear deformation. Damage variables can defined as

$$d_1 = d_{1+}\frac{\langle\sigma_{11}\rangle}{|\sigma_{11}|} + d_{1-}\frac{\langle-\sigma_{11}\rangle}{|\sigma_{11}|};\ d_2 = d_{2+}\frac{\langle\sigma_{22}\rangle}{|\sigma_{22}|} + d_{2-}\frac{\langle-\sigma_{22}\rangle}{|\sigma_{22}|}, \tag{3.2}$$

where angle brackets, "⟨ ⟩", signifies Macaulay operator. So, if the stress value in angle brackets is below zero then the result of the Macaulay operator function will be zero. Thus, the corresponding damage variable to the state of stress activated.

3.1.2 Fiber Response

Response of the material along fiber directions is defined with damaged elasticity. Fiber damage variables are assumed to be a function of corresponding effective stress in the model. Relation between effective stresses and damage variables are formulated as

$$\tilde{\sigma}_{1+} = \frac{\langle \sigma_{11} \rangle}{(1-d_{1+})}, \tilde{\sigma}_{1-} = \frac{\langle -\sigma_{11} \rangle}{(1-d_{1-})}, \tilde{\sigma}_{2+} = \frac{\langle \sigma_{22} \rangle}{(1-d_{2+})}, \tilde{\sigma}_{2-} = \frac{\langle -\sigma_{22} \rangle}{(1-d_{2-})}. \quad (3.3)$$

To simplify the notation, subscript "α" is used in equations to describe the corresponding stress. Subscript "α" get the values of "$1(+,-),\ 2(+,-)$", in equations where "1" and "2" indicates fiber direction, "$+$" and "$-$" indicates tension and compression respectively.

To be able to model failure in fiber directions, damage initiation and damage evolution mechanisms must be defined in the material model. Damage initiation is the start point where failure criteria is met and damage is started. Damage initiation criterion in fiber directions can be defined as

$$\phi_\alpha = \frac{\tilde{\sigma}_\alpha}{X_\alpha}; (\alpha = 1+, 1-, 2+, 2-), \quad (3.4)$$

where function noted as ϕ_α is used as a criterion for compressive and tensile fiber failure in both fiber directions. X_α, notes the compressive and tensile strength along the local fiber directions for uniaxial loading.

Damage evolution that takes place after damage initiation defined in the material model by the damage evolution law given as

$$d_\alpha = 1 - \frac{1}{r_\alpha} \exp\left[-\frac{2 g_0^\alpha L_c}{G_f^\alpha - g_0^\alpha L_c} (r_\alpha - 1) \right];\ (\alpha = 1+, 1-, 2+, 2-), \quad (3.5)$$

where L_c, represent the characteristic length of the element, G_f^α, denotes the fracture energy per unit area of composite material under uniaxial tensile or compressive loading along fiber directions, g_0^α, is the elastic energy per unit volume under uniaxial tensile or compressive loading along fiber directions at damage initiation and r_α, denotes the damage threshold for fiber damage.

Damage variable evolutions are functions of damage thresholds and fracture energy per unit area. Damage thresholds, r_α, are non-decreasing quantities that reflect the historical damage of the material. Damage variable is directly related to damage threshold and as it increases the damage increases. Damage thresholds are set to the value of 1 until the damage initiation. Once damage initiation is reached, the damage threshold will be equal to maximum value of the failure criteria function that exceeds the value of 1 as it is stated as [39, 50]

$$r_\alpha = \max(1, \phi_\alpha). \tag{3.6}$$

Fracture energy per unit area can be described as the required energy to cause complete fracture separation from the initial point of loading. Elastic energy density at the point of damage initiation can be defined as

$$g_0^\alpha = \frac{X_\alpha^2}{2E_\alpha}. \tag{3.7}$$

Characteristic length of the element in FE mesh is very important to predict the energy dissipation correctly. In a material subjected to uniaxial loading in a fiber direction the dissipated energy per unit area will be equal to fracture energy per unit area in the end of the fracture.

Since elastic energy density will only include the energy values in elastic region, the fracture energy per unit area must be higher than the elastic energy per unit area. This fact provides the maximum value of L_c as it is expressed as

$$G_f^\alpha - g_0^\alpha L_c > 0 \Leftrightarrow L_c < L_{max} = \frac{G_f^\alpha}{g_0^\alpha}. \tag{3.8}$$

If characteristic length L_c is greater in the generated mesh, then analysis will over-predict the value of energy dissipation in crushing.

3.1.3 Shear Response

Experimental studies that examined woven composites subjected to in-plane shear loading has shown that, unlike fibers, shear response is dominated by non-linear plastic behavior. This plastic behavior caused by matrix microcracking during shear loading. The elastic shear stress-strain equations can be rewritten as

$$\tilde{\sigma}_{12} = \frac{\sigma_{12}}{1 - d_{12}} = 2G_{12}\varepsilon_{12}^{el} = 2G_{12}\left(\varepsilon_{12} - \varepsilon_{12}^{pl}\right), \tag{3.9}$$

yield function defined in material model is given as

$$F = |\tilde{\sigma}_{12}| - \tilde{\sigma}_0(\varepsilon^{pl}) \leq 0, \tag{3.10}$$

hardening law is defined as it is given as

$$\tilde{\sigma}_0(\varepsilon^{pl}) = \tilde{\sigma}_{y0} + C(\varepsilon^{pl})^p, \tag{3.11}$$

where $\tilde{\sigma}_{y0}$, denotes the initial effective shear yield stress, C and p are the constants of the hardening equation. ε^{pl}, is the equivalent plastic strain. After yield point is reached, effective stress values increases as strain rate increases to the damage initiation point. Shear damage initiation criterion of the matrix is given as

$$\phi_{12} = \left|\frac{\tilde{\sigma}_{12}}{S}\right|, \tag{3.12}$$

where, S is the in-plane shear strength. As it was in the fiber response, damage evolution is directly related to shear damage threshold. Damage threshold for shear loading is formulated as

$$r_{12} = \max(1, \phi_{12})\,. \tag{3.13}$$

Shear damage variable evolution is assumed that it is equal to the logarithm of the damage threshold and it increases with it until the maximum value of the damage variable, which is equal to 1, is reached. Shear damage variable evolution is mathematically defined as

$$d_{12} = \min(\alpha_{12}\ln(r_{12})\,, d_{12}^{max})\,, \alpha_{12} > 0, d_{12}^{max} \leq 1, \tag{3.14}$$

where α_{12}, denotes the shear damage variable coefficient, which is a material property that can be determined experimentally. To be able to express the behavior difference between loading in fiber directions and in-plane shear direction, stress strain curve of a CFRP material that is subjected to tensile tests and shear tests is given in Figure 3.2 [39].

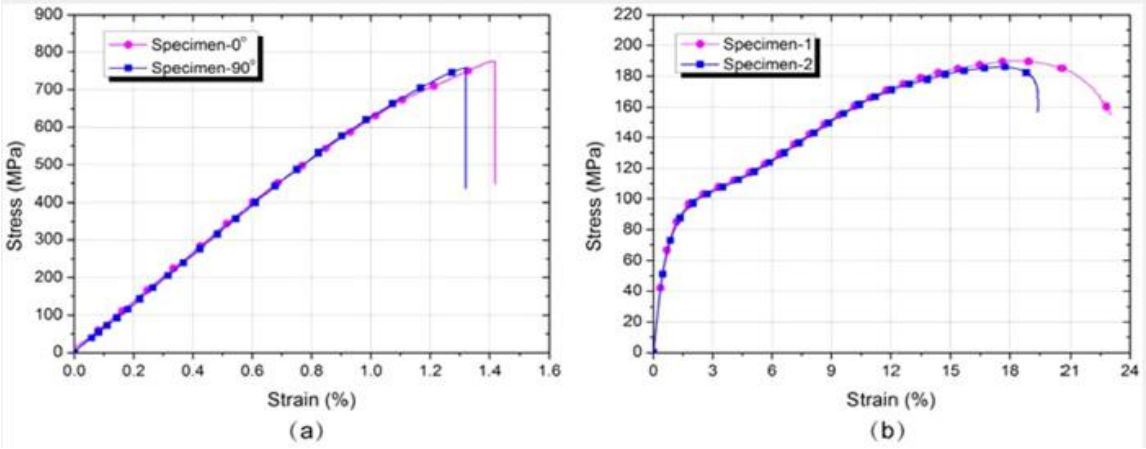

Figure 3.2. Typical stress-strain curves of a CFRP material that subjected to loading; a) Tensile loading, b) Shear loading [39].

As it is observed in the Figure 3.2., elastic behavior followed by damage initiation and damage evolution in fiber direction loading. However, stress strain behavior is dominated by plastic behavior of shear loading.

3.1.4 Setting the User Interface and Element Deletion

In this section, the element deletion methods and defining the user interface in ABAQUS software will be discussed. Damage variables in corresponding loading evolves to a value of failure that set in material module of ABAQUS as the material is subjected to loading. Once the damage variable reach the maximum specified value the element will be deleted. ABQ_PLY_FABRIC VUMAT has two options to define the deletion of elements [50]:

1) In first option, the element is deleted when any damage variable in fiber directions reaches to specified damage value, $d_{1+/-} = d_{max}$ or $d_{2+/-} = d_{max}$, or the plastic strain caused by shear loading reaches to a specified value, $\varepsilon^{pl} = \varepsilon^{pl}_{max}$.

2) In second option, the element is deleted when damage variables in both fiber directions reaches to specified damage value, $d_{1+/-} = d_{2+/-} = d_{max}$, or the plastic strain caused by shear loading reaches to a specified value, $\varepsilon^{pl} = \varepsilon^{pl}_{max}$.

One of these two options can be chosen and activated by setting value of element deletion flag, 1DelFlag, as 1 or 2 respectively. These two options can also be combined with a deformation based element deletion method. Deformation based element method can be defined with a criterion that sets the principal logarithmic strains can sustain before its deleted, $\tilde{\varepsilon}_{max} > 0, \tilde{\varepsilon}_{min} < 0, \tilde{\varepsilon}_{max} > \tilde{\varepsilon} > \tilde{\varepsilon}_{min}$.

It is stated before, that to use ABQ_PLY_FABRIC material model, the user material name defined in property module in ABAQUS must start with string of "ABQ_PLY_FABRIC". The number of solution dependent variables (*DEPVAR) is 16 and "DELETE" parameter is set to 16 in property module. Brief summary of the VUMAT in keyword interface is given in Figure 3.3 [50].

```
*MATERIAL, NAME= ABQ_PLY_FABRIC
*DENSITY
 ρ
*USER MATERIAL, CONSTANTS=40
** Line 1:
 E1+ , E2+ , ν12+ , G12 , E1- , E2- , ν12-
** Line 2:
 X1+ , X1- , X2+ , X2- , S
** Line 3:
 G_f^1+ , G_f^1- , G_f^2+ , G_f^2- , α12 , d12^max
** Line 4:
 σ̄y0 , C , p
** Line 5:
 lDelFlag, dmax , ε̄^pl max , ε̂max , ε̂min
*DEPVAR, DELETE=16
 16
```

Figure 3.3. User material constants and property modelling prescription of material model [50].

VUMAT consists 40 constant rows to be defined in the user material module. The number of significant variables to define user material is 26. So, some of the constant rows are not used and must be typed 0 to the relevant constant row in the user material module. E.g. to define the first line of the constants the first 7 row in the user interface module, the elastic properties must be typed in the order given in Figure 3.3.

The 8th row must be typed 0 because it is not used. To define the second line the first 5 properties must be set then the last 3 rows must be typed 0 because they are not used as well. Line 5 is about the controls of the material point failure. Running VUMAT is possible without using the three strain criterions involves shear plasticity.

To be able to see the results of intra-laminar behavior of material after the simulation the solution dependent output variables (SDV) must be selected from "Field Output Request" module. Output variables that have special meaning for intra-laminar behavior of fabric-reinforced composites is given in Table 3.1.

Table 3.1. Output variables of Intra-laminar behavior.

Output Variable	Symbol	Description
SDV1	d_{1+}	Tensile damage along fiber direction 1
SDV2	d_{1-}	Compressive damage along fiber direction 1
SDV3	d_{2+}	Tensile damage along fiber direction 2
SDV4	d_{2-}	Compressive damage along fiber direction 2
SDV5	d_{12}	Shear damage
SDV6	r_{1+}	Tensile damage threshold along fiber direction 1
SDV7	r_{1-}	Compressive damage threshold along fiber direction 1
SDV8	r_{2+}	Tensile damage threshold along fiber direction 2
SDV9	r_{2-}	Compressive damage threshold along fiber direction 2
SDV10	r_{12}	Shear damage threshold
SDV11	$\tilde{\varepsilon}^{pl}$	Equivalent plastic strain
SDV12	ε_{11}^{el}	Elastic strain component 11
SDV13	ε_{22}^{el}	Elastic strain component 22
SDV14		Not used
SDV15	ε_{12}^{el}	Elastic strain component 12
SDV16	MpStatus	Material point status;1 if active, 0 if failed

3.2. Inter-laminar Failure Modelling with Cohesive Surface Method

Inter-laminar damage, in other words delamination, is one of the predominant failure modes in crushing of the laminated woven carbon fiber-reinforced composites. It is the separation of lamina layers that forms the laminate. Delamination failure can be modelled easily by generating cohesive connections between plies. By generating cohesive contacts, the damage initiation and damage evolution of delamination behavior can be simulated. Generating cohesive contacts between surfaces of plies is called cohesive surface method or cohesive contact method. Using cohesive contacts is simpler than using cohesive elements.

Cohesive contacts generated between plies are based on traction-separation law. Traction-separation law defined in contact constitutive equation account for the relationship between traction vectors and separation vectors acts in cohesive interfaces. Inter-laminar behavior is considered as linear elastic behavior before the initiation of delamination occurred. After the initiation of damage, it is generally assumed that cohesive contact exhibit linear softening to the fail separation. Typical traction separation response curve for shear loading is illustrated in Figure 3.4 [17].

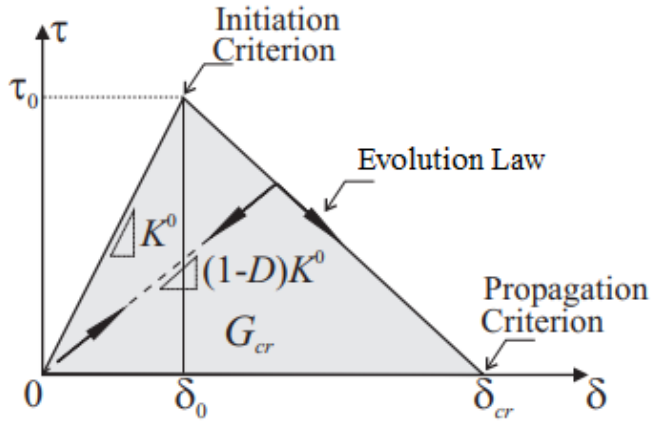

Figure 3.4. Typical traction separation response in shear loading [51].

In Figure 3.4, K^0, denotes for the stiffness of cohesive contact in shear loading, S_0, refers to the strength of contact in shear loading, G_{cr}, refers to the fracture energy in normal shear (Mode I,II delamination), δ_0 and δ_{cr} refers to the damage initiation separation and complete fail separation respectively and D refers to the damage variable.

There are three possible crack growth mode in delamination failure these are delamination in normal direction (mode I, opening), delamination in first shear direction (mode II, sliding) and delamination in second shear direction (mode III, scissoring). Delamination modes is illustrated in Figure 3.5 [51].

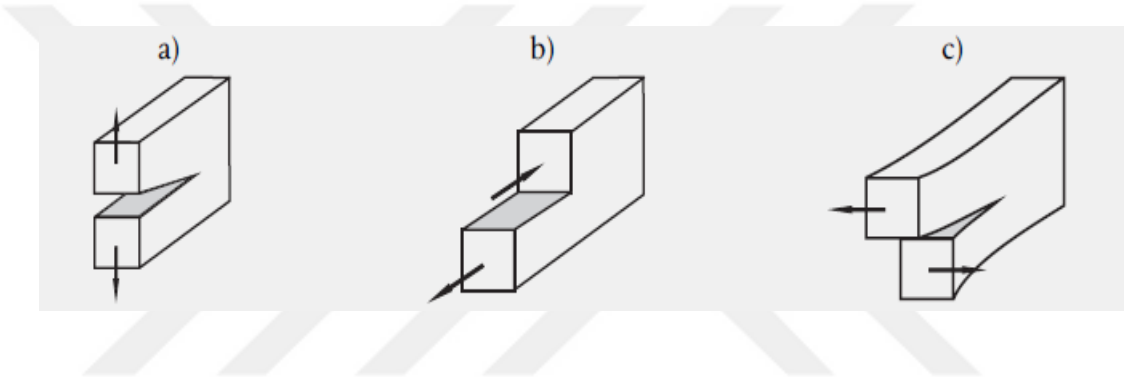

Figure 3.5. Delamination modes, a) mode I b) mode II c) mode III [51].

Cohesive traction-separation behavior exhibit uncoupled behavior in delamination, which means any loading in a direction does not cause any other cohesive forces in other directions, e.g. normal separation does not cause a cohesive force in shear direction. Elastic behavior of cohesive contacts is given as [17, 39]

$$\boldsymbol{t} = \begin{Bmatrix} t_n \\ t_s \\ t_t \end{Bmatrix} = \begin{bmatrix} K_n & 0 & 0 \\ 0 & K_s & 0 \\ 0 & 0 & K_t \end{bmatrix} \begin{Bmatrix} \delta_n \\ \delta_s \\ \delta_t \end{Bmatrix} = \boldsymbol{K}\delta, \tag{3.15}$$

where $\boldsymbol{t}$, denotes the traction stress vector and δ, denotes the contact separation. Subscripts *n*, *s* and *t* refers to the normal, first shear and second shear directions in this order. $\boldsymbol{K}$, refers to the stiffness matrix of cohesive interaction. Typical traction separation behavior involves the traction stresses and contact separation, however constitutive equations of traction separation behavior can be interpreted differently in some studies according to the method of using cohesive elements or cohesive surfaces to model delamination. Separation, in cohesive elements can be defined with nominal strain of the cohesive elements. In cohesive surface method separation defined with contact separation between plies surfaces.

Main purpose of the cohesive surface modelling is to simulate delamination fractures. Fictional cohesive contribution to the elastic strain of the laminate must be small for simulating delamination accurately. So, the cohesive contact stiffness in loading directions must have very high values. Extremely high values of stiffness also may cause numerical problems in simulation. Camanho et al. [52], suggested using a value of $10^6\ N/mm^3$ for cohesive stiffness and Turon et al., suggested a method for selecting cohesive stiffness values by deriving equilibrium conditions on delamination [53].

From the equilibrium condition, relationship between lamina through-the-thickness stiffness and cohesive contact stiffness can be formulated as

$$\sigma = E_3\varepsilon = K\delta, \tag{3.16}$$

where σ is the normal traction stress, E_3 is the lamina through-the-thickness stiffness, ε is the lamina transverse strain, K is the cohesive stiffness and δ is the cohesive contact separation. Effective strain of the composite laminate is formulated as [53]:

$$\varepsilon_{eff} = \varepsilon + \frac{\delta}{\mathrm{t}}, \tag{3.17}$$

where, t denotes the lamina thickness and δ denotes cohesive surface separation. Elastic deformation behavior of the laminate in cohesive surface method is illustrated in schematic at Figure 3.6 [53].

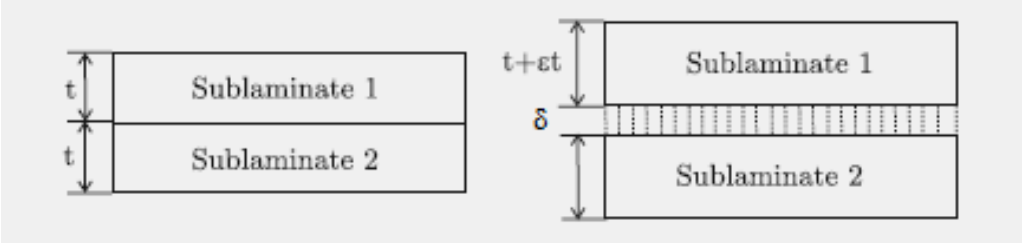

Figure 3.6. Elastic deformation behavior of the laminate in cohesive surface method [53].

Elastic deformation behavior defined in the cohesive surface method considers the separation between two cohesive zones as an elastic deformation until the point of damage initiation. Appointing a high value of K cohesive stiffness restricts high values of δ separation and providing this model to be accurate.

Using equilibrium conditions effective Young modulus can be derived as [53]

$$\sigma = E_3\varepsilon = K\delta = E_{eff}\varepsilon_{eff}, \tag{3.18}$$

$$E_{eff} = \frac{E_3\varepsilon}{\varepsilon_{eff}} = E_3\left(\frac{\varepsilon}{\varepsilon + \frac{\delta}{\mathrm{t}}}\right) = E_3\left(\frac{1}{1 + \frac{E_3}{\mathrm{Kt}}}\right). \tag{3.19}$$

To prevent the effect of cohesive contacts on the compliance of the laminate, Effective young modulus must be close to lamina through-the-thickness stiffness. So, as it can be understood from (3.19), cohesive surface between plies doesn't affect the compliance of the composite laminate if $E_3 \ll Kt$. Thus a relation between lamina stiffness and cohesive stiffness can be derived as [53]

$$K = \frac{mE_3}{\mathrm{t}}, m \gg 1. \tag{3.20}$$

Turon et al., suggested that m value can be taken as 50 [53]. In their study, cohesive interface stiffness of carbon fiber epoxy composite laminates that has thickness between 0.125 and 5mm is calculated as in the range of 10^5 and $5x10^6\ N/mm^3$. These results agree with the results of Camanho [52]. Cohesive stiffness values were chosen as $10^6\ N/mm^3$ in this study.

As the modelled cohesive surfaces completes the artificial elastic behavior with a suitable stiffness value, the separation and traction values gets to the damage initiation point. There are four possible criterion to model damage initiation in cohesive surface model. These are, maximum stress criterion, maximum separation criterion, quadratic stress criterion and quadratic separation criterion. In maximum stress and maximum separation criterion, damage is initiated when one of the traction or separation, according to used criterion, in different loading directions (normal, first shear, second shear) reaches to a critical value. In quadratic criterions, damage is initiated when sum of the squares of the failure criterions in three different loadings is equal to one. In many studies quadratic stress criterion used to model damage initiation and it is used in this study as well. Quadratic stress damage initiation criterion is given as

$$\left(\frac{\langle t_n \rangle}{t_n^{max}}\right)^2 + \left(\frac{t_s}{t_s^{max}}\right)^2 + \left(\frac{t_t}{t_t^{max}}\right)^2 = 1. \tag{3.21}$$

Once the quadratic stress damage initiation criterion is fulfilled, damage propagation of delamination takes place. Damage evolution law of the mixed behavior can be defined either separation based or energy based. Energy based damage evolution is widely used to model damage evolution and it can be defined by using a tabular form or one of two analytical forms. These two analytical criterions are Power Law criterion and Benzeggagh-Kane criterion. In this study, Benzeggagh-Kane Criterion was used. Benzeggagh-Kane damage evolution law is given as [17, 38]

$$G^c = G_n^c + (G_s^c - G_n^c)\left(\frac{(G_s, G_t)}{G_n + G_s + G_t}\right)^{\eta}, \tag{3.22}$$

where, G denotes the fracture energy, superscript c denotes critical fracture energy and η refers to the Benzeggagh-Kane cohesive property.

Quadratic stress damage initiation criterion and Benzeggagh-Kane energy based damage evolution criterion works efficiently to model mixed mode delamination behavior. To give a better understanding of mixed mode delamination response of cohesive surfaces a schematic representation of damage initiation and damage evolution of mixed mode delamination is illustrated in Figure 3.7 [54].

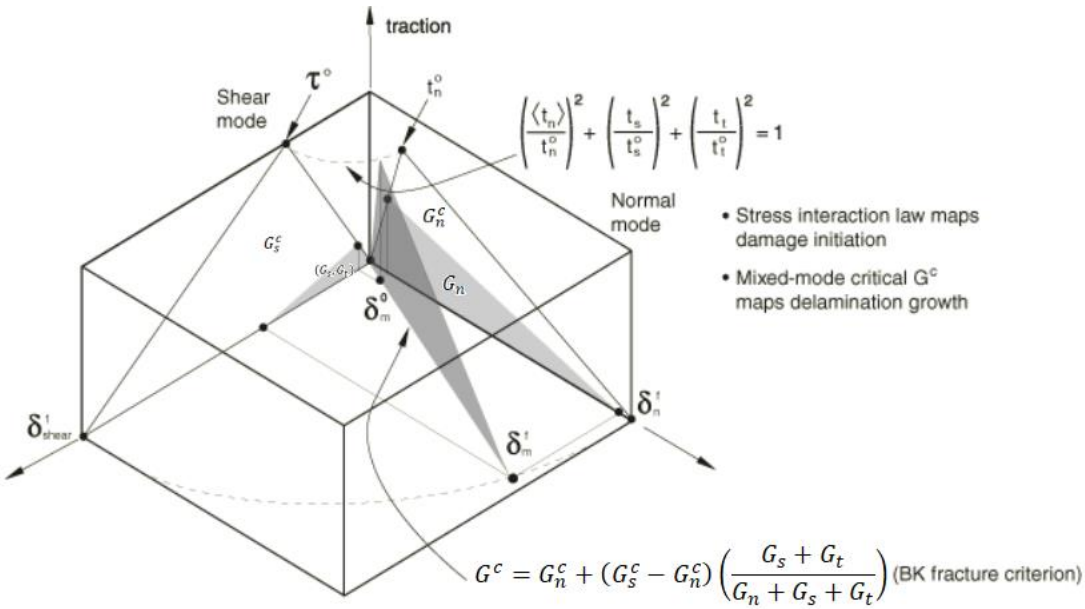

Figure 3.7. Mixed mode traction-separation response of cohesive surfaces [54].

Mixed mode traction-separation response chart in the Figure 3.7 is the developed type of the typical traction-separation curves for the three directions of normal traction direction, first shear direction, second shear direction. Shear traction-separation curve on Figure 3.7 refers to the resultant traction separation curve of the first shear direction curve and second shear direction curve. Shear traction-separation curves and normal traction separation curves resultant generates the mixed mode separation curve as in the formulas of quadratic stress damage initiation and Benzeggagh-Kane damage evolution.

3.3. Construction of the Axial Crush Simulation Model

Construction of the model starts with generating 3D models of specimens. Composite tubes of manufactured specimens consists 6 plies with 0.2 mm thickness and the tube length is 40 mm. To create 3D model of the composite tubes, one ply of elements was modelled in the “part” module first. Then this ply was meshed with explicit hex SC8R continuum shell elements with approximate element size of 1 mm by using “sweep” technique from “mesh controls” and a mesh part was created from meshed ply. After mesh part was created, the tube stacked shell geometry was generated by offsetting solid meshed layers from “edit mesh” module. Chamfer trigger was modelled by offsetting elements from the plies in longitudinal direction. After geometry of the tube modelled. Stack directions of the plies were orientated for mesh edit module as well. Thus the 3D model of the composite tubes were generated and meshing operation were completed for composite tubes. Sets were appointed to plies and their surfaces to define material properties easily. Generated stacked shell model of the tubes are shown in Figure 3.8.

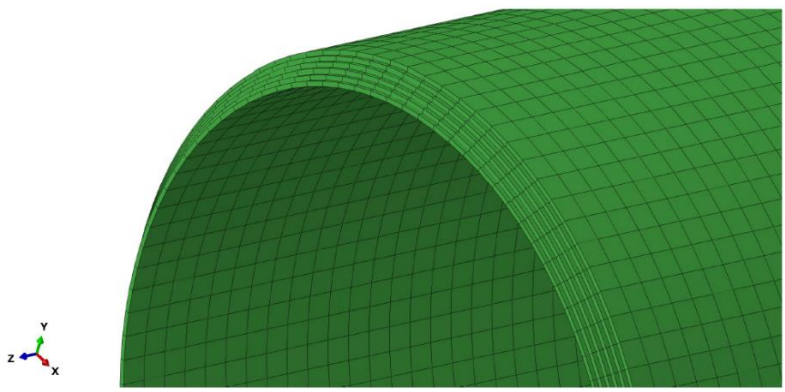

Figure 3.8. Generated stacked shell model of the composite tubes.

Rigs of the test machine and crush plugs were modelled by generating discrete rigid shell parts. Test rigs were modelled as rectangular rigid planes and crush plugs were modelled by revolution of their section. Quasi-static modelling was carried out by crushing the model of specimen between these rigid parts. Reference points were generated on center points of top and bottom rigid parts to define load and boundary conditions and creating load displacement curve of the simulation. Explicit quad R3D4 discrete rigid elements were used in meshing of the rigid plates. Mesh size of the rigid parts generated to model test rigs doesn't affect the crushing behavior so much. But radius portion of the crash plugs were meshed with approximate element size of 0.1 mm to create mesh with a smooth radius curve to model crushing behavior accurately. Virtual debris wedge was modelled as crush plugs modelled. Virtual debris wedge provides fronds to move both inwards and outwards directions and the resulting failure modes is more representative of the actual modes observed during experiments. Section of the tubes with modelled inwards-folding crush plug, outwards-folding crush plug, virtual debris wedge and flat plate are shown in Figure 3.9.

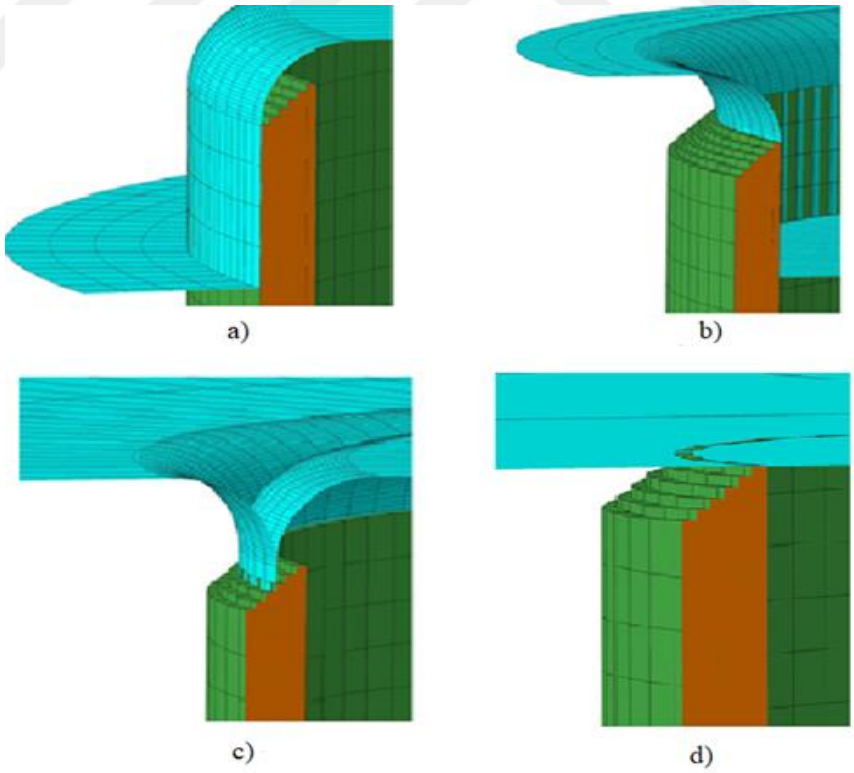

Figure 3.9. Assembly of the rigid parts and tubes model; a) Inwards folding crush plug model, b) Outwards folding crush plug model, c) Virtual debris crushing, d) Rigid flat plate crushing.

Next step is defining material properties. Intra-laminar material properties of composite tubes were defined using ABQ_PLY_FABRIC VUMAT and they were assigned to ply sets from "composite layup" module. Intra-laminar properties to model the composites numerically, are given in Table 3.2 [39].

Table 3.2. Intra-laminar material properties used to model composite structures [39].

Description	Variable	Value
Density $[g/cm^3]$	ρ	1.56
Young Modulus along fiber direction 1 $[GPa]$	E_1	65.1
Young Modulus along fiber direction 2 $[GPa]$	E_2	64.4
Shear Modulus $[GPa]$	G_{12}	4.5
Principal Poisson Ratio	v_{12}	0.037
Tensile Strength along fiber direction 1 $[MPa]$	X_{1+}	776
Compressive Strength along fiber direction 1 $[MPa]$	X_{1-}	704
Tensile Strength along fiber direction 2 $[MPa]$	X_{2+}	760
Compressive Strength along fiber direction 2 $[MPa]$	X_{2-}	698
Shear Stress at the initiation of shear damage $[MPa]$	S	95
Tensile fracture energy per unit area along fiber direction 1 $[kJ/m^2]$	G_f^{1+}	125
Compressive fracture energy per unit area along fiber direction 1 $[kJ/m^2]$	G_f^{1-}	250
Tensile fracture energy per unit area along fiber direction 2 $[kJ/m^2]$	G_f^{2+}	95
Compressive fracture energy per unit area along fiber direction 1 $[kJ/m^2]$	G_f^{2-}	245
Shear damage equation parameter	α_{12}	0.18
Max shear damage	d_{12}^{max}	0.99
Initial effective shear yield stress $[MPa]$	$\tilde{\sigma}_{y0}$	185
Hardening equation coefficient	C	1053
Hardening equation power term	p	0.41
Element deletion flag	1DelFlag	1
Max value of damage variable	d_{max}	0.99

Intra-laminar properties listed in the Table 3.2 have been adapted from the study of Zhou et al. [39]. In the study of Zhou et al., the composite tubes are manufactured from T300/epoxy plain weave woven fabric carbon fiber composite. Composite prepreg used in Zhou et al. study is very similar with the prepreg used in this study, which is manufactured by KordSA with a designation KOM10T HSCF 3KD PL200 and consists of plain weave T300 carbon fibers manufactured by TORAYCA with a TEX number of 3K. Resin system in both prepregs are epoxy resin and resin content is around 42%, and the thickness of the plies is around 0.22 mm in both prepregs. Due to the similarities between prepregs used in this study to prepregs used in Zhou et al.'s study, intra-laminar properties taken from Zhou et al.'s study.

Polyurethane foam was modelled with *CRUSHABLE FOAM model. Density of the foam was defined as 0.158 g/cm^3. Elastic modulus was defined as 49.4 MPa and elastic Poisson's ratio was defined as 0. Volumetric Hardening option was selected for *CRUSHABLE FOAM model. Compression yield stress ratio was appointed as 1 and hydrostatic yield stress ratio was appointed as 0.5 which are default values. Crushable foam hardening was defined by entering plastic region stress and strain values of the PU foam in the module. Stress and strain values are obtained from engineering stress strain curve of the crushing results of PU foam since Poisson's ratio is assumed as zero. Stress-strain curve of used PU foam is given in Figure 3.10.

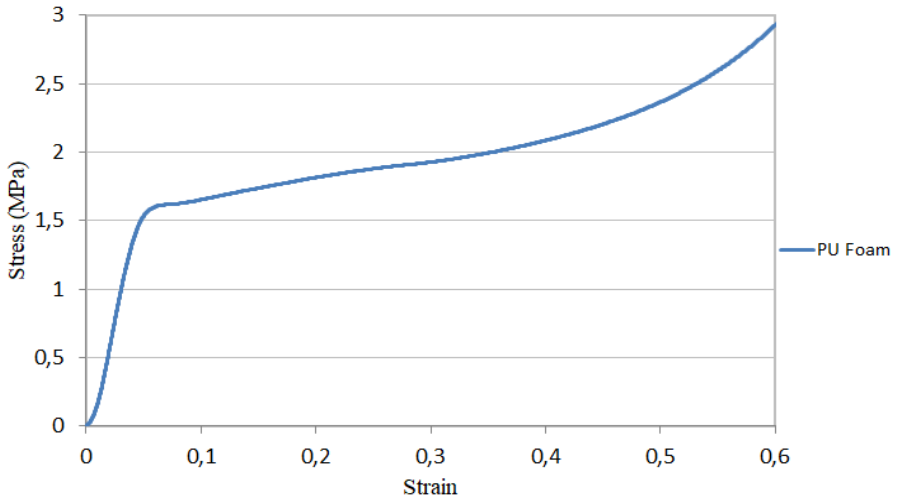

Figure 3.10. Stress-strain curve of the PU foam obtained experimentally and used in simulations.

After property values were defined, required parts to model testing of the specimen were brought together in the “assembly” module. Tube specimens were positioned between impactor and the lower plate as in the start of the experimental testing. An example of the assembly of testing specimen using outer-folding crush plug is shown in Figure 3.11.

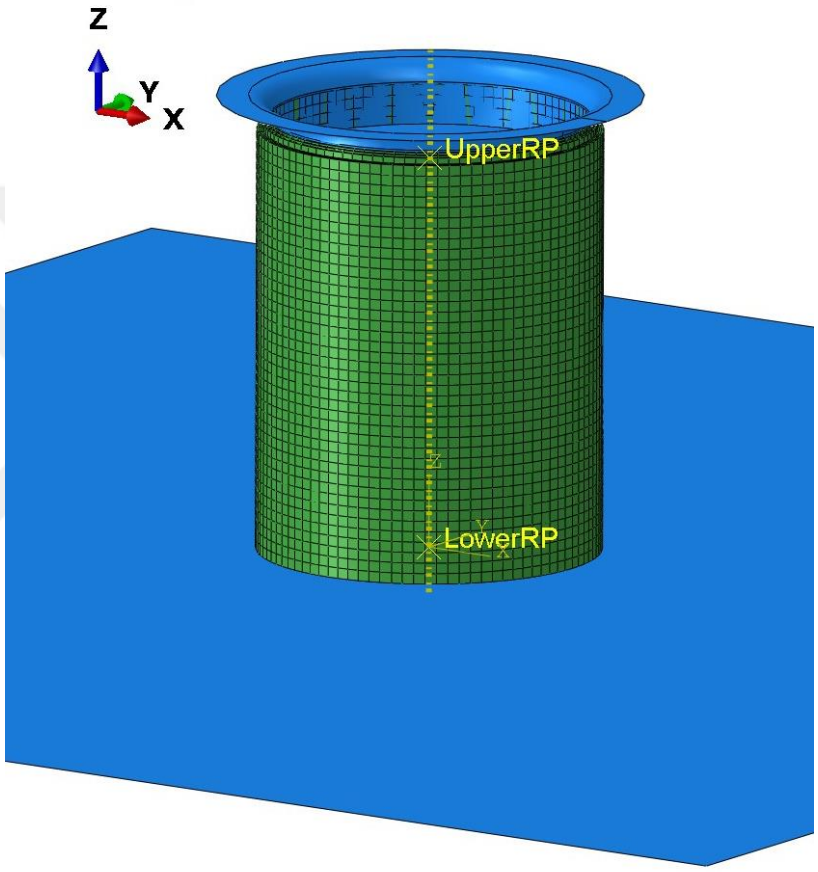

Figure 3.11. Test model generated in assembly module.

After creating assembly of the test parts, Dynamic/Explicit test procedure was created from “step” module. Quasi-static tests on ABAQUS can be performed either using implicit or explicit solver. However, explicit algorithm has some advantages over implicit algorithm in quasi-static axial crushing of composite tubes. Implicit solver uses iterations to ensure equilibrium of the internal forces at every time increment. On the other hand, explicit solver calculates the state of the next increment from the state of the previous increment. Explicit solver gives accurate results with suitable amount of increments [55].

In complex structures with a large number of degree of freedom, implicit algorithm will be more time consuming due to the high number of nonlinear equations that must be solved in each iteration. Contacts that exhibit nonlinear changes, such as cohesive surface contacts, can be solved more efficiently by using explicit solver as well [55].

Another point that must be enlightened is modelling of the axial quasi-static crushing using Dynamic/Explicit step. To model quasi-static tests specimens must be crushed with constant crushing speed. No effect of the accelerations or gravity is considered in the quasi-static crushing. Dynamic/Explicit step with constant test speed defined on the rigid impactors is suitable for modelling axial quasi-static crushing of specimens.

Mass scaling method was used for whole model with the target time increment of 1e-7. Mass scaling is a method used to reduce computational time of the dynamic or quasi-static analysis by adding nonphysical mass to assembly to achieve suitable number of time increments. Semi-automatic mass scaling method is used which scales the elements mass if time increment is below the target. Time period is defined according to crushing speed of the modelled test. In this study, crushing speed was defined as 2 m/s and 20 mm displacement was investigated. Time period of the test is defined as 0.01 s. It is important to state that in numerical simulations a very higher value of crushing rate than experimental test crushing rate was used. High crushing rate was used to decrease the computational cost of the simulation. Increasing the crushing speed does not differ the crushing mode and it does not affect the energy absorption characteristics excessively [44]. In the studies of Mamalis et al. [38] and Zhou et al. [39] similar approach is used with increased speed rates in the numerical simulations.

Next step after creating the assembly of the test parts is defining interactions of the test model. To prevent crushing in the bottom of the tube, tie constraints were created between bottom nodes of the tube specimen and bottom rigid plate nodes. Friction between parts were modelled by tangential behavior with a friction coefficient of 0.2. Tangential behavior define the contact behavior of a part slips on the surface of the other part, such as friction and elastic slip. Normal behavior define the contact behaviors when a part contacts and tends to move towards the other part in a normal axis, such as hard contact, soft contact and damped contact. Hard contact was selected to define normal behavior.

Tangential behavior, normal behavior, cohesive behavior and damage contact properties were assigned to contacts between plies. Friction between plies was selected as 0.2 and hard contact defined between plies as well. Cohesive behavior and damage contact defines the delamination as they were explained in the inter-laminar behavior modelling section. Cohesive behavior defines sticky surfaces and damage defines the delamination damage initiation and damage evolution values.

Inter-laminar behavior of composites were defined by creating cohesive contact from "interaction" module after the assembly is created. To define cohesive contact between plies, general contact cohesive behavior and damage properties were created first. Uncoupled traction separation behavior was defined in "cohesive behavior" option with a penalty stiffness value of 10e6 in three different delamination modes. Quadratic damage initiation and Benzeggagh-Kane damage evolution methods were defined to "damage behavior" option. Inter-laminar values are quite hard to achieve experimentally. In this study, inter-laminar values of Zhou et al.'s study were used as well since the resin system of examined specimens in this study and Zhou et al.'s are both epoxy [39]. Inter-laminar values are given in Table 3.3 [39].

Table 3.3. Inter-laminar properties used to model delamination [39].

Description	Variable	Value
Damage initiation stress for normal traction $[MPa]$	t_n^0	54
Damage initiation stress for first shear traction $[MPa]$	t_s^0	70
Damage initiation stress for second shear traction $[MPa]$	t_t^0	70
Fracture energy per unit area for normal traction $[J/m^2]$	G_n^c	504
Fracture energy per unit area for first shear traction $[J/m^2]$	G_s^c	1566
Fracture energy per unit area for second shear traction $[J/m^2]$	G_t^c	1566
Benzeggagh-Kane cohesive property	η	2.284

Interaction properties were assigned to the general contacts created between parts. Interactions between tubes, foams and rigid parts consists tangential behavior and normal behavior. Interaction property group created for contacts between tubes, foams and rigid parts are assigned as global property to the created general contact. Interaction of the plies between them consists tangential behavior, normal behavior, cohesive behavior and damage properties. Interaction of the plies are assigned from “individual property assignments” section by selecting the relative ply surfaces.

Next step of the modelling is defining load and boundary conditions. “Load” module is used to define load and boundary conditions. During axial crush testing, the bottom plate is keep in its position and upper impactor moves towards bottom plate along the central axis. So, by using the reference points created in rigid parts, “encastre” condition was defined in the lower reference point which constrain any movement in six degrees of freedom and displacement/rotation condition defined in the upper reference point which constrain movement in five degrees of freedom and only lets movement in axial direction. Crushing speed was defined by creating “predefined field” to the upper reference as 2m/s.

Mesh is generated in the first place while creating the geometrical parts. SC8R hex elements used to model composite tubes, C3DR8 elements used to model foam cores and R3D4 elements used to model rigid parts. Enhanced hourglass control was used on simulations to prevent hourglass effect on elements. Hourglass effect may occur on the elements with reduced integration points. Reducing the integration points causes elements to be less stiff in some points inside of the element. Elements with reduced integration points may exhibit zero energy modes similar to the shapes of hourglass when they are subjected to loads. Hourglass effect may result with excessive distortion of elements and this generally aborts the simulation.

To obtain meaningful results, necessary output variables were selected from “Field Output Request” section. Many output variables are selected as default. To observe inter-laminar failure, “CSDMG” and “CSQUADSCRT” variables must be selected. “CSDMG” shows scalar stiffness degradation for cohesive surfaces and “CSQUADSCRT” shows quadratic damage initiation criterion for cohesive surfaces. Intra-laminar failure results are activated by “SDVs” or solution dependent state variables. Meanings of the “SDV” variables are given in previous chapters (see Table 3.1). Lastly, “STATUS” variable must be activated to see which element failed during a time point of axial crushing. Final part of the modelling is job creation from in “Job” module.

In order to give a better explanation of modelling process and to state all of the selected modelling options, construction of finite element models of specimens subjected to axial crushing is summarized in the finite element solution that is given in below;

Module: Part

To create composite tube specimen parts,

Create Part => select 3D, Deformable, Solid, Extrusion => Continue => Create Circle => Sketch the first ply of the tube with the thickness of 0.2 mm => Extrude for 39mm.

To create foam cylinder parts,

Create Part => select 3D, Deformable, Solid, Extrusion => Continue => Create Circle => Sketch the cross section of foam => Extrude for 40mm.

Partition cell: Define Cutting Plane => select 3 Points method => Create quarter circle cylinder partition cells.

To create rigid flat plate parts,

Create Part => select 3D, Discrete Rigid, Shell, Planar => Continue => Sketch the plate.

Tools => Reference Point => Assign RP to the middle point of the rigid plate.

To create rigid crush plug and virtual debris wedge impactor parts,

Create Part => select 3D, Discrete Rigid, Shell, Sweep => Continue => Sketch the cross-section of the impactor.

Tools => Reference Point => Assign RP to the middle point of the rigid impactor.

Module: Mesh

To mesh and generate full model of composite tubes,

Object => Part: Composite Tube => Seed Part => Approximate element size: 1 => OK => Done.

Assign Mesh Controls => Element Shape: Hex => Technique: Sweep => Algorithm: Medial Axis.

Assign Element Type => Element Library: Explicit => Family: Continuum Shell => Hourglass control: Enhanced.

Assign Stack Direction => select outer surface of the tube

Mesh => Create Mesh Part, Object => Part, select created mesh part => Mesh => Edit => Category: Mesh => Method: Offset (create solid layers) => generate other plies by offsetting from outer surface of first ply => Method: Offset (create solid layers) => generate chamfer section from the top surface of plies.

To mesh foam cylinder structures,

Assign Mesh Controls => Element Shape: Hex-dominated => Technique: Sweep => Algorithm: Medial Axis.

Assign Element Type => Element Library: Explicit => Family: 3D Stress.

Seed Part => Approximate global size: 4.

Mesh part.

To mesh rigid flat plates,

Assign Element Type => Element Library: Explicit => Family: Discrete Rigid Element => Mesh part.

To mesh rigid plugs and virtual debris wedge impactor,

Assign Element Type => Element Library: Explicit => Family: Discrete Rigid Element.

Assign Mesh Controls => Element Shape: Quad-dominated => Technique: Sweep.

Seed Part => Approximate global size: 1.

Seed Edges => Select the radius edge => Approximate element size: 0.1.

Mesh part.

Module: Property

To define intralaminar damage of composites,

Create Material => Name: ABQ_PLY_FABRIC_1 => select Density, Depvar, User Material behaviors => define relative values according to Table 3.2, select both Depvar values as 16.

Create Composite Layup => Assign intralaminar damage properties to the plies using sets.
To define foam material behavior,
Create Material => Name: PU Foam => select Density, Elastic, Crushable Foam and Crushable Foam Hardening behaviors => set density as 1.58e-10, set Young's Modulus as 49.4, set Poisson's ratio as 0, set Hardening as Volumetric, set Compression Yield Stress Ratio as 1, set Hydrostatic Yield Stress Ratio as 0.5, set Crushable Foam Hardening Stress-strain values according to Figure 3.10.
Create Section => select Solid, Homogeneous, choose material as PU Foam.
Assign Section => select Foam part and assign PU Foam properties.
To define point mass to the upper impactor,
Special => Inertia => Create Point mass/Inertia => select Upper plate reference point => set Mass, Isotropic as 300 (It must be stated that this point mass has no effect to the quasi-static crushing behavior of the specimen, it is only generated to define a constant speed to the upper impactor, it is selected as a high valued mass to provide a low decrease in the kinetic energy thus crushing speed).

Module: Assembly
Create Instance => select required parts to simulate the desired specimen subjected to axial crushing => use Translate Instance and Rotate Instance to set position of the parts accurately.

Module: Step
Create Step => Name: Step-1, Dynamic/Explicit => select time period as 0.01 (10ms).
Field Output Request => select F-Output-1 => activate "CSDMG", "CSQUADSCRT", "STATUS" and "SDV".

Module: Interaction
Create Constraints => Tie Contacts => select master surface as bottom rigid plate, select slave surface as bottom nodes of the foam and composite tubes (create tie constraints for tube and foam separately), specify position tolerance distance as 5 and check on tie rotational DOFs if applicable option.

Create Interaction Property => select Contact => Name: friction, select Tangential Behavior and Normal Behavior options => select Tangential Behavior friction formulation as Penalty and set Friction Coefficient as 0.2 => select Normal Behavior Pressure-Overclosure option as “Hard” Contact.

Create Interaction Property => select Contact => Name: L2L, select Tangential Behavior, Normal Behavior, Cohesive Behavior and Damage options => select Tangential Behavior friction formulation as Penalty and set Friction Coefficient as 0.2 => select Normal Behavior Pressure-Overclosure option as “Hard” Contact => select Cohesive Behavior and Damage option values according to the Table 3.3 and information given in section 3.2.

Create General Contact (Explicit) => select Contact Domain Included Surface Pairs as “All with self” => select Global Property Assignment as defined “friction” contact => generate individual contacts between ply surfaces with “L2L” property from Individual Property Assignments.

Module: Load

Create Boundary Condition => Step: Initial, Category: Mechanical, Type: Encastre => assign “Encastre” boundary condition to the reference point of the lower plate.

Create Boundary Condition => Step: Initial, Mechanical, Displacement/Rotation boundary condition => set displacement boundary conditions of U1=0, U2=0, UR1=0, UR2=0, UR3=0 to the upper rigid impactor reference point.

Create Predefined Field => Step: Initial, Category: Mechanical, Type: Velocity => assign V3= -2000 (2m/s crushing speed).

Module: Job

Create Job => Name: Simulated Specimen Name, Model: Model-1 => Job Type: Full Analysis.

4. RESULTS AND DISCUSSION

Obtained results of experimental tests and numerical analyses are discussed in this section. Results of the experimental tests are examined first. Then, results of the numerical analyses examined and compared to the experimental test results.

4.1. Experimental Test Results

Experimental tests carried out in this study are focused on quasi-static crushing tests of empty composite tubes, PU foam filled composite tubes and HGMS/epoxy syntactic foam filled composite tubes. Effect of different diameters and different crush plugs were examined during the tests of empty composite tubes. Foam filled tests were carried out according to results of the empty tubes.

Results of the experimental tests were evaluated using load displacement curves. SEA-displacement curves derived from load-displacement curves of specimens were investigated as well. SEA values on SEA-displacement curves refers to the absorbed energy divided by crushed weight on relative displacement. Crushing modes of the empty tubes were also examined to develop a better understanding of crushing behavior of crash box specimens.

Load-displacement curves, SEA-displacement curves and crushing response of empty tubes, PU foam filled tubes and HGMS/epoxy syntactic foam filled tubes are discussed in this section consecutively. Two tests were done for every test specimen. Results of the experimental tests were coherent with each other and no great difference exists between them. So one of the results of experimental tests were selected and discussed for each test specimen.

4.1.1 Empty Tubes Experimental Test Results

Specimens of circular composite tubes were manufactured in three different diameters of Ø30mm, Ø40mm and Ø50mm. To be able to model composite crushing efficiently and to develop a better understanding of crushing, three different diameter tubes were tested by using inwards-crushing crush plug, outwards-crushing crush plug other than using only flat test rigs. Results of empty tubes were examined in order of smallest to largest diameter.

Load-displacement curves of Ø30mm tubes tested with three different method is shown in Figure 4.1, SEA-displacement curve of Ø30mm tubes are shown in Figure 4.2 and crushing modes of Ø30mm tubes are shown in Figure 4.3.

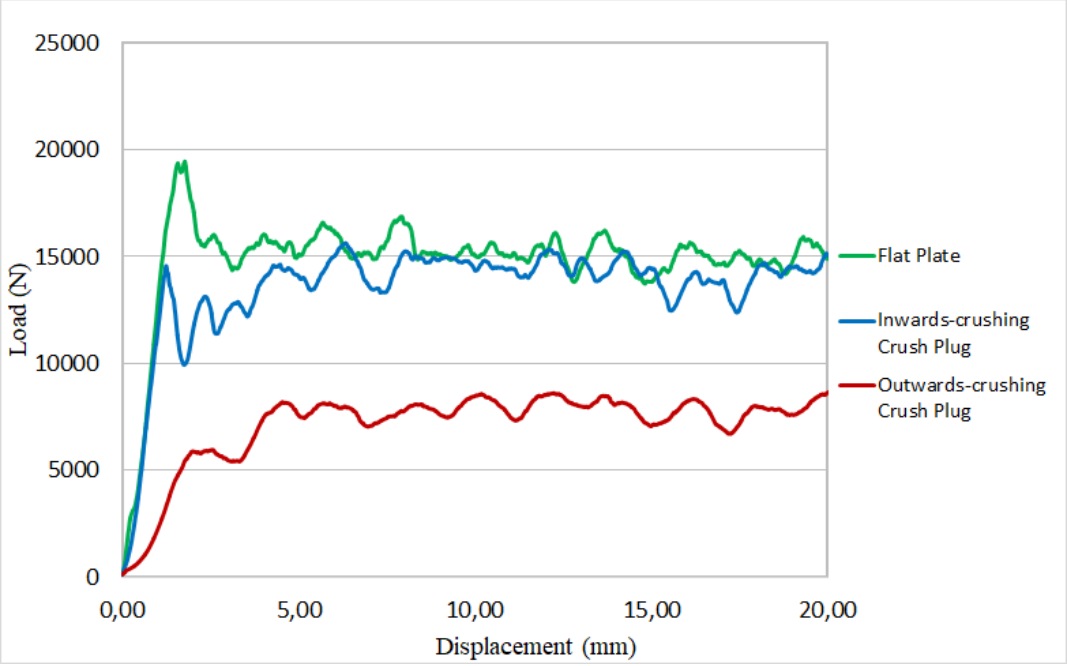

Figure 4.1. Load-displacement curves of Ø30mm tubes tested with three different method.

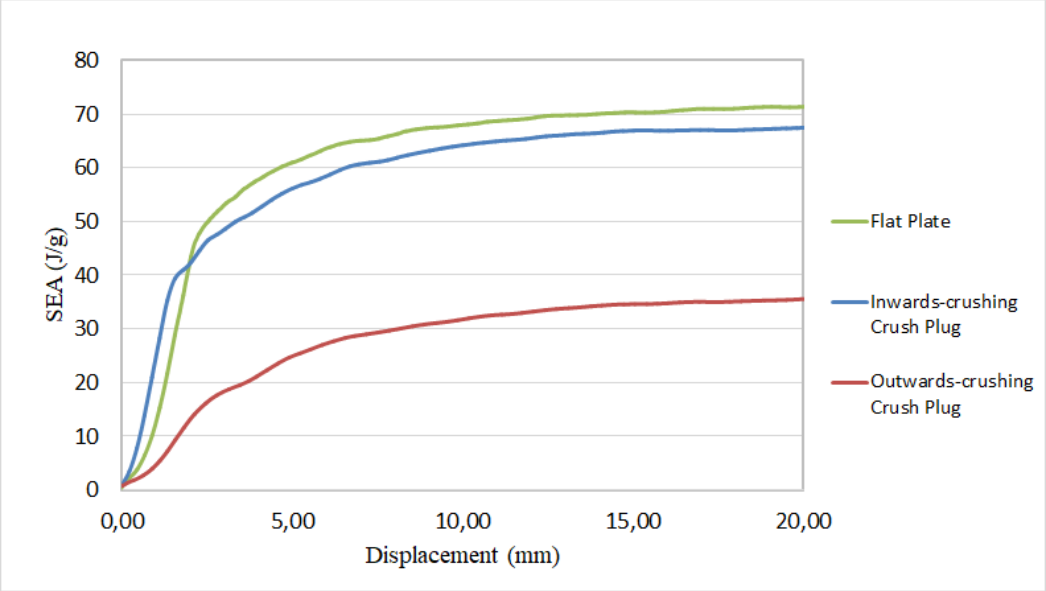

Figure 4.2. SEA-displacement curves of Ø30mm tubes tested with three different method.

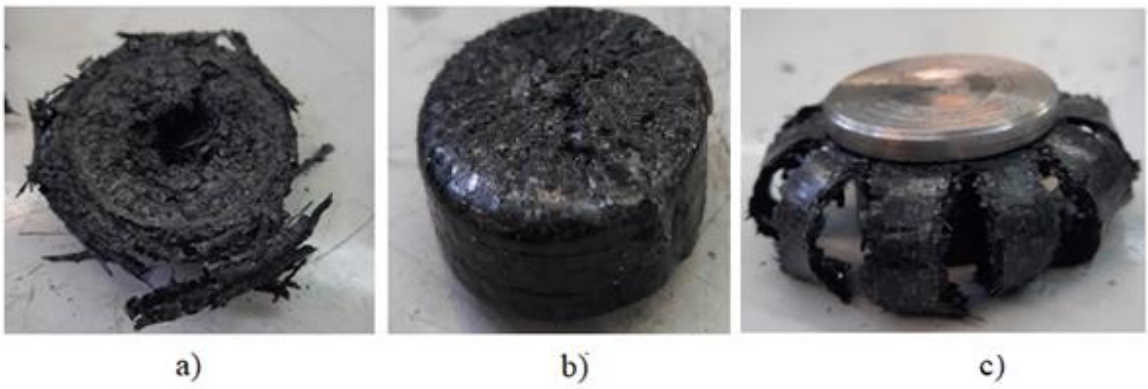

Figure 4.3. Crushing modes for Ø30mm empty tube with three different methods, a) Flat plate crushing, b) Inwards crushing c) Outwards crushing.

In the load-displacement curves of Ø30mm tubes quasi-static crushing given in Figure 4.1, it is observed that the most efficient crushing method is using flat plates and not to use any crush plug. Flat plate crushing is the most efficient because it causes fragmentation of larger regions of the tube.

Test results by using inwards-crushing crush cap are relatively close to the flat plate crushing results because while the parts of the tube axially split and fronds inwards during crushing they intertwine with each other as axial crushing progresses. This cause fragmentation of a large portion of the tube with a crushing load close to the flat plate crushing. As tubes are progressively crushed, fragmented parts of the tube is trapped to the inside of the tube and this results in increasing load values after a point is reached since fragmented parts filling inside the uncrushed part of the tube develops a resistance load and act as a solid column when they fill the space between bottom rig and crush cap.

Using outwards-crushing crush cap is the least efficient of the methods examined. Main failure behavior of this method is the axial splits caused from tensile failure of material along hoop direction. Required loads to cause these axial splits and outwards splaying are rather lower than other flat plate crushing and inwards frond crushing. However, this crushing method provides a good progressive crushing behavior.

Similar behavior observed in crushing tests of other diameters. In Figure 4.4, load-displacement curves of Ø40mm tubes tested with three different method are shown. In Figure 4.5, SEA-displacement curves of Ø40mm tubes are shown. In Figure 4.6, crushing modes of Ø40mm tubes are shown.

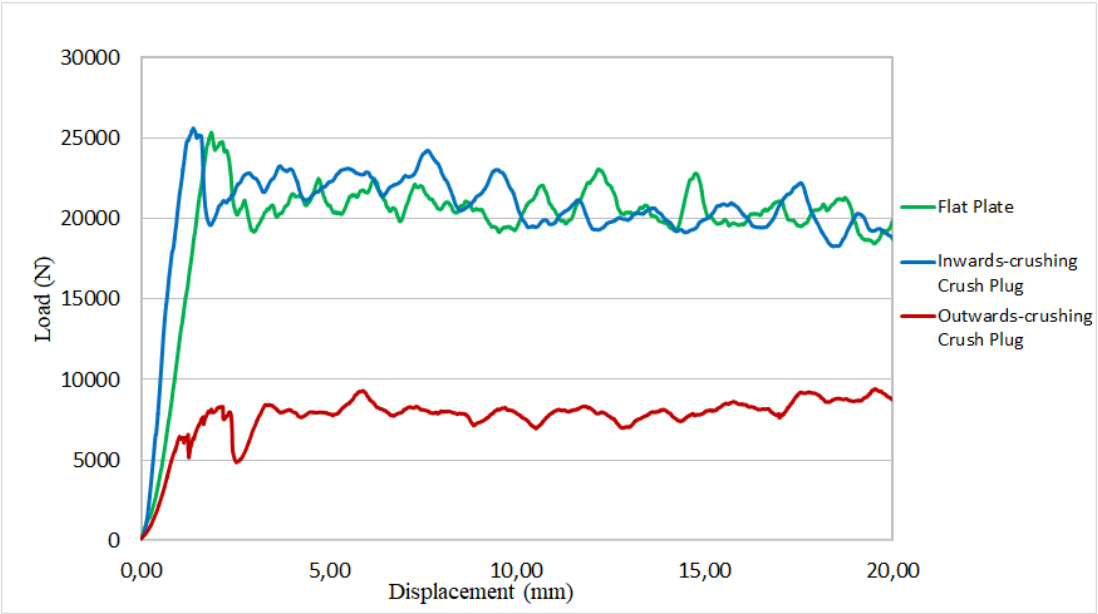

Figure 4.4. Load-displacement curves of Ø40mm tubes tested with three different method.

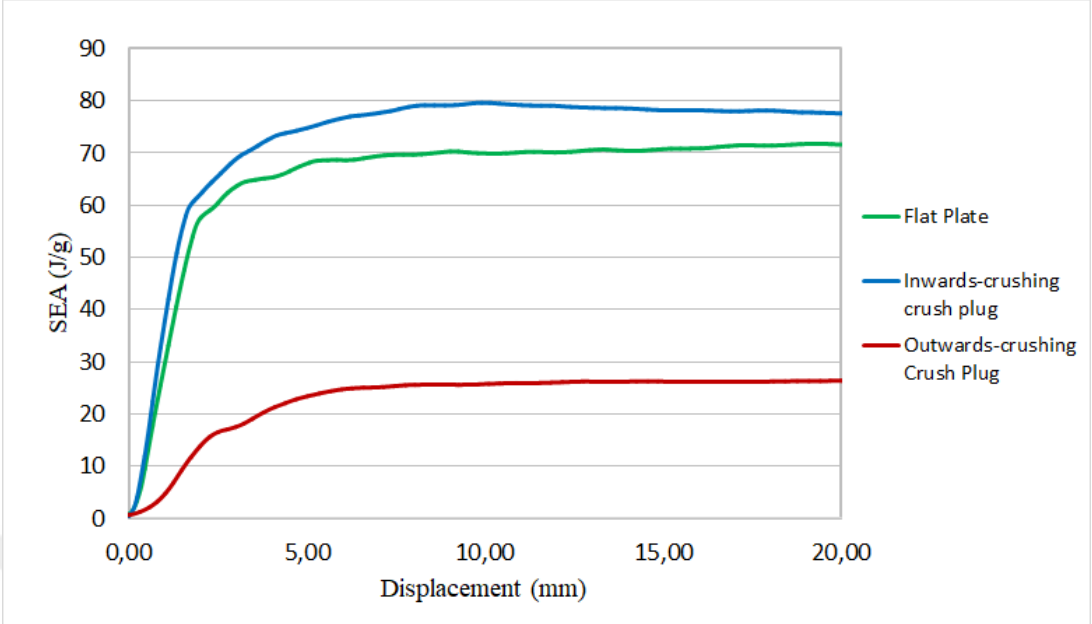

Figure 4.5. SEA-displacement curves of Ø40mm tubes tested with three different method.

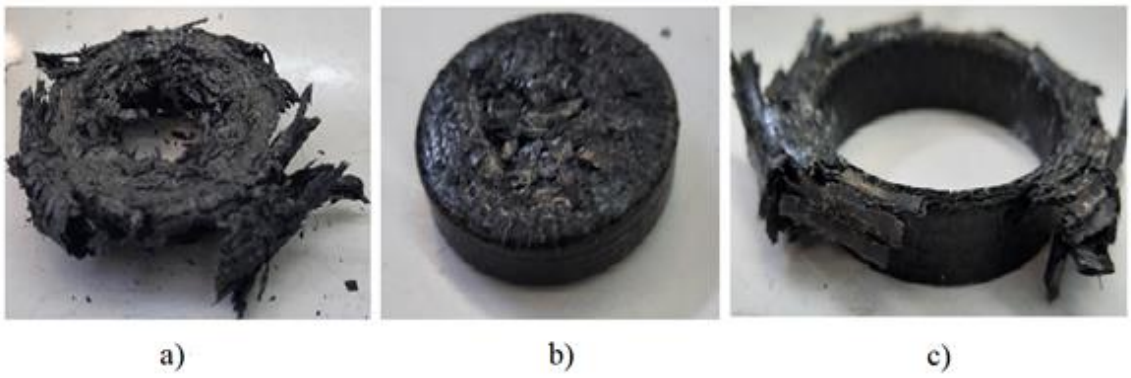

Figure 4.6. Crushing modes for Ø40mm empty tube with three different methods, a) Flat plate crushing, b) Inwards crushing, c) Outwards crushing.

In Figure 4.7, load-displacement curves of Ø50mm tubes tested with three different method are shown. In Figure 4.8, SEA-displacement curves of Ø50mm tubes are shown. In Figure 4.9, crushing modes of Ø50mm tubes are shown.

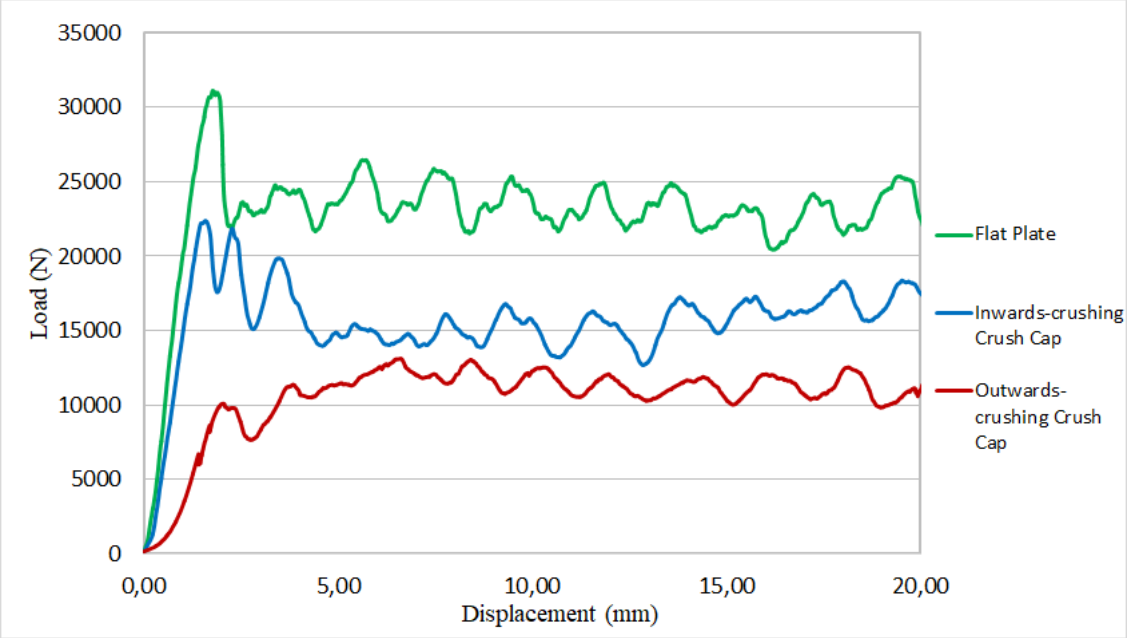

Figure 4.7. Load-displacement curves of Ø50mm tubes tested with three different method.

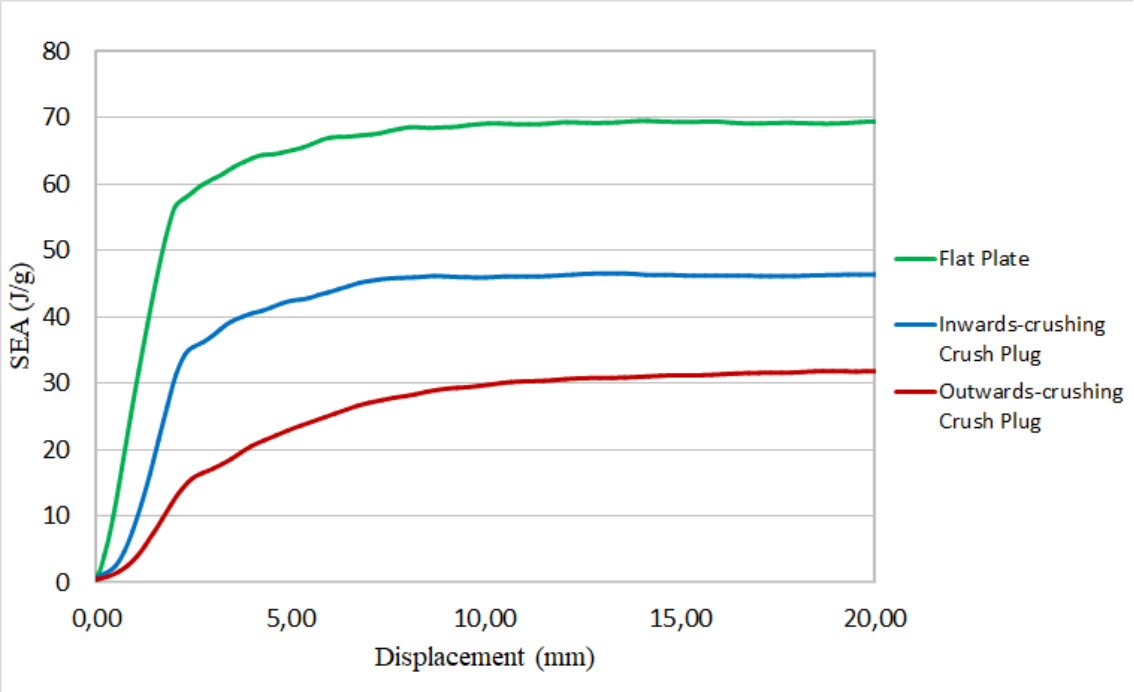

Figure 4.8. SEA-displacement curves of Ø50mm tubes tested with three different method.

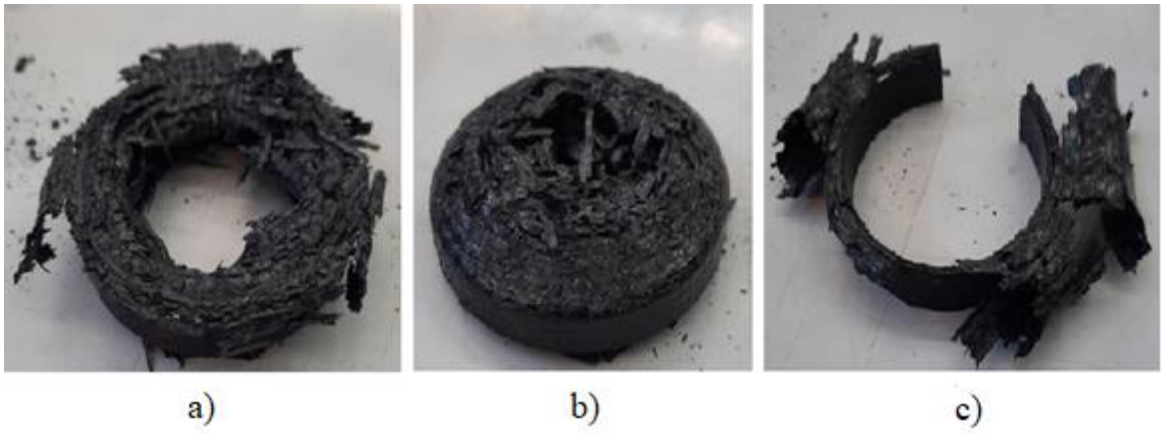

Figure 4.9. Crushing modes for Ø50mm empty tube with three different methods, a) Flat plate crushing, b) Inwards crushing, c) Outwards crushing.

From the test results, it is observed that flat plate crushing is the most efficient method in energy absorption terms. Load-displacement curves of flat plate crushing for three different diameters are compared in Figure 4.10. SEA-displacement curves are compared in Figure 4.11.

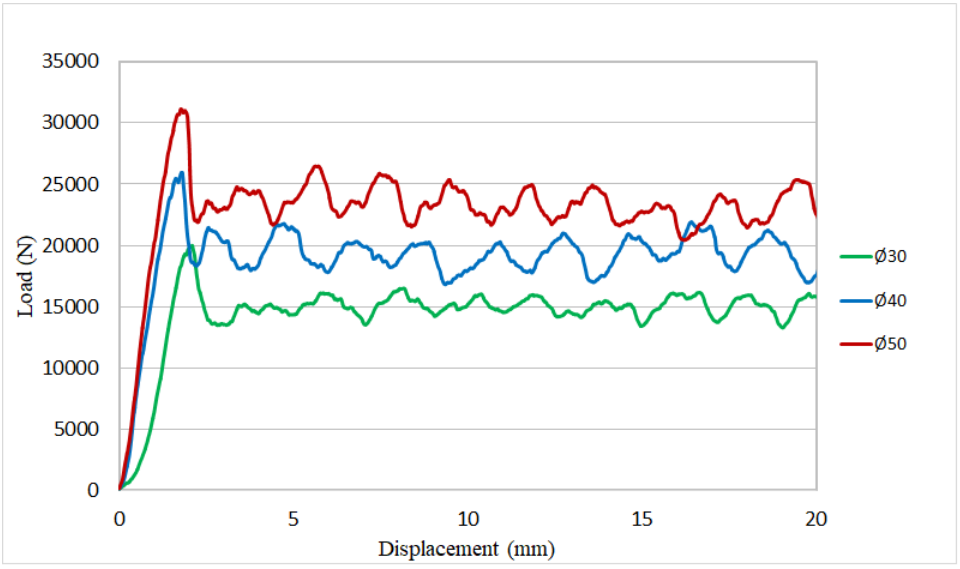

Figure 4.10. Load-displacement curves of empty tubes with different diameter crushed with flat plate.

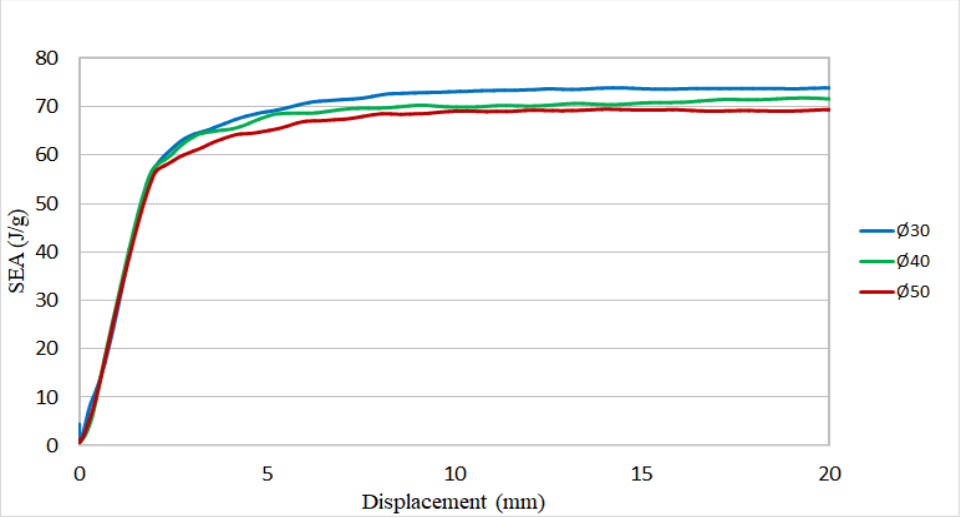

Figure 4.11. SEA-displacement curves of empty tubes with different diameter crushed with flat plate.

The experimental crushing test results of empty composite tubes shown that specific energy absorption values are very close to each other in flat plate crushing. As it is expected, the energy absorption value increases as diameter increases. Experimental axial crushing test results of empty tubes are summarized in Table 4.1.

Table 4.1. Summary of the crushing test results of empty tubes.

Diameter [mm]	Crushed Part Weight [g]	Crushing Method	Energy absorption at 20mm disp. [J]	SEA [J/g]
Ø30	4.02	Flat Plate	287.44	71.50
		Inwards Crushing	271.25	67.48
		Outwards Crushing	142.93	35.55
Ø40	5.28	Flat Plate	378.89	71.75
		Inwards Crushing	410.48	77.74
		Outwards Crushing	154.50	29.26
Ø50	6.58	Flat Plate	457.34	69.50
		Inwards Crushing	311.20	47.29
		Outwards Crushing	209.78	31.88

It can be seen that the SEA of all tubes are very close to each other when a flat plate is used. However, SEA values does not have a similar trend for inwards and outwards plugs, and the SEA values depend on the diameter with highest value obtained for Ø40 diameter inward crushing specimens. However during Ø50mm tube inwards crushing, specific energy absorption value is much smaller. This is because inner fronds are more relaxed in large diameter tubes and they do not intertwine with each other as in smaller diameter tubes. It can be suggested that after a certain diameter value, inner fronds occurring in inwards crushing tends to behave like outwards fronds without interacting each other.

4.1.2. Polyurethane Foam Filled Tube Experimental Test Results

Polyurethane foam filled tests were carried out on Ø50mm specimens crushed with flat plate. Polyurethane foam filled specimens are manufactured by stuffing polyurethane foam cylinder into Ø50mm composite tube. In this section, crushing of sole polyurethane foam and polyurethane foam filled composite tube are examined. It should be noted that all tests for foam filled tubes are made using flat compression plate.

Load-displacement curve of sole polyurethane foam is given in Figure 4.12. Load-displacement curve of polyurethane foam filled composite tube is given in Figure 4.13.

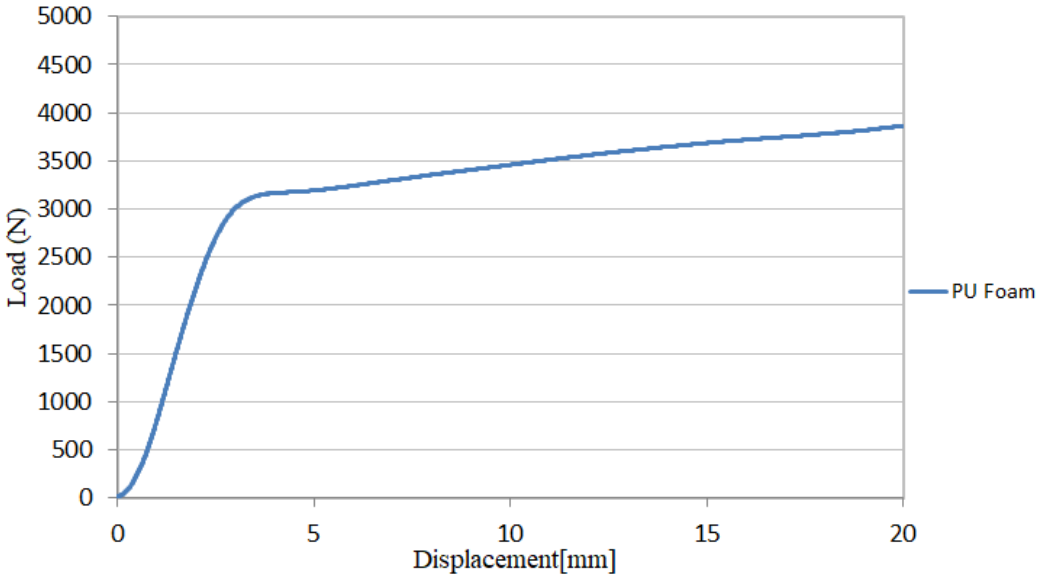

Figure 4.12. Ø50mm PU foam cylinder load-displacement curve.

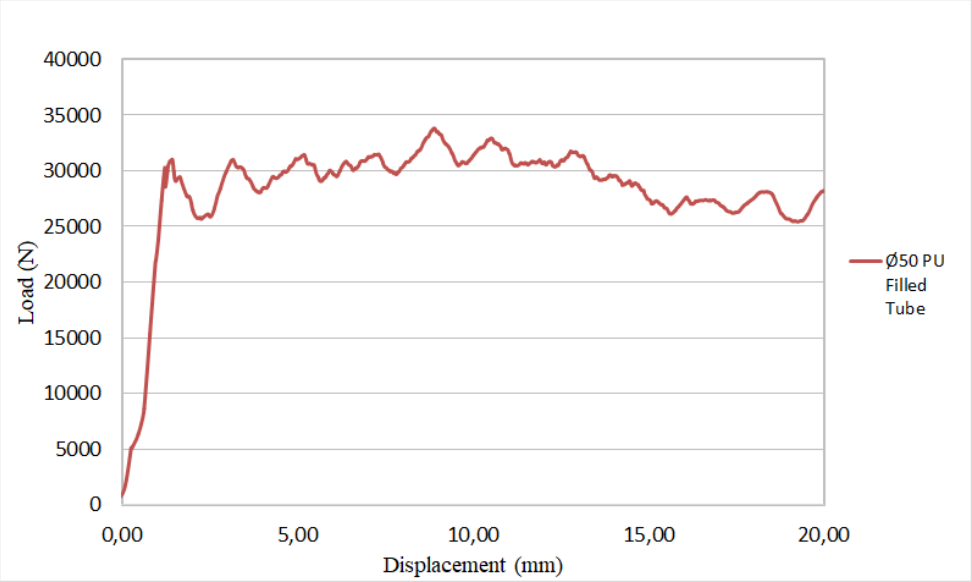

Figure 4.13. Ø50mm PU foam filled composite tube load-displacement curve.

Foam filled composite tube load displacement curve must be examined together with sole PU foam and empty composite tube curves to be able to observe the positive effect of interaction in foam filled tubes. Compared load displacement curves of PU foam filled composite tube, sole PU foam, empty composite tube are given in Figure 4.14 and SEA-displacement curves are given in Figure 4.15.

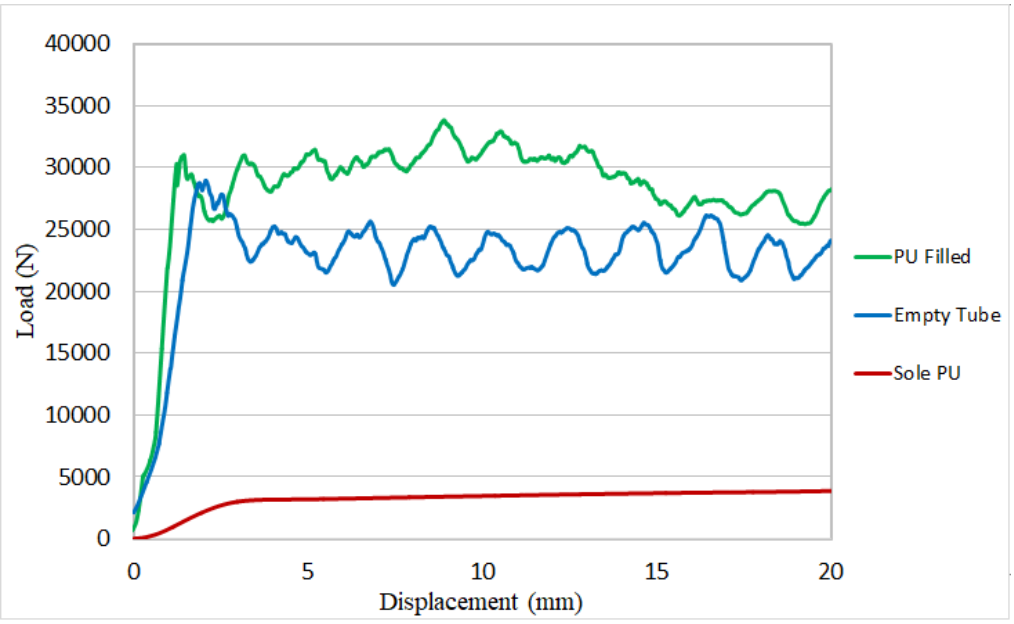

Figure 4.14. Ø50mm PU-filled composite tube load-displacement curves.

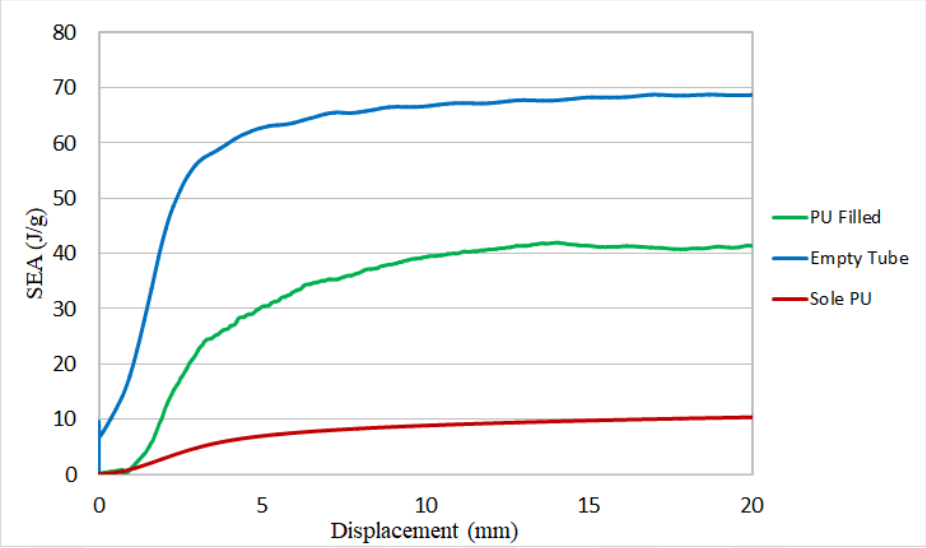

Figure 4.15. Ø50mm PU-filled composite tube SEA-displacement curves.

Crushing mode of foam-filled composite tube is shown in Figure 4.16. During crushing of PU filled composite tubes, a debris wedge occurred on the top end of the composite tube. Foam stuffed inside tube prevents fronds towards inside tube, so debris wedge acts as in splaying mode in the start and after some time wedge acts between foam and tube. This result with outwards fronds.

Figure 4.16. Crushing mode of PU foam filled tube, a) with debris wedge, b) debris wedge removed.

Summary of the Ø50mm PU foam-filled composite tubes test results are given in Table 4.2.

Table 4.2. Summary of the crushing test results of PU foam-filled composite tubes.

Test	Crushed Part Weight (g)	Absorbed energy at 20 mm disp. (J)	SEA (J/g)
Sole PU	6.2	68.04	10.97
Empty CFRP Tube	6.58	457.34	69.50
PU+CFRP Linear Sum	12.78	525.38	41.10
PU Filled CFRP Tube	12.78	565.69	44.25

Examining test results of PU foam filled composite tubes, it is found out that foam filling composite tubes does increase energy absorption slightly and creates a positive effect but stuffing PU foam inside tube also increases the weight of the crash box specimen. This results lower values of SEA.

4.1.3. Syntactic Foam Filled Tube Experimental Test Results

Only Ø30mm syntactic foam filled tubes are tested for comparison with empty and polyurethane foam filled tubes. Load displacement curves of empty tube, syntactic foam, and syntactic foam filled tube tests are given in Figure 4.17. SEA-displacement curves are given in Figure 4.18.

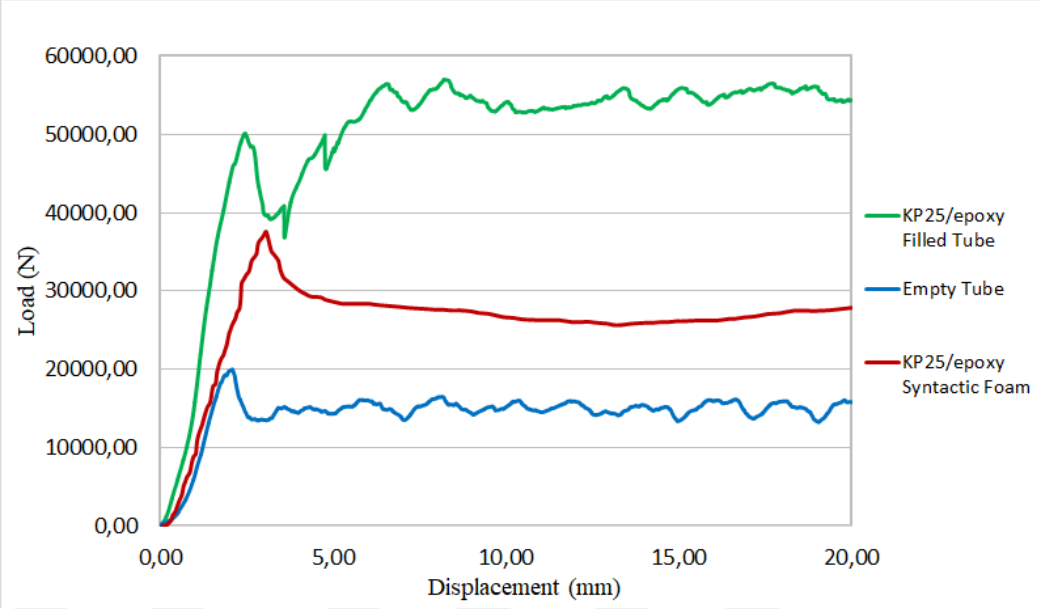

Figure 4.17. Load displacement curves of Ø30mm HGMS/epoxy filled tube specimen.

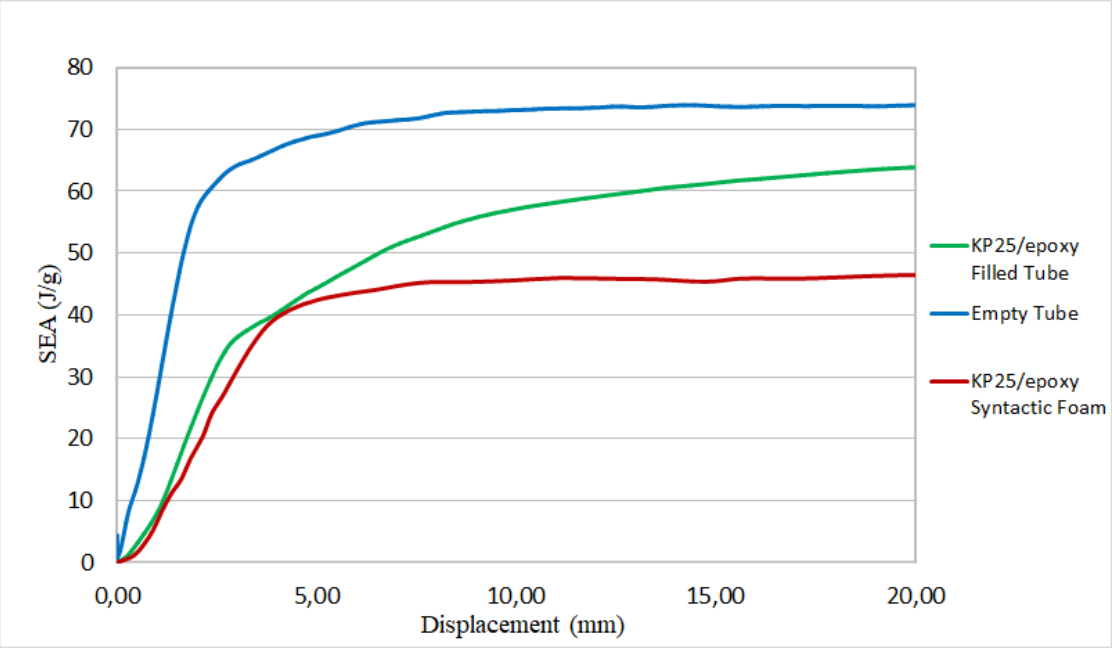

Figure 4.18. SEA-displacement curves of Ø30mm HGMS/epoxy filled tube specimen.

Crushing mode of the Ø30mm HGMS/epoxy filled specimen is given in Figure 4.19. Crushing mode of the HGMS/epoxy filled tubes is not stable as in PU filled tubes. This is because PU is a cellular foam that its plastic Poisson's ratio is close to zero. However, HGMS/epoxy foam is a composite material itself and it doesn't have large cavities in its structure as PU foam. HGMS diameter used in syntactic foams is around 90μm and they do not act as hollow portions inside PU foam [50]. Thus, Poisson's ratio of HGMS/epoxy foam is much higher than PU foams and it expands outwards when subjected to compression. In axial crushing of HGMS/epoxy filled tubes, syntactic foam core tears off the outer composite tube at a certain level of load. This kind of behavior possess the risk of catastrophic crushing as well.

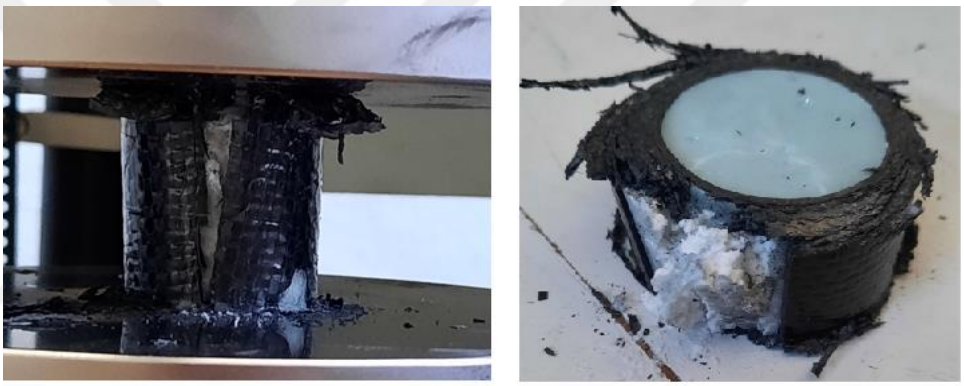

a) b)

Figure 4.19. Crushing modes of Ø30mm HGMS/epoxy filled tube, a) During testing b) Final crushing mode.

Summary of the Ø30mm HGMS/epoxy filled composite tubes test results are given in Table 4.3.

Table 4.3. Summary of the crushing test results of Ø30mm HGMS/epoxy filled composite tubes.

Test	Crushed Part Weight (g)	Absorbed energy at 20 mm disp. (J)	SEA (J/g)
Sole KP25/epoxy	11.45	527.95	46.11
Empty CFRP Tube	4.02	287.44	71.50
HGMS/epoxy foam + CFRP Linear Sum	15.47	815.39	52.71
HGMS/epoxy filled CFRP Tube	15.47	987.98	63.87

4.2. Numerical Study Results

Results of the numerical analysis performed to simulate axial crush of the specimens are discussed in this section. All numerical simulations are carried out on ABAQUS/Explicit commercial FEA software. First simulation results of empty tube specimens are examined and then the results of foam filled tube specimens are discussed.

4.2.1. Numerical Study Results of Empty Composite Tubes

Experimental tests of empty composite tubes are done using three different methods on three different diameter tubes. Composite tubes with the diameters of Ø30mm, Ø40mm and Ø50mm are tested by crushing with flat plate rigs and crush caps. First, numerical works are demonstrated by modelling the crushing of the tube using flat rigid part. It is observed that numerical results of the tubes differs from the experimental results. Crushing mode is rather local buckling than progressive crushing in the simulations. Crushing mode of the numerical simulation using flat rigid part is shown in Figure 4.20.

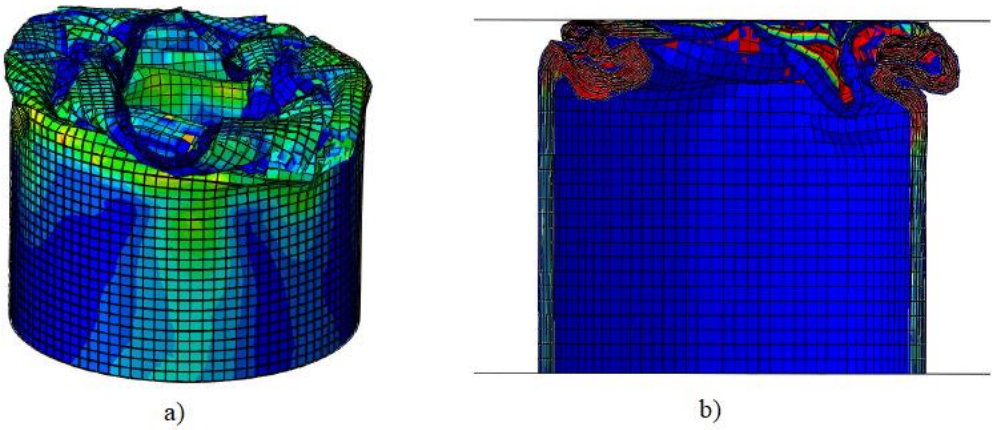

Figure 4.20. Crushing mode using flat rigid plates; a) 3D view, b) Section view.

Load displacement curve of this method also shows differences from the experimental results. Comparison of the numerical load displacement curve using this method and experimental load displacement curve is given in Figure 4.21. SEA displacement curve of the numerical simulation and experimental tests were given in Figure 4.22. It can be seen that, due to the high peak force occurs using rigid flat plates, SEA values also gives a peak in the curve but they converges to a constant SEA value after some point.

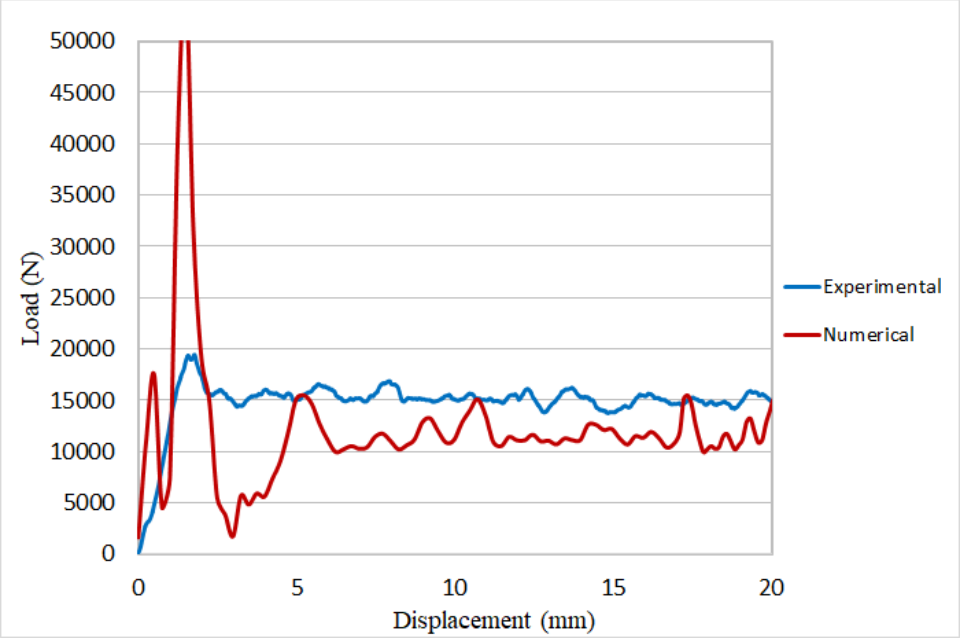

Figure 4.21. Load displacement curves of Ø30mm empty tube experimental test and numerical simulation using rigid flat plate.

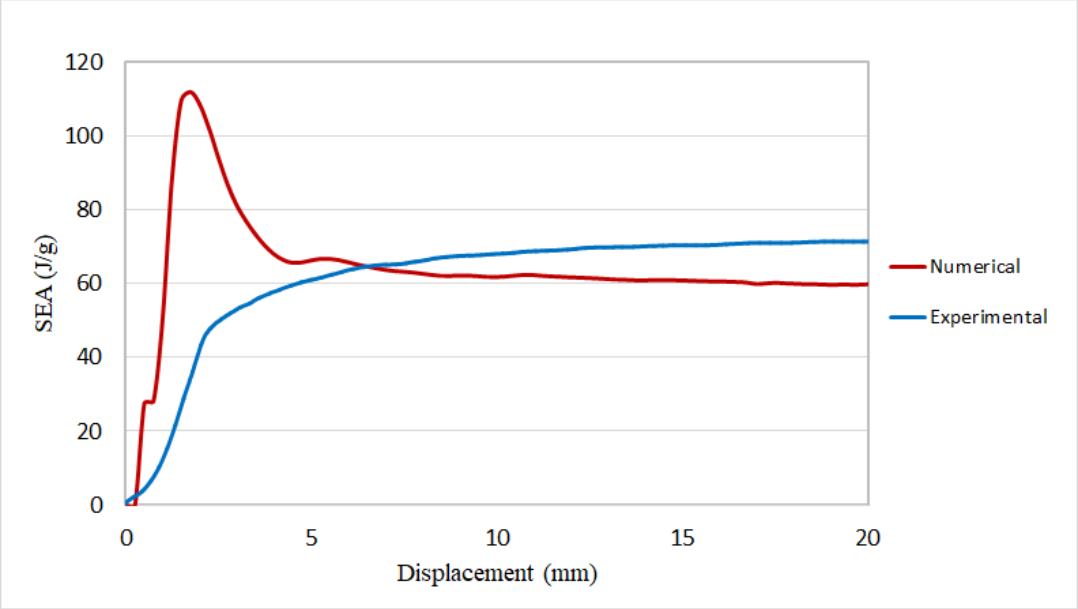

Figure 4.22. SEA displacement curves of Ø30mm empty tube experimental test and numerical simulation using rigid flat plate.

There is a high initial load and then the tube buckles locally with a sudden drop of load. It is understood from the load displacement curves and the obtained crushing mode, numerical modelling using rigid flat plate doesn't simulate real crushing behavior accurately. It is due to the lack of the debris wedge in simulation that causes splaying of the tube walls.

To be able to simulate axial crushing of composite tubes used by flat test rigs accurately, a virtual debris wedge modelled on the top rigid plate. This debris wedge is simulating the debris formed due to the fragmentation of the material filling the space between delaminated layers. Simulation results of the axial crushing tests using flat plates, inwards-crushing caps and outwards-crushing caps are examined respectively.

Crushing mode obtained in the numerical simulation using a debris wedge compared to the crushing mode of specimen tested experimentally using flat plates in Figure 4.23. Section view of the crushing mode obtained from simulation is given in Figure 4.24.

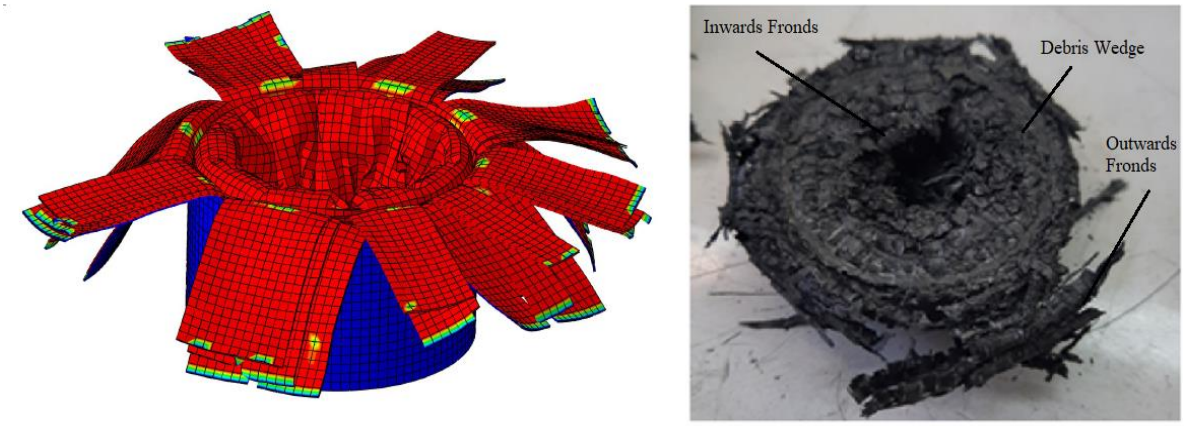

Figure 4.23. Crushing modes of Ø30mm empty tube flat plate crushing a) Numerical simulation using debris wedge b) Experimental test.

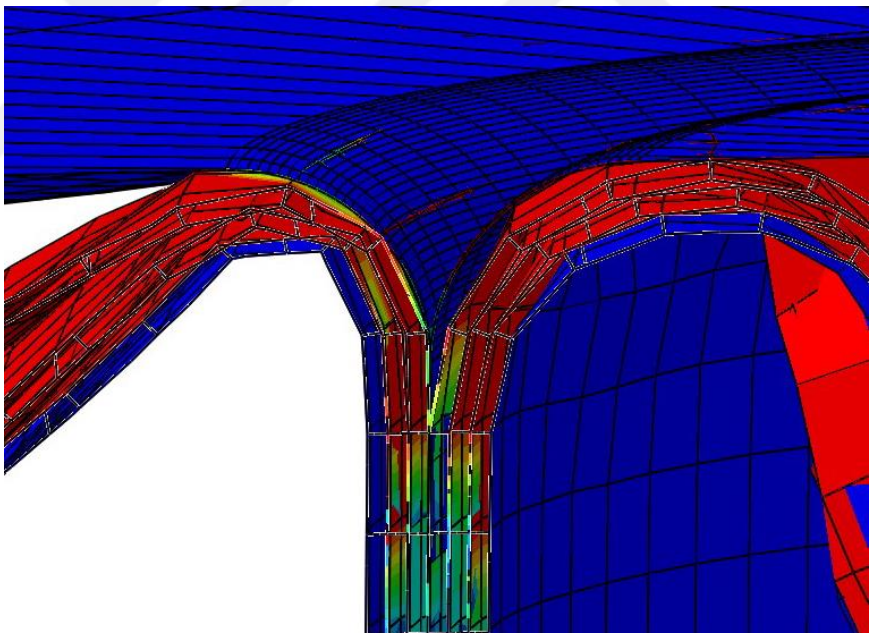

Figure 4.24. Section view of the tube wall simulated using virtual debris crushing.

Load displacement curves of numerical simulation using virtual debris wedge and flat plate crushing experimental test of Ø30mm tube are compared in Figure 4.25. SEA displacement curve of the debris wedge model is given in Figure 4.26. It can be seen that by using a debris wedge in the model, both crushing mode, load displacement curve and SEA displacement curve can be represented closer to experimental results.

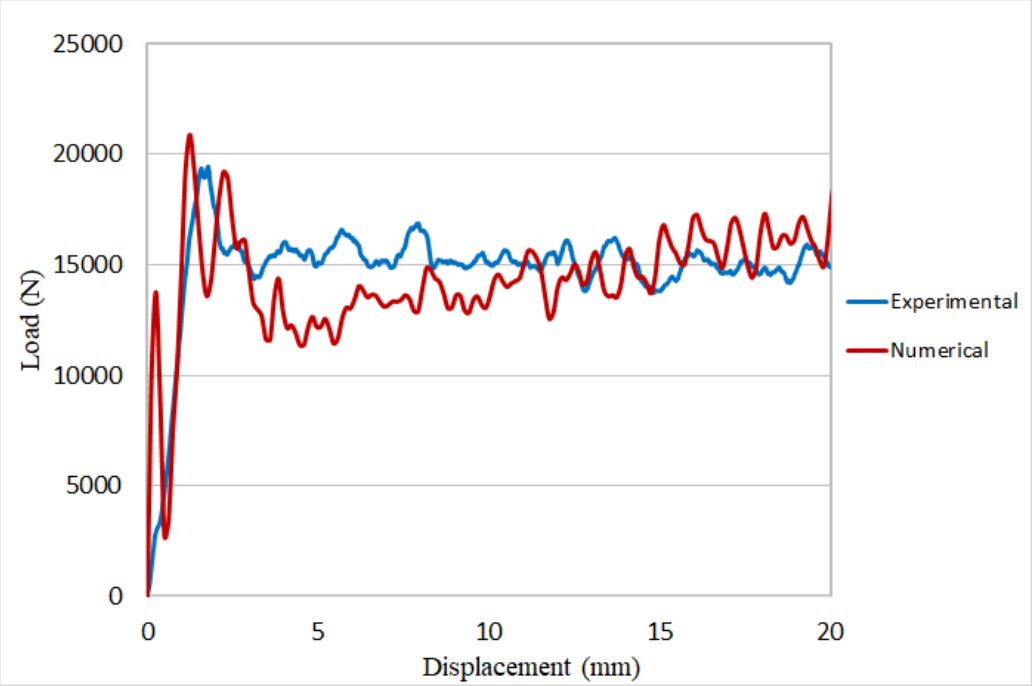

Figure 4.25. Load displacement curves of Ø30mm empty tube experimental test and numerical simulation using virtual debris wedge.

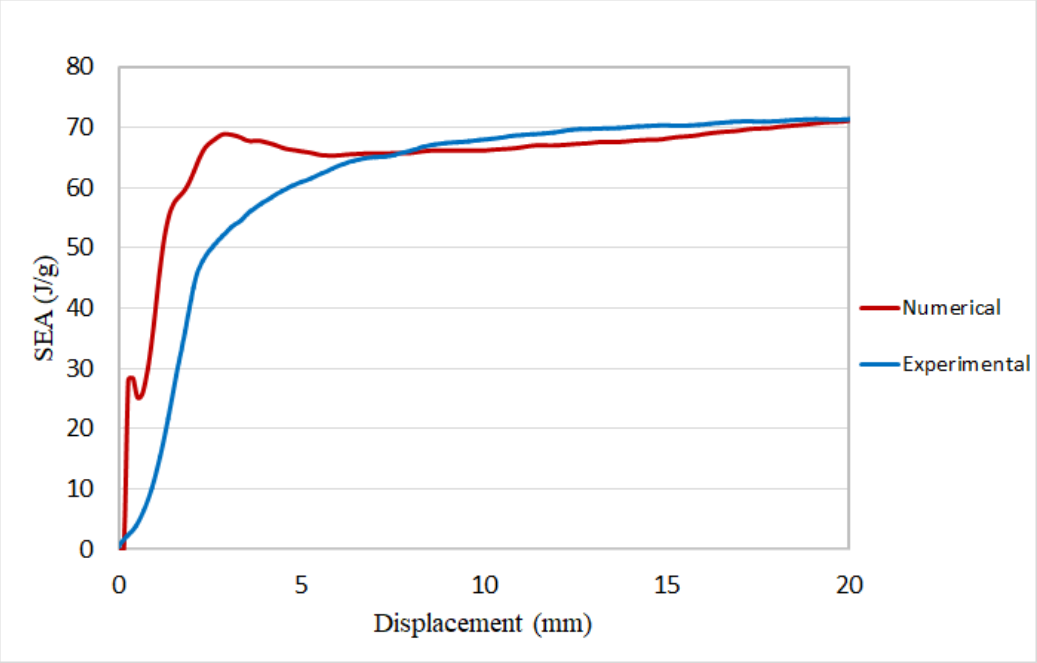

Figure 4.26. SEA displacement curves of Ø30mm empty tube experimental test and numerical simulation using virtual debris wedge.

Difference of SEA displacement curves between numerical simulation and experimental tests in first 2 mm in Figure 4.26 caused by high loads of numerical simulations and low crushed part weight. As crushing progresses, values show coherent behavior.

Crushing mode obtained from numerical simulation of the inwards crushing of empty tubes are compared to the experimental crushing mode in Figure 4.27. Section view of the crushing mode obtained from numerical simulation of the inwards crushing is given in Figure 4.28.

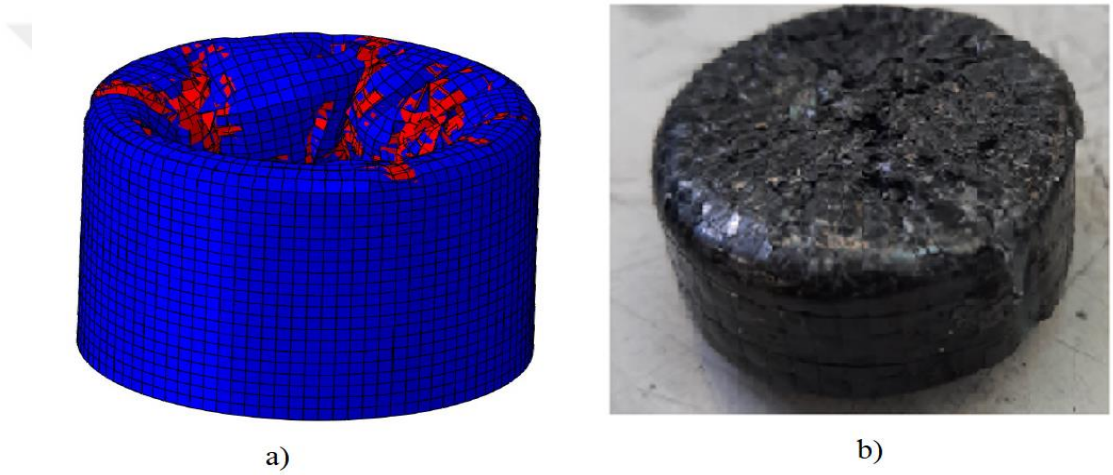

Figure 4.27. Crushing modes of Ø30mm empty tube inwards crushing a) Numerical simulation b) Experimental test.

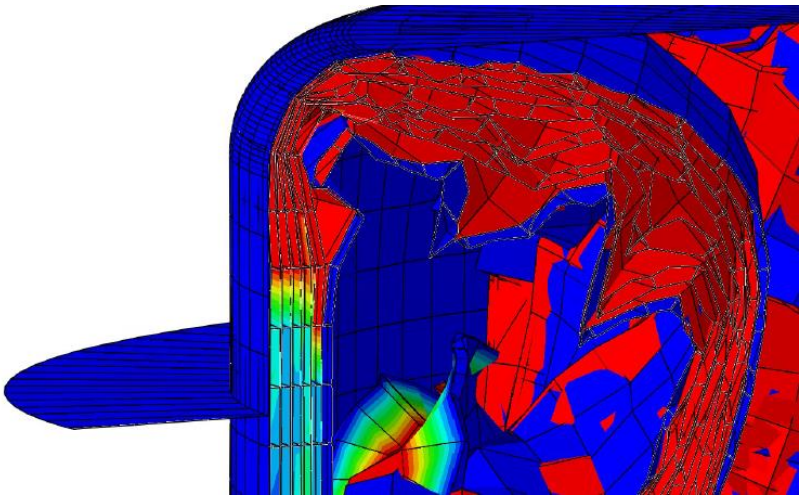

Figure 4.28. Section view of the tube wall simulated using inwards crush cap.

Load displacement curves of numerical simulation using inwards crush cap and inwards crushing experimental test of Ø30mm tube are compared in Figure 4.29. SEA displacement curves were given in Figure 4.30. It can be seen that the load displacement and SEA displacement curves obtained experimentally and numerically are very close to each other.

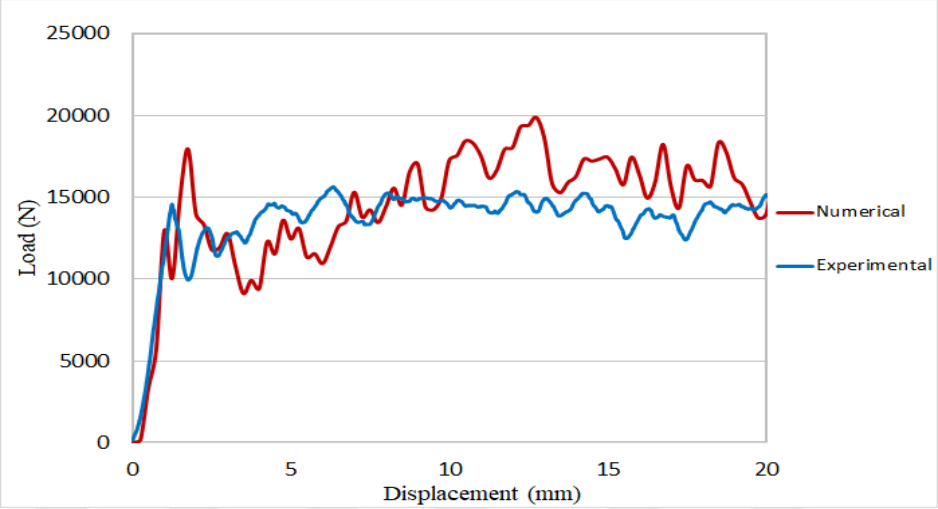

Figure 4.29. Load displacement curves of Ø30mm empty tube inwards crushing experimental test and numerical simulation.

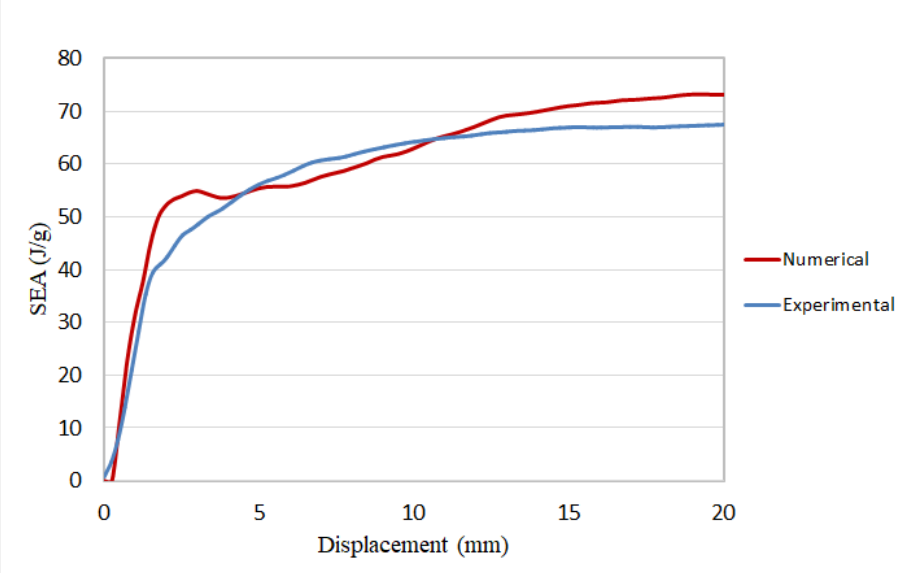

Figure 4.30. SEA displacement curves of Ø30mm empty tube inwards crushing experimental test and numerical simulation.

Crushing mode obtained from numerical simulation of the outwards crushing of empty tubes are compared to the experimental test crushing mode in Figure 4.31. Section view of the crushing mode obtained from numerical simulation of the outwards crushing is given in Figure 4.32.

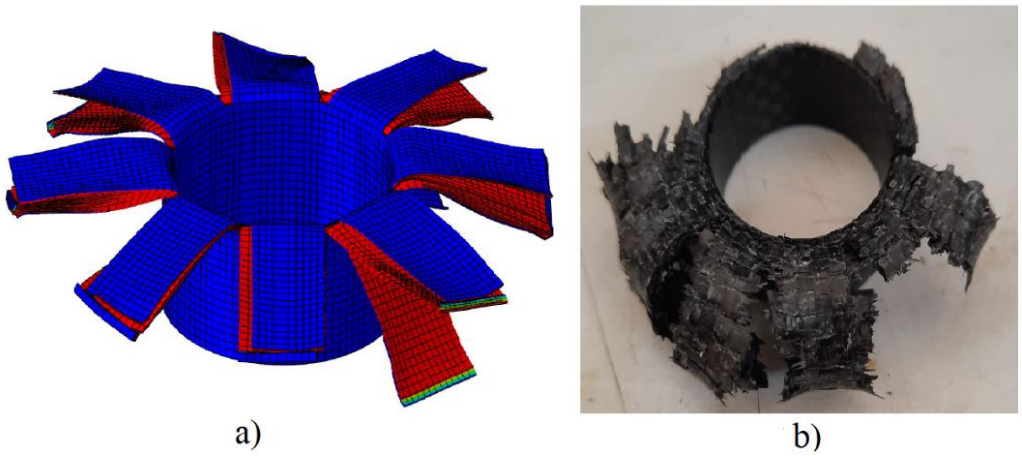

Figure 4.31. Crushing modes of Ø30mm empty tube outwards crushing a) Numerical simulation b) Experimental test.

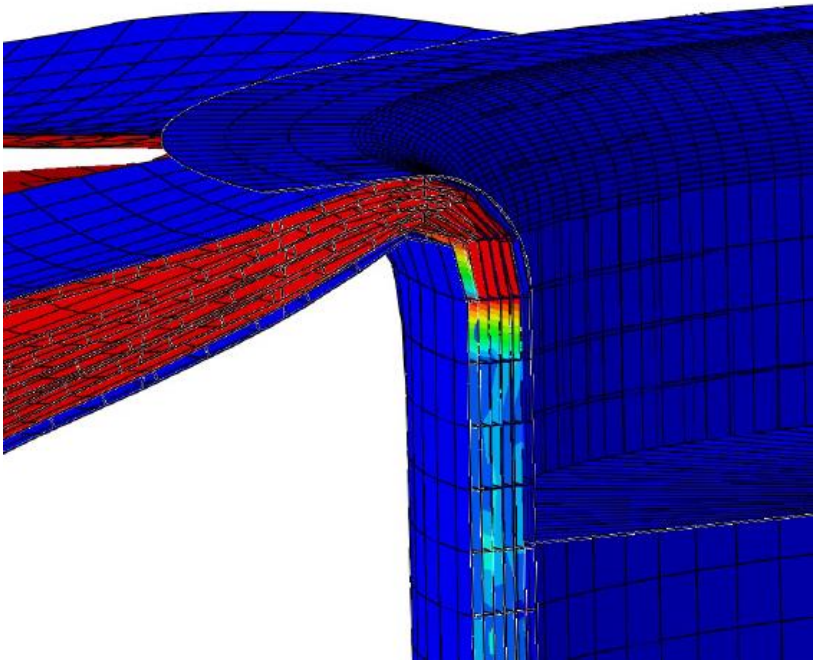

Figure 4.32. Section view of the tube wall simulated using outwards crush cap.

Load displacement curves of numerical simulation using outwards crush cap and outwards crushing experimental test of Ø30mm tube are compared in Figure 4.33. Although the initial portion of the simulated load-displacement curve exhibit large fluctuations due to behavior of the elements on the chamfer region, the stable portion of the curves are very close to each other. Chamfer elements in outwards crushing cause these fluctuations because when they subjected to outwards crushing, some of the elements stretches in the hoop direction until the axial splits occurs, this leads to the elements top surfaces hits the crush plug in normal axis in a direct way. Apparently modelled tube walls subjected to inwards crushing exhibit frond behavior more relaxed than outwards crushing in numerical simulations since some of the elements are squeezed. Outwards crushing simulations puts up this behavior until axial cracks are generated and wall fronds starts to slip rigid plugs surface smoothly.

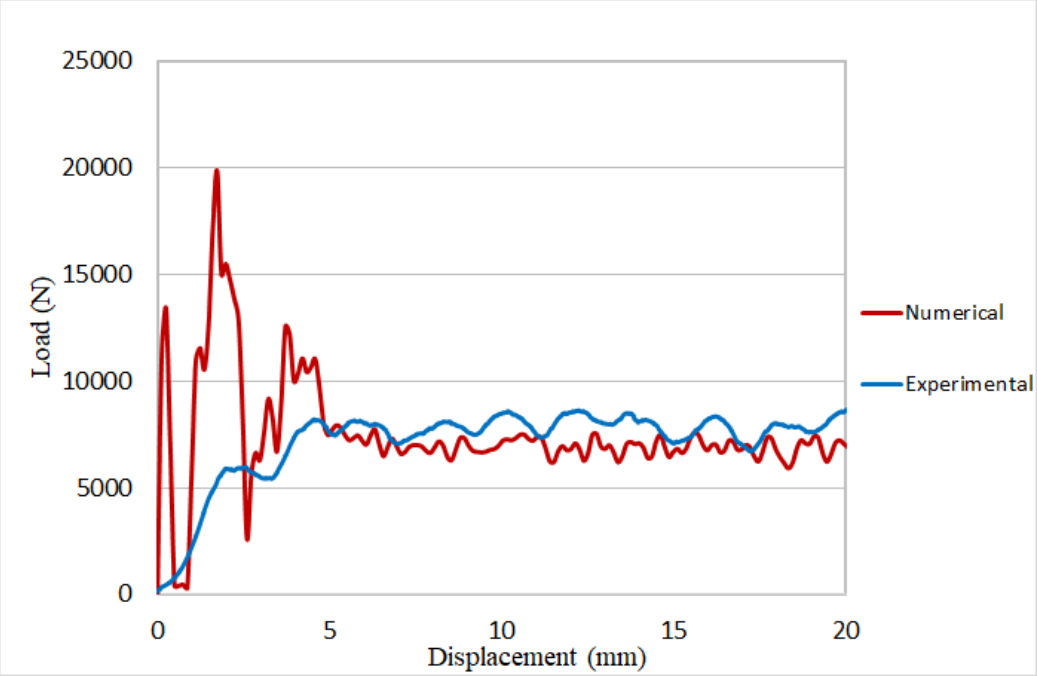

Figure 4.33. Load displacement curves of Ø30mm empty tube outwards crushing experimental test and numerical simulation.

Initial fluctuations also has effects on the SEA displacement curve since high energy absorption value of the numerical simulation divided by a small portion of the crushed weight in the start of the axial crushing. Yet SEA values approaches to an asymptotic value in the final stages of the crushing which gives coherent values. SEA displacement curves of numerical simulation and experimental test using outwards crush cap is given in Figure 4.34.

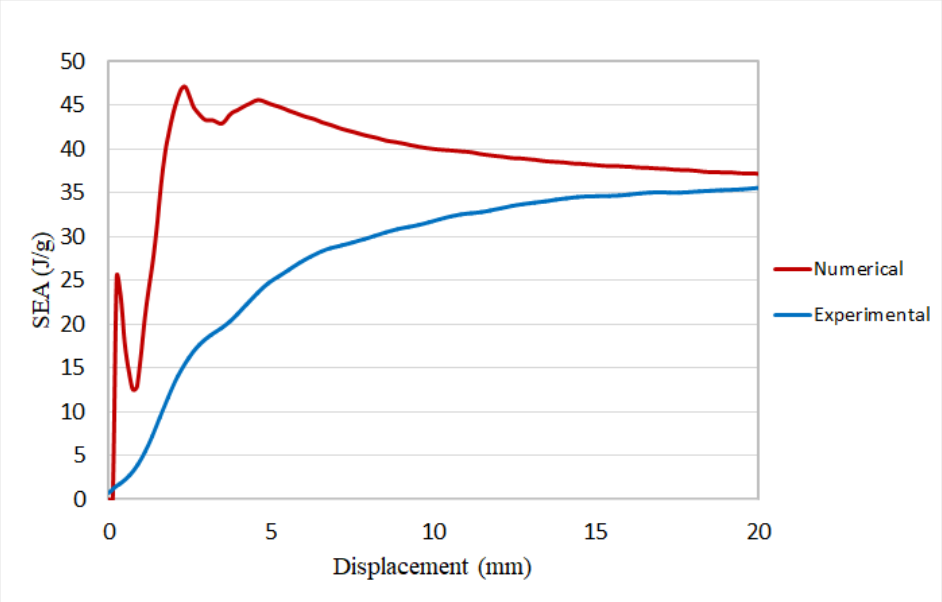

Figure 4.34. SEA displacement curves of Ø30mm empty tube outwards crushing experimental test and numerical simulation.

Summary of the numerical simulations on Ø30mm empty tubes are given in Table 4.4.

Table 4.4. Summary of the numerical simulations on Ø30mm tube.

Analysis	Absorbed Energy at 20mm (J)		SEA (J/g)	
	Num.	Exp.	Num.	Exp.
Flat Plate Crushing	260.22	287.44	64.73	71.50
Virtual Debris Crushing	289.15	287.44	71.92	71.50
Inwards Crushing	293.96	271.25	73.12	67.48
Outwards Crushing	151.98	142.93	37.80	35.55

Load displacement curves obtained from numerical simulations are consistent with the experimental ones, and the numerical and experimental values of total absorbed energy and SEA are very close. Also crushing modes of numerical simulations shows a good resemblance to the crushed tubes on experimental tests.

4.2.2. Numerical Study Results of PU Filled Composite Tube

In the experimental section of the study, Ø50mm PU foam filled tube tested to investigate the effects of the foam filling composite tubes in axial crushing. In this section, results of the developed simulation of the axial crushing of Ø50mm PU foam filled tube is compared to the experimental results. First PU foam is modelled using *CRUSHABLE FOAM material model. Since plastic Poisson's ratio is close to zero, no expansion occurred in 20mm crushing. Load displacement curves of experimental and numerical results of PU foam are compared in Figure 4.35.

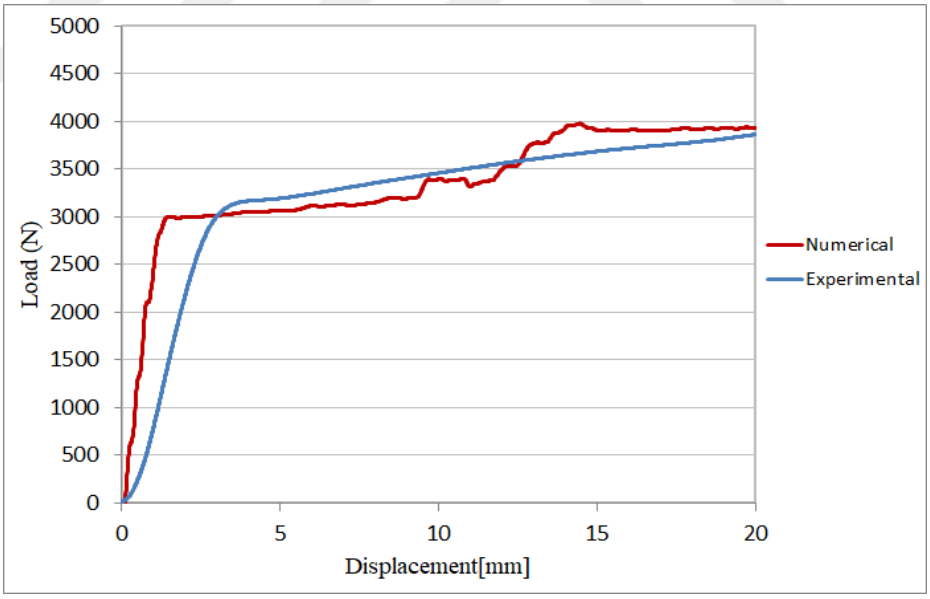

Figure 4.35. Load displacement curves of Ø50mm PU foam cylinder numerical simulation and experimental test.

Since plastic Poisson's ratio is assumed to zero, modelled PU foam is crushed in the simulation almost without expansion. Crushing behavior of the simulated PU foam is shown in Figure 4.36.

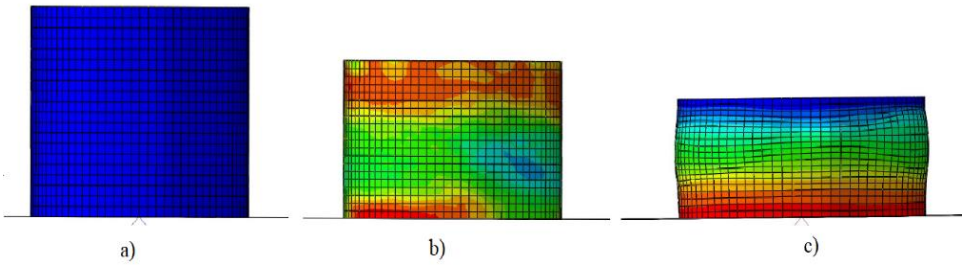

Figure 4.36. PU Foam numerical crushing modes, a) initial position, b) 10mm displacement c) 20mm displacement.

Modelled PU foam is positioned inside the tube in assembly module to model axial crushing of PU filled tube and virtual debris wedge used in simulating the composite tube. Crushing mode obtained from simulations is similar to the experimental crushing mode. Numerical crushing mode is compared to the experimental crushing mode in Figure 4.33. Composite tube is colored as grey and PU foam colored as yellow in numerical crushing to give a better illustration in Figure 4.37. Section view of the numerical tube is illustrated in Figure 4.38.

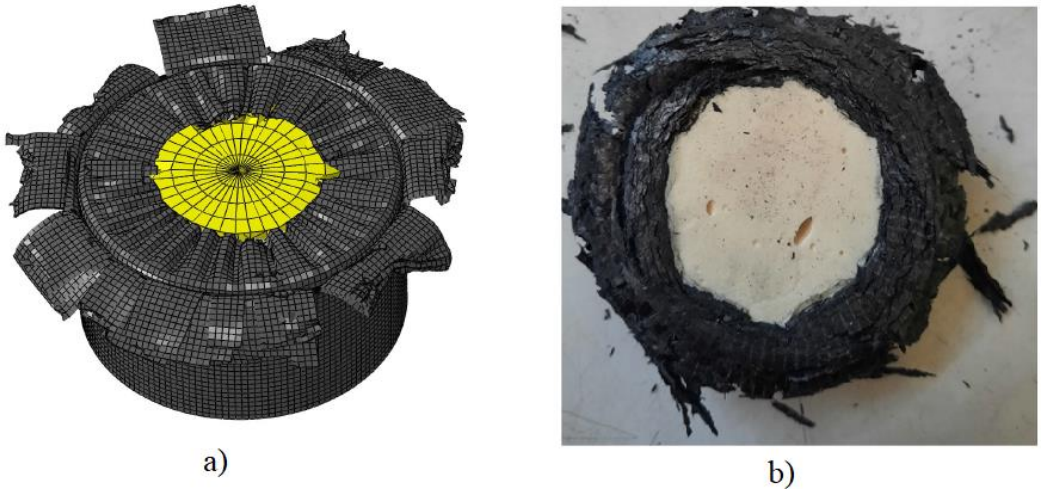

Figure 4.37. PU filled composite tubes crushing modes a) Numerical analysis crushing mode b) Experimental analysis crushing mode.

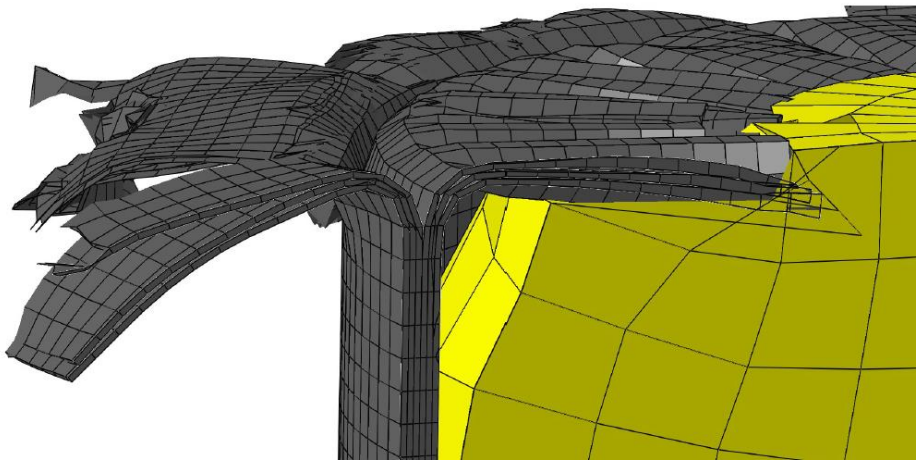

Figure 4.38. Section view of the simulation model of PU filled composite tube.

Foam filled composite tube shows a crushing mode similar to the experimental results in numerical simulations. However, in experimental results, inner fronds are fragmented at some point and work as a debris wedge between foam and tube. Thus outwards fronds occurs only after fracture of the inwards fronds. In numerical simulations, inwards fronds always compressing the foam inwards and no fracture in inwards fronds is observed. Delamination damage of the specimen is shown in Figure 4.39.

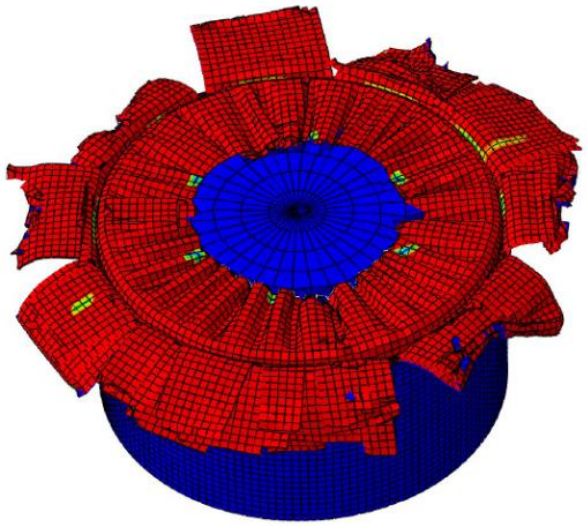

Figure 4.39. Delamination damage in numerical simulation.

.

Load displacement curves obtained from numerical simulations are close to the experimental results as well. Comparison of the numerical and experimental load displacement curves are given in Figure 4.40. SEA displacement curves of foam filled component given in Figure 4.41.

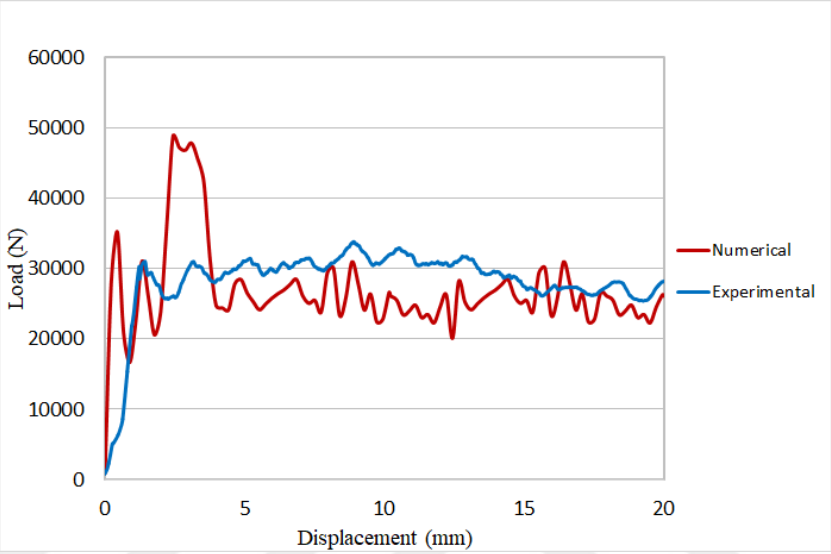

Figure 4.40. Load displacement curves Ø50mm foam filled composite tube numerical simulation and experimental test.

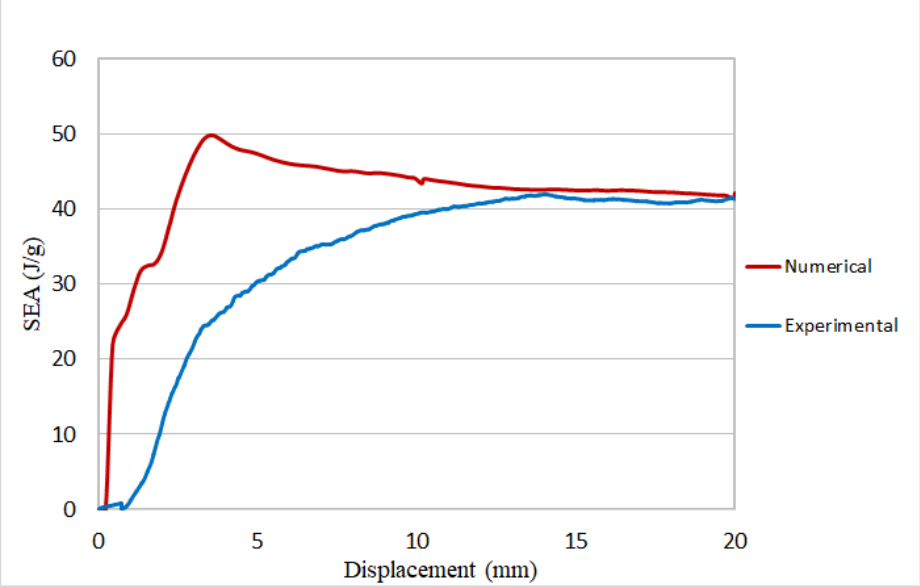

Figure 4.41. SEA displacement curves Ø50mm foam filled composite tube numerical simulation and experimental test.

Summary of the numerical simulation of Ø50mm PU filled tube is shown in Table 4.5.

Table 4.5. Summary of the numerical simulation of Ø50mm PU filled tube.

Analysis	Absorbed Energy at 20mm (J)		SEA (J/g)	
	Num.	Exp.	Num.	Exp.
PU Filled Tube Virtual Debris Crushing	538.51	565.59	42.13	44.25

It is found that SEA values decreases in foam filled components due to the increase in the weight of the components. Performed simulations and the experimental tests of the specimens shown coherent results. Increase in the energy absorption of foam filled tubes is observed but the increase in energy absorption caused from positive interaction behavior is not effective enough to increase SEA values.

Numerical analysis of HGMS/epoxy syntactic foam filled tubes was not performed in this thesis study, because that *CRUSHABLE FOAM is not appropriate for modelling syntactic foams since syntactic foams structure differs from cellular structure foams, which have a higher volumetric ratio of porosity inside. Syntactic foams also exhibit a brittle damage behavior when subjected to axial compression. Better modelling techniques are required for simulation of the syntactic foams, which is beyond the scope of this thesis.

5. CONCLUSION AND FUTURE WORK

In this thesis study, axial crushing behavior of composite circular tube structures and foam filled composite circular tube structures were examined experimentally and numerically. Experimental tests on crush specimens were carried out as quasi-static axial crushing tests on universal test machine Zwick Roell Z/100 with the upper limit of 100 kN. Numerical simulations are performed on ABAQUS/Explicit FEA software.

Circular composite tubes investigated in this study were manufactured from plain weave woven fabric carbon fiber prepreg of KordSA KOM10T HSCF 3KD PL200 by roll wrapping method and using heat shrink tapes. Manufactured composite tubes has six layers of woven carbon fiber prepreg. Composite tubes with three different diameters of Ø30mm, Ø40mm and Ø50mm were manufactured and tested. Experimental tests on manufactured composite tubes were performed using three different crushing methods. Three tubes for each diameter were crushed with inwards-crushing crush caps, outwards-crushing crush caps and flat plates of the test rigs. Top ends of the tubes also chamfered by machining before crushing to generate trigger mechanism on the tubes.

Achieved results of the experimental tests performed on empty composite tubes showed that external crush plug triggers has critical effect on crushing behavior. Both inwards crushing and outwards crushing methods showed progressive crushing behavior as well as crushing with flat plates. Crushing with flat plates exhibited better energy absorption capacity than inwards crushing and outwards crushing. Inwards crushing's energy absorption capacity is close to flat plate crushing in Ø30mm tubes and Ø40mm. In Ø50mm tubes results was rather lower than flat plate crushing values. Outwards crushing has the lowest energy absorption capacity. However, both inwards and outwards crushing showed progressive axial crushing behavior that is critical for simulating the axial crushing behavior.

According to the results of the empty tubes experimental tests, axial crushing tests on foam filled tubes were carried out on Ø50mm tubes filled with PU foam. Positive interaction effect on energy absorption is observed in the crushing of PU filled tubes. However, it is observed that specific energy absorption of the PU filled tube is lower than empty composite tubes due to the increased weight.

Effects of a different type of foam core is also examined in the study. Experimental tests are carried out on glass microballoon/epoxy syntactic foam filled composite tubes. Manufactured syntactic foams can reach the maximum load values of the 100kN of used test machine in large diameters. Because of this situation, syntactic foam filled tubes were examined with Ø30mm composite tubes. Experimental tests of the syntactic foam filled tubes gave better energy absorption capacity results than PU filled tubes. However, due to the high Poisson's ratio of the syntactic foams, HGMS/epoxy filled composite tubes exhibited vertical tears as HGMS/epoxy foam expands while crushing. Crushing mode of HGMS/epoxy foam filled tube is not very desirable because of the axial split that carries the risk of catastrophic crushing. Specific energy absorption value also found out to be lower than empty tubes.

Numerical simulations on ABAQUS/Explicit were carried out by modelling empty composite tubes axial crushing and PU filled composite tubes axial crushing. ABQ_PLY_FABRIC built-in VUMAT was used to model intra-laminar damage of composites tubes and cohesive surface method was used to model inter-laminar damage behavior. *CRUSHABLE FOAM material model was used to define material properties of cellular PU foam. Numerical simulations on empty composite tubes showed close results to the experimental tests. Inwards crushing simulations and outwards crushing simulations have shown that material models used gives accurate results on axial crushing. There is also another approach investigated in numerical studies. A virtual debris wedge was generated on the top rigid plate to model the effect of the debris wedge occurs in flat plate crushing. Virtual debris wedge modelling showed load displacement curves and crushing modes close to the experimental test results as well and it gave better results than crushing with rigid flat plate modelling. PU foam filled tubes also showed close crushing modes and load displacement curves when a virtual debris wedge is used in simulations.

For future work, modelling method of axial crushing of composite tubes needs to be developed in a way that natural formation of debris wedge due to fragmentation is involved. Macro modelling of the intra-laminar damage of the composite tubes deletes the element when it is failed. However, fractured portion of the tube is generally remain in between two plies and acts as a wedge that splays the wall of the composite tube. Modelling technique of the composite tubes for flat plate crushing must be able to model the effect of the debris wedge to model composite tubes more accurately.

It is observed in the results that crush plugs can change the crushing characteristics of the tube extremely. Novel crush plugs designs may bring forth better crushing characteristics and higher energy absorption values. Also, effects of the crush plugs needs to be examined on foam filled tubes as well.

Numerical analysis of HGMS/epoxy syntactic foam is not performed in this thesis study. It is because HGMS/epoxy foams does not have a cellular structure as PU foams have. *CRUSHABLE FOAM material model is not appropriate for HGMS/epoxy foam. As a future work, better modelling techniques are required to simulate HGMS/epoxy foam.

SEA values of the foam filled tubes found out to be lower than empty tubes. This is because SEA values of the foam cores is much less than composite tubes. Influence of the interaction effect that provides higher energy absorption is not effective as much as the increased weight of the component because of the foam. So more efficient foam structures with lower density and higher crush loads should be designed.

REFERENCES

1. EU 2019/631 Regulation, "CO_2 Emission Performance Standards for Cars and Vans", https://ec.europa.eu/clima/eu-action/transport-emissions/road-transport-reducing-co2-emissions-vehicles/co2-emission-performance-standards-cars-and-vans_en, accessed in January 2022.

2. Reinforced Plastics, "Carbon Composites and Cars – Technology Watch 2012", 2013, https://www.reinforcedplastics.com/content/features/carbon-composites-and-cars-technology-watch-2012-1, accessed in August 2022.

3. Feraboli, P., "Advanced Composites for the Body and Chassis of A Production High Performance Car", *International Journal of Vehicle Design*, Vol. 15, No. 3/4, pp. 233-246, 2007.

4. Türkiye İstatistik Kurumu, TÜİK, "Road Traffic Accident Statistics, 2020", 2021, https://data.tuik.gov.tr/Bulten/Index?p=Road-Traffic-Accident-Statistics-2020-37436&dil=2, accessed on November 30, 2021.

5. Hussain, N. N., S. P. Regalla and Y. V. D. Rao, "Comparative Study of Trigger Configuration for Enhancement of Crashworthiness of Automobile Crash Box Subjected to Axial Impact Loading", *Procedia Engineering*, Vol. 173, pp. 1390-1398, 2017.

6. Ramakrishna, S., "Microstructural Design of Composite Materials for Crashworthy Structural Applications", *Materials & Design*, Vol. 18, No.3, pp. 167-173, 1997.

7. Wang, H., W. Wang, P. Wang, F. Jin and H. Fan, "Foam-Filled Lightweight Braided-Textile Reinforced and Nested Tubular Structures for Energy Absorption Applications", *Composites Part A: Applied Science and Manufacturing*, Vol. 149, No. 106569, pp. 1-16, 2021.

8. Sun, G., Z. Wang, H. Yu, Z. Gong and Q. Li, "Experimental and Numerical Investigation into the Crashworthiness of Metal-Foam-Composite Hybrid Structures", *Composite Structures*, Vol. 209, pp. 535-547, 2019.

9. Hanssen, A. G., O. S. Hopperstad and M. Langseth, "Design of Aluminium Foam-Filled Crash Boxes of Square and Circular Cross-Sections", *International Journal of Crashworthiness*, Vol. 6, No. 2, pp. 177-188, 2001.

10. Hull, D., "A Unified Approach to Progressive Crushing of Fibre-Reinforced Composite Tubes", *Composites Science and Technology*, Vol. 40, No.4, pp. 371-421, 1991.

11. Farley, G. L. and R. M. Jones, *Energy Absorption Capability of Composite Tubes and Beams*, NASA Technical Memorandum 101634, AVSCOM Technical Report 89-B-003, 1989.

12. Deepak, S., G. Henderson, D. Mikita, K. Mirarchi, R. Park, J. Smolko, J. Awerbuch and T. Tan, "An Experimental Study on the Effect of Failure Trigger Mechanisms on the Energy Absorption Capability of CFRP Tubes Under Axial Compression", *Composites Part A: Applied Science and Manufacturing*, Vol. 64, pp. 25-35, 2014.

13. Ghasemnejad, H. and Rabiee A., "Progressive Crushing of Polymer Matrix Composite Tubular Structures: Review", *Open Journal of Composite Materials*, Vol. 7, pp. 14-48, 2007.

14. Feraboli P., B. Wade., F. Deleo and M. Rassaian, "Crush Energy Absorption of Composite Channel Section Specimens", *Composites Part A: Applied Science and Manufacturing*, Vol. 40, No. 8, pp. 1248-1256, 2009.

15. Sokolinsky, V. S., K. C. Indermuehle and J. A. Hurtado, "Numerical Simulation of The Crushing Process of A Corrugated Composite Plate", *Composites Part A: Applied Science and Manufacturing*, Vol. 42, No. 9, pp. 1119-1126, 2011.

16. Dalli, D., *Experimental and Numerical Developments in Predicting the Crashworthiness of Formula One Composite Structures*, Ph.D. Thesis, Queen's University Belfast, 2020.

17. Analysis of Composite Materials with ABAQUS (ABAQUS Technical Document), Dassault Systémes, 2009.

18. Tobby, E. R. and A. Bahaadini, *Design, Analysis and Verification of Composite Components Subjected to Crash Load Cases*, M.S. Thesis, Blekinge Institute of Technology, 2015.

19. Zarei, H., M. Kröger and H. Albertsen, "An Experimental and Numerical Crashworthiness Investigation of Thermoplastic Composite Crash Boxes", *Composite Structures*, Vol. 85, No.3, pp. 245-257, 2008.

20. Savage, G, I. Bomphray and M. Oxley, "Exploiting the Fracture Properties of Carbon Fibre Composites to Design Lightweight Energy Absorbing Structures", *Engineering Failure Analysis*, Vol. 11, No. 5, pp. 677-694, 2004.

21. Dhaliwal, G. S. and G. M. Newaz, "Effect of Resin Rich Veil Cloth Layers on the Uniaxial Tensile Behavior of Carbon Fiber Reinforced Fiber Metal Laminates", *Journal of Composite Science*, Vol. 2, pp. 1-32, No. 61, 2018.

22. Massoom, Z. F. and H. A. Kishawy, "Prediction of Critical Thrust Force Generated at the Onset of Delamination in Machining Carbon Reinforced Composites", *The International Journal of Advanced Manufacturing Technology*, Vol. 103, pp. 2751-2759, 2019.

23. Thornton, P., "Energy Absorption in Composite Structures", *Journal of Composite Materials*, Vol. 13, No. 3, pp. 248-262, 1979.

24. Schmuesser, D. and L. Wickcliffe, “Impact Energy Absorption of Continuous Fiber Composite Tubes”, *Journal of Engineering Material and Technology*, Vol. 109, No. 1, pp. 72-77, 1987.

25. Farley, G. L. “Energy Absorption of Composite Materials”, *Journal of Composite Materials*, Vol. 17, No. 3, pp. 267-279, 1983.

26. Hamada, H., J. Coppola, D. Hull, Z. Maekawa and H. Sato, "Comparison of Energy Absorption of Carbon/Epoxy and Carbon/PEEK Composite Tubes," *Composites*, Vol. 23, No. 4, pp. 245-252, 1992.

27. Hamada, H., S. Ramakrishna and H. Satoh, "Crushing Mechanism of Carbon Fibre/PEEK Composite Tubes," *Composites*, Vol. 26, No. 11, pp. 749-755, 1995.

28. Berry, J. P., *Energy Absorption and Failure Mechanisms of Axially Crushed GRP tubes,* Ph.D. Thesis, University of Liverpool, 1984.

29. Mamalis, A. G., M. Robinson, D. E. Manolakos, G. A. Demosthenus, M. B. Ioannidis and J. Carruthers, “Review, Crashworthy Capability of Composite Material Structures”, *Composite Structures*, Vol. 37, No. 2, pp. 109-134, 1997.

30. Thornton, P. H. and P.J. Edwards, “Energy Absorption in Composite Tubes”, *Journal of Composite Materials*, Vol. 16, No. 6, pp. 541-545, 1982.

31. Kindervater, C. M., “Compression and Crush Energy Absorption Behavior of Composite Laminates”, in *Proceedings of the E/MRS Conference*, Strasbourg, Federal Republic of Germany, 1985.

32. Yao, S., Z. Chen, P. Xu, Z. Li and Z. Zhao, “Experimental and Numerical Study on the Energy Absorption of Polyurethane Foam-Filled Metal/Composite Hybrid Structures”, *Metals*, Vol. 11, No. 118, pp. 1-19, 2021.

33. Costas, M., D. Morin, M. Langseth, L. Romera and J. Diaz, "Axial Crushing of Aluminum Extrusions Filled with PET Foam and GFRP. An Experimental Investigation", *Thin-Walled Structures,* Vol. 99, pp. 45-57, 2016.

34. Pietras, D., E. Linul, T. Sadowski and A. Rusinek, "Out-of-Plane Crushing Response of Aluminium Honeycombs in-situ Filled with Graphene-Reinforced Polyurethane Foam", *Composite Structures,* Vol. 246, pp. 112548-112565, 2020.

35. Zhou, J., Z. Guan and W. Cantwell, "Modelling Compressive Crush of Composite Tube Reinforced Foam Sandwiches", in *ICCM2014,* Cambridge, England, 2014.

36. Marszalek, J., J. Stadnicki and P. Danielczyk, "Finite Element Model of Laminate Construction Eement with Multi-Phase Microstructure", *Science and Engineering of Composite Materials,* Vol. 27, No. 1, pp. 405-414, 2020.

37. Bussadori, B. P., K. Schuffenhauer and A. Scattina, "Modelling of CFRP Crushing Structures in Explicit Crash Analysis", *Composites Part B: Engineering,* Vol. 60, pp. 725-735, 2014.

38. Mamalis, A. G., D. E. Manolakos, M. B. Ioannidis, P. K. Kostazos and D. P. Papapostolou, "Axial Collapse of Hybrid Square Sandwich Composite Tubular Components with Corrugated Core: Numerical Modelling", *Composite Structures,* Vol. 58, No. 4, pp. 571-582, 2002.

.

39. Zhou, G., G. Sun, G. Li, A. Cheng and Q. Li, "Modelling for CFRP Structures Subjected to Quasi-Static Crushing", *Composite Structures,* Vol. 184, pp. 41-55, 2018.

40. Lombarkia, R., A. Gakwaya, D. Nandlall, M. L. Dano, J. Lévesque and P. Vachon-Joanette, "Experimental Investigation and Finite-Element Modelling of the Crushing Response of Hat Shape Open Section Composite", *International Journal of Crashworthiness,* Vol. 27, No. 3, pp. 772-783, 2020.

41. ABAQUS Web Documentation, "Crushable Foam Plasticity Models", https://ABAQUS-docs.mit.edu/2017/English/SIMACAEMATRefMap/simamat-c-crushfoam.htm, accessed in January 2022.

42. McGregor, C., R. Vaziri and X. Xiao, "Finite Element Modelling of the Progressive Crushing of Braided Composite Tubes Under Axial Impact", *International Journal of Impact Engineering*, Vol. 37, No. 6, pp. 662-672, 2010.

43. Farley, G. L., "The Effects of Crushing Speed on the Energy-Absorption Capability of Composite Tubes", *Journal of Composite Materials*, Vol. 25, No. 10, pp. 1314-1329, 1991.

44. Jackson, A., S. Dutton, A.J. Gunnion and D. Kelly, "Investigation into Laminate Design of Open Carbon-Fibre/Epoxy Sections by Quasi-Static and Dynamic Crushing", *Composite Structures*, Vol. 93, No. 10, pp. 2646-2656, 2011.

45. Eyer, G., O. Montagnier, J. P. Charles and C. Hochard, "Design of a Composite Tube to Analyze the Compressive Behavior of CFRP", *Composites Part A: Applied Science and Manufacturing*, Vol. 87, pp. 115-122, 2016.

46. Dunstone Hi Shrink Tapes, "Dunstone Shrink Tape Product Information", https://www.shrinktape.com/products/hi-shrink-tapes/, accessed in March 2022.

47. OM10 Resin System Prepregs Technical Data Sheet, KordSA. Accessed in February 2022.

48. EPIKOTE™ Resin MGS® LR285 Technical Data Sheet, HEXION Specialty Chemicals. Accessed in February 2022. https://r-g.com.pl/pl/p/file/7160c686048aa59257decd7ee895c247/L285-TSDS.pdf.

49. Hollow Glass Sphere KP25 Technical Data Sheet, Zhengzhou Hollowlite Materials Company. Accessed in February 2022. https://drive.google.com/file/d/1MruEx6ota1sO4sw1h3SxuOAxjgVnpwpI/view.

50. VUMAT for Fabric Reinforced Composites (ABAQUS Technical Document), Dassault Systémes, 2008.

51. Burlayenko, V. N. and T. Sadowski, “FE Modelling of Delamination Growth in Interlaminar Fracture Specimens”, *Budownictwo I Architektura*, Vol. 2, No. 1, pp. 95-109, 2008.

52. Camanho, P.P., C.G. Davila and M. F. de Moura, “Numerical Simulation of Mixed-Mode Progressive Delamination in Composite Materials”, *Journal of Composite Materials*, Vol. 37, No. 16, pp. 1415-1438, 2003.

53. Turon, A., C. G. Davila, P. P. Camanho and J. Costa, “An Engineering Solution for Mesh Size Effects in Simulation of Delamination Using Cohesive Zone Models”, *Engineering Fracture Mechanics*, Vol. 74, No. 10, pp. 1665-1682, 2007.

54. ABAQUS Web Documentation, “Defining the Constitutive Response of Cohesive Elements Using a Traction-Separation Description”, https://ABAQUS-docs.mit.edu/2017/English/SIMACAEELMRefMap/simaelm-c-cohesivebehavior.htm, accessed in March 2022.

55. Obbink-Huizer C., SIMULEON FEA Blog, “Implict vs Explicit Finite Element Analysis: When to Use Which?”, https://info.simuleon.com/blog/implicit-vs-explicit-finite-element-analysis, accessed in May 2022.

APPENDIX A: COPYRIGHT PERMISSIONS FOR FIGURES AND TABLES

Permissions for reused visual materials are given in this appendix.

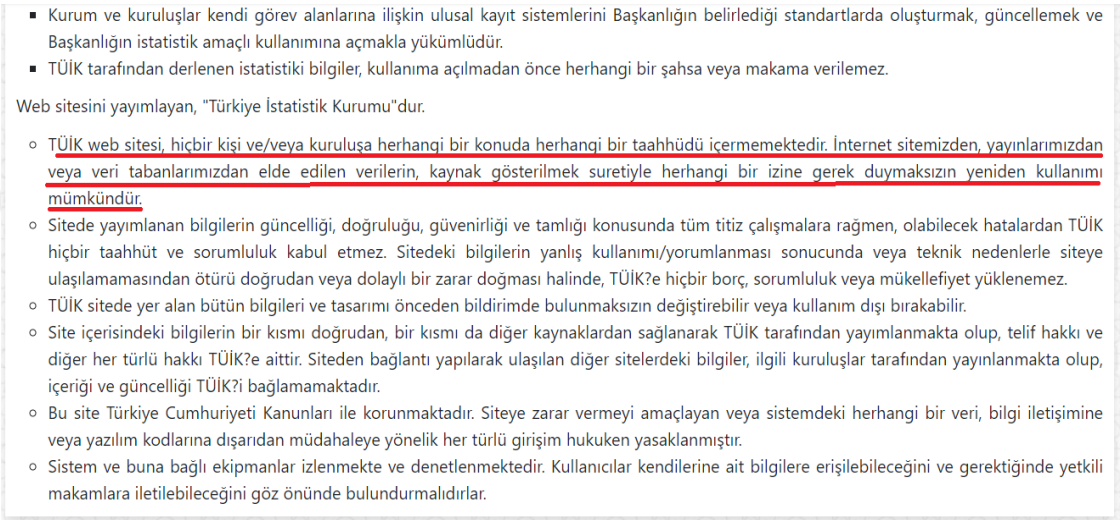

- Kurum ve kuruluşlar kendi görev alanlarına ilişkin ulusal kayıt sistemlerini Başkanlığın belirlediği standartlarda oluşturmak, güncellemek ve Başkanlığın istatistik amaçlı kullanımına açmakla yükümlüdür.
- TÜİK tarafından derlenen istatistiki bilgiler, kullanıma açılmadan önce herhangi bir şahsa veya makama verilemez.

Web sitesini yayımlayan, "Türkiye İstatistik Kurumu"dur.

- TÜİK web sitesi, hiçbir kişi ve/veya kuruluşa herhangi bir konuda herhangi bir taahhüdü içermemektedir. İnternet sitemizden, yayınlarımızdan veya veri tabanlarımızdan elde edilen verilerin, kaynak gösterilmek suretiyle herhangi bir izine gerek duymaksızın yeniden kullanımı mümkündür.
- Sitede yayımlanan bilgilerin güncelliği, doğruluğu, güvenirliği ve tamlığı konusunda tüm titiz çalışmalara rağmen, olabilecek hatalardan TÜİK hiçbir taahhüt ve sorumluluk kabul etmez. Sitedeki bilgilerin yanlış kullanımı/yorumlanması sonucunda veya teknik nedenlerle siteye ulaşılamamasından ötürü doğrudan veya dolaylı bir zarar doğması halinde, TÜİK?e hiçbir borç, sorumluluk veya mükellefiyet yüklenemez.
- TÜİK sitede yer alan bütün bilgileri ve tasarımı önceden bildirimde bulunmaksızın değiştirebilir veya kullanım dışı bırakabilir.
- Site içerisindeki bilgilerin bir kısmı doğrudan, bir kısmı da diğer kaynaklardan sağlanarak TÜİK tarafından yayımlanmakta olup, telif hakkı ve diğer her türlü hakkı TÜİK?e aittir. Siteden bağlantı yapılarak ulaşılan diğer sitelerdeki bilgiler, ilgili kuruluşlar tarafından yayınlanmakta olup, içeriği ve güncelliği TÜİK?i bağlamamaktadır.
- Bu site Türkiye Cumhuriyeti Kanunları ile korunmaktadır. Siteye zarar vermeyi amaçlayan veya sistemdeki herhangi bir veri, bilgi iletişimine veya yazılım kodlarına dışarıdan müdahaleye yönelik her türlü girişim hukuken yasaklanmıştır.
- Sistem ve buna bağlı ekipmanlar izlenmekte ve denetlenmektedir. Kullanıcılar kendilerine ait bilgilere erişilebileceğini ve gerektiğinde yetkili makamlara iletilebileceğini göz önünde bulundurmalıdırlar.

Figure A.1. Permission for Figure 1.1.

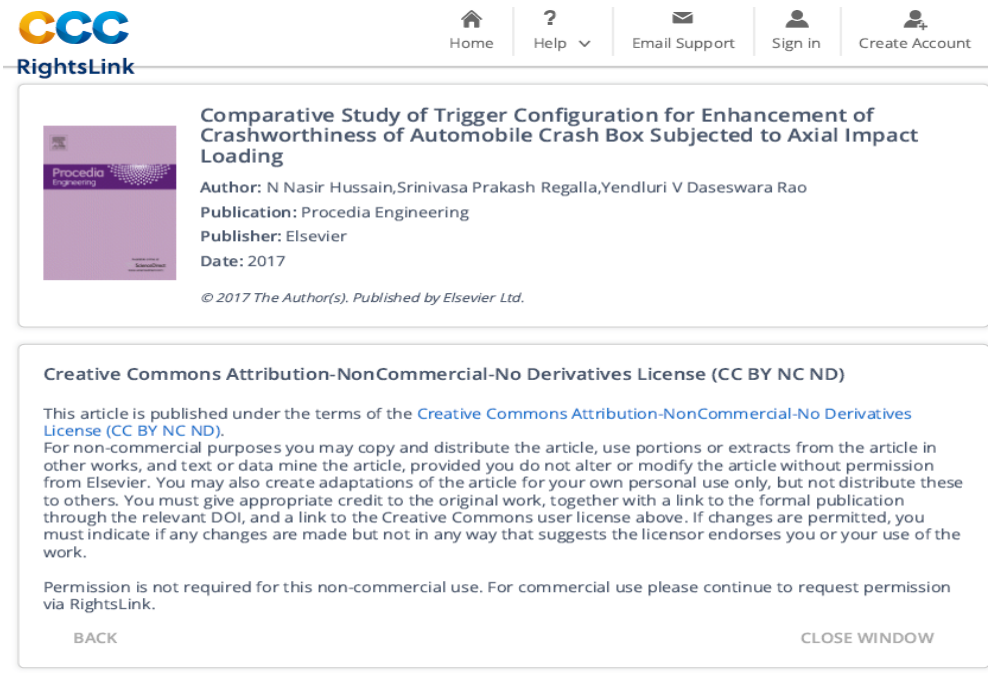

Figure A.2. Permission for Figure 1.2.

CCC RightsLink

Help | Live Chat | Serdar Demir

Microstructural design of composite materials for crashworthy structural applications

Author: S Ramakrishna
Publication: Materials & Design
Publisher: Elsevier
Date: 1 October 1997

Copyright © 1998 Elsevier Science Ltd. All rights reserved.

Order Completed

Thank you for your order.

This Agreement between Serdar Demir ("You") and Elsevier ("Elsevier") consists of your order details and the terms and conditions provided by Elsevier and Copyright Clearance Center.

License number	Reference confirmation email for license number
License date	Jun, 21 2022

Licensed Content

Licensed Content Publisher	Elsevier
Licensed Content Publication	Materials & Design
Licensed Content Title	Microstructural design of composite materials for crashworthy structural applications
Licensed Content Author	S Ramakrishna
Licensed Content Date	1 October 1997
Licensed Content Volume	18
Licensed Content Issue	3
Licensed Content Pages	7

Order Details

Type of Use	reuse in a thesis/dissertation
Portion	figures/tables/illustrations
Number of figures/tables/illustrations	2
Format	both print and electronic
Are you the author of this Elsevier article?	No
Will you be translating?	No

About Your Work

Title	EXPERIMENTAL AND NUMERICAL ANALYSIS OF FOAM-FILLED COMPOSITE STRUCTURES SUBJECTED TO AXIAL CRUSHING
Institution name	Boğaziçi University, Institute for Graduate Studies in Science and Engineering
Expected presentation date	Aug 2022

Additional Data

Portions	Figure 2, Figure 3

Figure A.3. Permission for Figures 1.3 and 1.24.

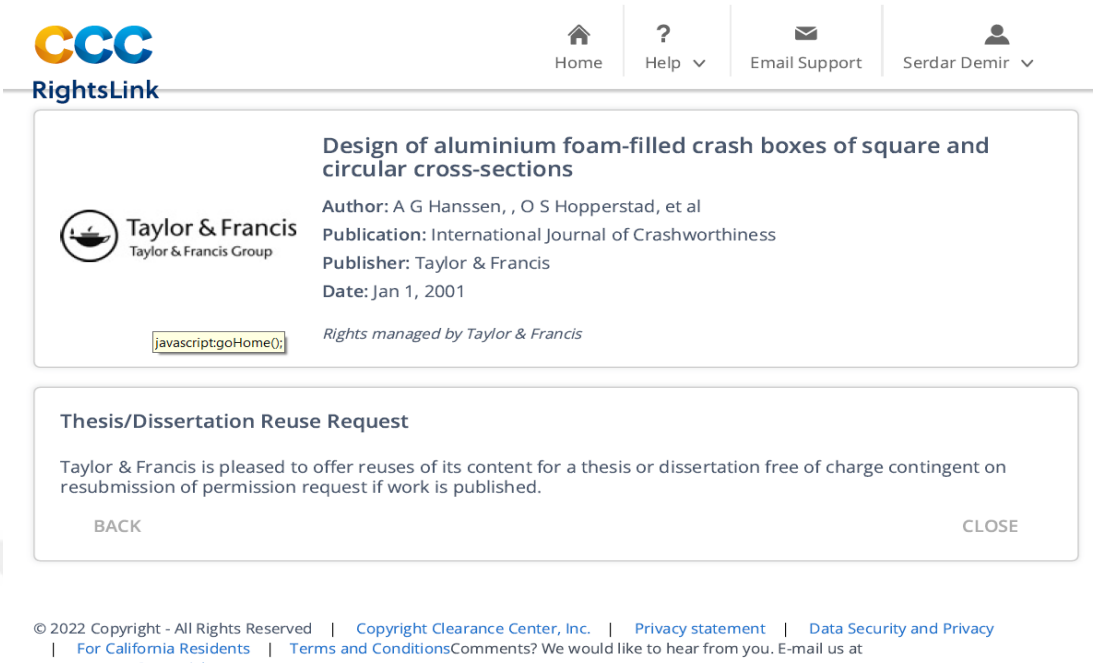

Figure A.4. Permission for Figures 1.4, 1.28 and 1.29.

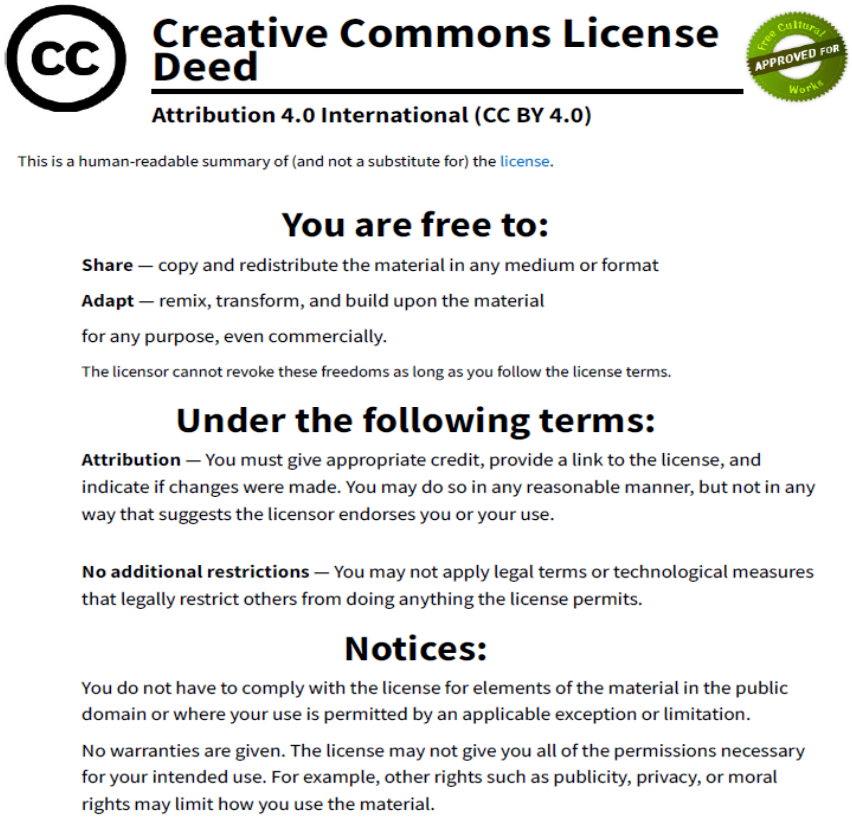

Figure A.5. Permission for Figures 1.5 and 1.34.

CCC RightsLink

Help | Email Support | Serdar Demir

A unified approach to progressive crushing of fibre-reinforced composite tubes

Author: D. Hull
Publication: Composites Science and Technology
Publisher: Elsevier
Date: 1991

Copyright © 1991 Published by Elsevier Ltd.

Order Completed

Thank you for your order.

This Agreement between Serdar Demir ("You") and Elsevier ("Elsevier") consists of your order details and the terms and conditions provided by Elsevier and Copyright Clearance Center.

License number	Reference confirmation email for license number
License date	Jun, 21 2022

Licensed Content

Licensed Content Publisher	Elsevier
Licensed Content Publication	Composites Science and Technology
Licensed Content Title	A unified approach to progressive crushing of fibre-reinforced composite tubes
Licensed Content Author	D. Hull
Licensed Content Date	1991
Licensed Content Volume	40
Licensed Content Issue	4
Licensed Content Pages	45

Order Details

Type of Use	reuse in a thesis/dissertation
Portion	figures/tables/illustrations
Number of figures/tables/illustrations	14
Format	both print and electronic
Are you the author of this Elsevier article?	No
Will you be translating?	No

About Your Work

Title	EXPERIMENTAL AND NUMERICAL ANALYSIS OF FOAM-FILLED COMPOSITE STRUCTURES SUBJECTED TO AXIAL CRUSHING
Institution name	Boğaziçi University, Institute for Graduate Studies in Science and Engineering
Expected presentation date	Aug 2022

Additional Data

Portions	Figure 1, Figure 2, Figure 3, Figure 4, Figure 5, Figure 8, Figure 9, Figure 11, Figure 17, Figure 19, Figure 20, Figure 22, Figure 23, Figure 25

Figure A.6. Permission for Figures 1.6, 1.12, 1.14, 1.15, 1.16, 1.17, 1.18, 1.19, 1.20, 1.21, 1.22, 1.25, 1.26 and 1.27.

CCC RightsLink

Help | Email Support | Serdar Demir

Crush energy absorption of composite channel section specimens

Author: Paolo Feraboli,Bonnie Wade,Francesco Deleo,Mostafa Rassaian

Publication: Composites Part A: Applied Science and Manufacturing

Publisher: Elsevier

Date: August 2009

Copyright © 2009 Elsevier Ltd. All rights reserved.

Order Completed

Thank you for your order.

This Agreement between Serdar Demir ("You") and Elsevier ("Elsevier") consists of your order details and the terms and conditions provided by Elsevier and Copyright Clearance Center.

License number	Reference confirmation email for license number
License date	Jun, 21 2022

Licensed Content

Licensed Content Publisher	Elsevier
Licensed Content Publication	Composites Part A: Applied Science and Manufacturing
Licensed Content Title	Crush energy absorption of composite channel section specimens
Licensed Content Author	Paolo Feraboli,Bonnie Wade,Francesco Deleo,Mostafa Rassaian
Licensed Content Date	August 2009
Licensed Content Volume	40
Licensed Content Issue	8
Licensed Content Pages	9

Order Details

Type of Use	reuse in a thesis/dissertation
Portion	figures/tables/illustrations
Number of figures/tables/illustrations	2
Format	both print and electronic
Are you the author of this Elsevier article?	No
Will you be translating?	No

About Your Work

Title	EXPERIMENTAL AND NUMERICAL ANALYSIS OF FOAM-FILLED COMPOSITE STRUCTURES SUBJECTED TO AXIAL CRUSHING
Institution name	Boğaziçi University, Institute for Graduate Studies in Science and Engineering
Expected presentation date	Aug 2022

Additional Data

Portions	Figure 7, Figure 12

Figure A.7. Permission for Figure 1.7.

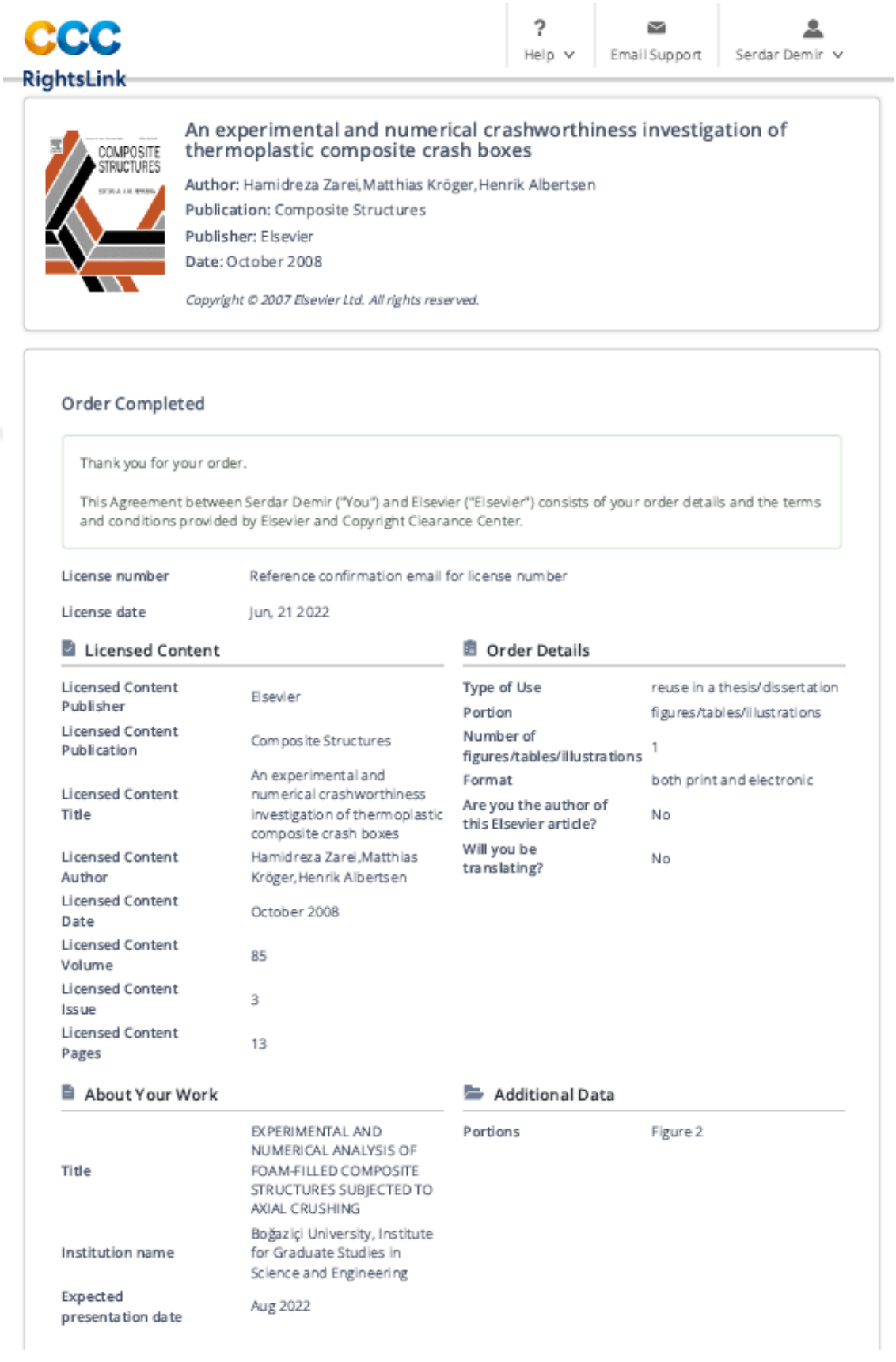

RightsLink

Help | Email Support | Serdar Demir

COMPOSITE STRUCTURES

An experimental and numerical crashworthiness investigation of thermoplastic composite crash boxes

Author: Hamidreza Zarei,Matthias Kröger,Henrik Albertsen
Publication: Composite Structures
Publisher: Elsevier
Date: October 2008

Copyright © 2007 Elsevier Ltd. All rights reserved.

Order Completed

Thank you for your order.

This Agreement between Serdar Demir ("You") and Elsevier ("Elsevier") consists of your order details and the terms and conditions provided by Elsevier and Copyright Clearance Center.

License number	Reference confirmation email for license number
License date	Jun, 21 2022

Licensed Content

Licensed Content Publisher	Elsevier
Licensed Content Publication	Composite Structures
Licensed Content Title	An experimental and numerical crashworthiness investigation of thermoplastic composite crash boxes
Licensed Content Author	Hamidreza Zarei,Matthias Kröger,Henrik Albertsen
Licensed Content Date	October 2008
Licensed Content Volume	85
Licensed Content Issue	3
Licensed Content Pages	13

Order Details

Type of Use	reuse in a thesis/dissertation
Portion	figures/tables/illustrations
Number of figures/tables/illustrations	1
Format	both print and electronic
Are you the author of this Elsevier article?	No
Will you be translating?	No

About Your Work

Title	EXPERIMENTAL AND NUMERICAL ANALYSIS OF FOAM-FILLED COMPOSITE STRUCTURES SUBJECTED TO AXIAL CRUSHING
Institution name	Boğaziçi University, Institute for Graduate Studies in Science and Engineering
Expected presentation date	Aug 2022

Additional Data

Portions	Figure 2

Figure A.8. Permission for Figure 1.9.

CCC RightsLink

Help | Email Support | Serdar Demir

Exploiting the fracture properties of carbon fibre composites to design lightweight energy absorbing structures

Author: G Savage,I Bomphray,M Oxley
Publication: Engineering Failure Analysis
Publisher: Elsevier
Date: October 2004

Copyright © 2004 Published by Elsevier Ltd.

Order Completed

Thank you for your order.

This Agreement between Serdar Demir ("You") and Elsevier ("Elsevier") consists of your order details and the terms and conditions provided by Elsevier and Copyright Clearance Center.

License number	Reference confirmation email for license number
License date	Jun, 21 2022

Licensed Content

Licensed Content Publisher	Elsevier
Licensed Content Publication	Engineering Failure Analysis
Licensed Content Title	Exploiting the fracture properties of carbon fibre composites to design lightweight energy absorbing structures
Licensed Content Author	G Savage,I Bomphray,M Oxley
Licensed Content Date	October 2004
Licensed Content Volume	11
Licensed Content Issue	5
Licensed Content Pages	18

Order Details

Type of Use	reuse in a thesis/dissertation
Portion	figures/tables/illustrations
Number of figures/tables/illustrations	1
Format	both print and electronic
Are you the author of this Elsevier article?	No
Will you be translating?	No

About Your Work

Title	EXPERIMENTAL AND NUMERICAL ANALYSIS OF FOAM-FILLED COMPOSITE STRUCTURES SUBJECTED TO AXIAL CRUSHING
Institution name	Boğaziçi University, Institute for Graduate Studies in Science and Engineering
Expected presentation date	Aug 2022

Additional Data

Portions	Figure 15

Figure A.9. Permission for Figure 1.10.

MDPI Open Access Information and Policy

All articles published by MDPI are made immediately available worldwide under an open access license. This means:

- everyone has free and unlimited access to the full-text of *all* articles published in MDPI journals;
- everyone is free to re-use the published material if proper accreditation/citation of the original publication is given;
- open access publication is supported by the authors' institutes or research funding agencies by payment of a comparatively low **Article Processing Charge (APC) (/about/apc)** for accepted articles.

https://www.mdpi

Permissions

No special permission is required to reuse all or part of article published by MDPI, including figures and tables. For articles published under an open access Creative Common CC BY license, any part of the article may be reused without permission provided that the original article is clearly cited. Reuse of an article does not imply endorsement by the authors or MDPI.

Figure A.10. Permission for Figures 1.11, 1.30 and 1.31.

RightsLink

Help | Email Support | Serdar Demir

SPRINGER NATURE

Prediction of critical thrust force generated at the onset of delamination in machining carbon reinforced composites

Author: Z. Fattahi Massoom et al
Publication: The International Journal of Advanced Manufacturing Technology
Publisher: Springer Nature
Date: Apr 27, 2019

Copyright © 2019, Springer-Verlag London Ltd., part of Springer Nature

Order Completed

Thank you for your order.

This Agreement between Serdar Demir ("You") and Springer Nature ("Springer Nature") consists of your order details and the terms and conditions provided by Springer Nature and Copyright Clearance Center.

License number	Reference confirmation email for license number
License date	Jun, 22 2022

Licensed Content

Licensed Content Publisher	Springer Nature
Licensed Content Publication	The International Journal of Advanced Manufacturing Technology
Licensed Content Title	Prediction of critical thrust force generated at the onset of delamination in machining carbon reinforced composites
Licensed Content Author	Z. Fattahi Massoom et al
Licensed Content Date	Apr 27, 2019

Order Details

Type of Use	Thesis/Dissertation
Requestor type	academic/university or research institute
Format	print and electronic
Portion	figures/tables/illustrations
Number of figures/tables/illustrations	1
Will you be translating?	no
Circulation/distribution	1 - 29
Author of this Springer Nature content	no

About Your Work

Title	EXPERIMENTAL AND NUMERICAL ANALYSIS OF FOAM-FILLED COMPOSITE STRUCTURES SUBJECTED TO AXIAL CRUSHING
Institution name	Boğaziçi University, Institute for Graduate Studies in Science and Engineering
Expected presentation date	Aug 2022

Additional Data

Portions	Figure 1

Figure A.11. Permission for Figure 1.13.

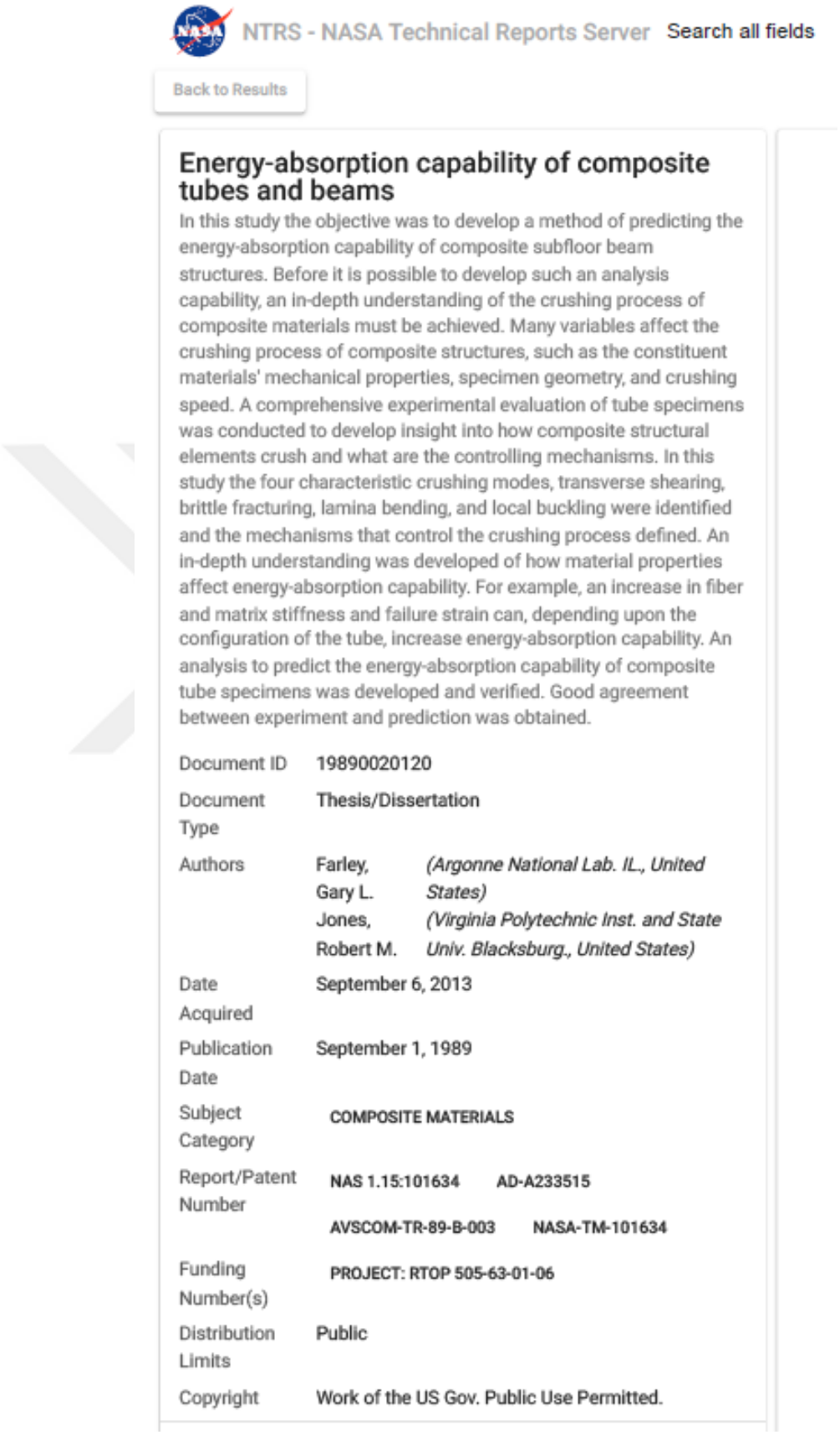

Figure A.12. Permission for Figure 1.23.

RightsLink

Help | Email Support | Serdar Demir

Axial crushing of aluminum extrusions filled with PET foam and GFRP. An experimental investigation

Author: M. Costas,D. Morin,M. Langseth,L. Romera,J. Díaz
Publication: Thin-Walled Structures
Publisher: Elsevier
Date: February 2016

Copyright © 2015 Elsevier Ltd. All rights reserved.

Order Completed

Thank you for your order.

This Agreement between Serdar Demir ("You") and Elsevier ("Elsevier") consists of your order details and the terms and conditions provided by Elsevier and Copyright Clearance Center.

License number	Reference confirmation email for license number
License date	Jun, 21 2022

Licensed Content

Licensed Content Publisher	Elsevier
Licensed Content Publication	Thin-Walled Structures
Licensed Content Title	Axial crushing of aluminum extrusions filled with PET foam and GFRP. An experimental investigation
Licensed Content Author	M. Costas,D. Morin,M. Langseth,L. Romera,J. Díaz
Licensed Content Date	February 2016
Licensed Content Volume	99
Licensed Content Issue	n/a
Licensed Content Pages	13

Order Details

Type of Use	reuse in a thesis/dissertation
Portion	figures/tables/illustrations
Number of figures/tables/illustrations	3
Format	both print and electronic
Are you the author of this Elsevier article?	No
Will you be translating?	No

About Your Work

Title	EXPERIMENTAL AND NUMERICAL ANALYSIS OF FOAM-FILLED COMPOSITE STRUCTURES SUBJECTED TO AXIAL CRUSHING
Institution name	Boğaziçi University, Institute for Graduate Studies in Science and Engineering
Expected presentation date	Aug 2022

Additional Data

Portions	Figure 1, Figure 12, Figure 16

Figure A.13. Permission for Figure 1.32 and 1.33.

CCC RightsLink

Help | Email Support | Serdar Demir

Modeling for CFRP structures subjected to quasi-static crushing

Author: Guohua Zhu,Guangyong Sun,Guangyao Li,Aiguo Cheng,Qing Li

Publication: Composite Structures

Publisher: Elsevier

Date: 15 January 2018

© 2017 Published by Elsevier Ltd.

Order Completed

Thank you for your order.

This Agreement between Serdar Demir ("You") and Elsevier ("Elsevier") consists of your order details and the terms and conditions provided by Elsevier and Copyright Clearance Center.

License number	Reference confirmation email for license number
License date	Jun, 21 2022

Licensed Content

Licensed Content Publisher	Elsevier
Licensed Content Publication	Composite Structures
Licensed Content Title	Modeling for CFRP structures subjected to quasi-static crushing
Licensed Content Author	Guohua Zhu,Guangyong Sun,Guangyao Li,Aiguo Cheng,Qing Li
Licensed Content Date	15 January 2018
Licensed Content Volume	184
Licensed Content Issue	n/a
Licensed Content Pages	15

Order Details

Type of Use	reuse in a thesis/dissertation
Portion	figures/tables/illustrations
Number of figures/tables/illustrations	2
Format	both print and electronic
Are you the author of this Elsevier article?	No
Will you be translating?	No

About Your Work

Title	EXPERIMENTAL AND NUMERICAL ANALYSIS OF FOAM-FILLED COMPOSITE STRUCTURES SUBJECTED TO AXIAL CRUSHING
Institution name	Boğaziçi University, Institute for Graduate Studies in Science and Engineering
Expected presentation date	Aug 2022

Additional Data

Portions	Figure 3, Figure 7

Figure A.14. Permission for Figure 1.36 and 3.2.

RightsLink

Help | Email Support | Serdar Demir

Finite element modelling of the progressive crushing of braided composite tubes under axial impact

Author: Carla McGregor,Reza Vaziri,Xinran Xiao

Publication: International Journal of Impact Engineering

Publisher: Elsevier

Date: June 2010

Copyright © 2009 Elsevier Ltd. All rights reserved.

Order Completed

Thank you for your order.

This Agreement between Serdar Demir ("You") and Elsevier ("Elsevier") consists of your order details and the terms and conditions provided by Elsevier and Copyright Clearance Center.

License number	Reference confirmation email for license number
License date	Jun, 21 2022

Licensed Content

Licensed Content Publisher	Elsevier
Licensed Content Publication	International Journal of Impact Engineering
Licensed Content Title	Finite element modelling of the progressive crushing of braided composite tubes under axial impact
Licensed Content Author	Carla McGregor, Reza Vaziri,Xinran Xiao
Licensed Content Date	June 2010
Licensed Content Volume	37
Licensed Content Issue	6
Licensed Content Pages	11

Order Details

Type of Use	reuse in a thesis/dissertation
Portion	figures/tables/illustrations
Number of figures/tables/illustrations	1
Format	both print and electronic
Are you the author of this Elsevier article?	No
Will you be translating?	No

About Your Work

Title	EXPERIMENTAL AND NUMERICAL ANALYSIS OF FOAM-FILLED COMPOSITE STRUCTURES SUBJECTED TO AXIAL CRUSHING
Institution name	Boğaziçi University, Institute for Graduate Studies in Science and Engineering
Expected presentation date	Aug 2022

Additional Data

Portions	Figure 6

Figure A.15. Permission for Figure 1.37.

CCC RightsLink

Help | Email Support | Serdar Demir

Design of a composite tube to analyze the compressive behavior of CFRP

Author: G. Eyer,O. Montagnier,J.-P. Charles,C. Hochard
Publication: Composites Part A: Applied Science and Manufacturing
Publisher: Elsevier
Date: August 2016

© 2016 Elsevier Ltd. All rights reserved.

Order Completed

Thank you for your order.

This Agreement between Serdar Demir ("You") and Elsevier ("Elsevier") consists of your order details and the terms and conditions provided by Elsevier and Copyright Clearance Center.

License number	Reference confirmation email for license number
License date	Jun, 21 2022

Licensed Content

Licensed Content Publisher	Elsevier
Licensed Content Publication	Composites Part A: Applied Science and Manufacturing
Licensed Content Title	Design of a composite tube to analyze the compressive behavior of CFRP
Licensed Content Author	G. Eyer,O. Montagnier,J.-P. Charles,C. Hochard
Licensed Content Date	August 2016
Licensed Content Volume	87
Licensed Content Issue	n/a
Licensed Content Pages	8

Order Details

Type of Use	reuse in a thesis/dissertation
Portion	figures/tables/illustrations
Number of figures/tables/illustrations	1
Format	both print and electronic
Are you the author of this Elsevier article?	No
Will you be translating?	No

About Your Work

Title	EXPERIMENTAL AND NUMERICAL ANALYSIS OF FOAM-FILLED COMPOSITE STRUCTURES SUBJECTED TO AXIAL CRUSHING
Institution name	Boğaziçi University, Institute for Graduate Studies in Science and Engineering
Expected presentation date	Aug 2022

Additional Data

Portions	Figure 1

Figure A.16. Permission for Figure 2.1.

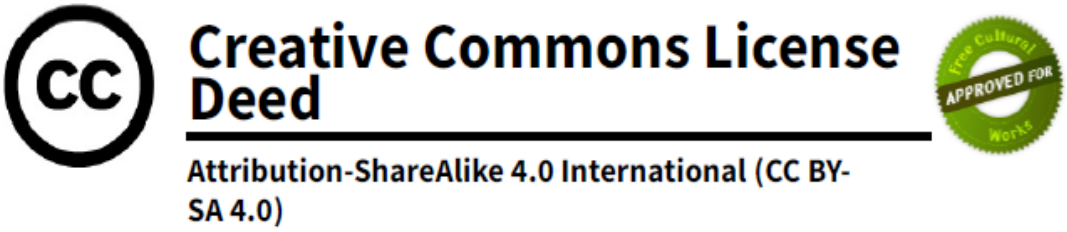

Creative Commons License Deed

Attribution-ShareAlike 4.0 International (CC BY-SA 4.0)

This is a human-readable summary of (and not a substitute for) the license.

You are free to:

Share — copy and redistribute the material in any medium or format

Adapt — remix, transform, and build upon the material

for any purpose, even commercially.

The licensor cannot revoke these freedoms as long as you follow the license terms.

Under the following terms:

Attribution — You must give appropriate credit, provide a link to the license, and indicate if changes were made. You may do so in any reasonable manner, but not in any way that suggests the licensor endorses you or your use.

ShareAlike — If you remix, transform, or build upon the material, you must distribute your contributions under the same license as the original.

No additional restrictions — You may not apply legal terms or technological measures that legally restrict others from doing anything the license permits.

Notices:

You do not have to comply with the license for elements of the material in the public domain or where your use is permitted by an applicable exception or limitation.

No warranties are given. The license may not give you all of the permissions necessary for your intended use. For example, other rights such as publicity, privacy, or moral rights may limit how you use the material.

Figure A.17. Permission for Figures 3.4 and 3.5.

RightsLink

Help | Email Support | Serdar Demir

An engineering solution for mesh size effects in the simulation of delamination using cohesive zone models

Author: A. Turon,C.G. Dávila,P.P. Camanho,J. Costa
Publication: Engineering Fracture Mechanics
Publisher: Elsevier
Date: July 2007

Copyright © 2006 Elsevier Ltd. All rights reserved.

Order Completed

Thank you for your order.

This Agreement between Serdar Demir ("You") and Elsevier ("Elsevier") consists of your order details and the terms and conditions provided by Elsevier and Copyright Clearance Center.

License number	Reference confirmation email for license number
License date	Jun, 22 2022

Licensed Content

Licensed Content Publisher	Elsevier
Licensed Content Publication	Engineering Fracture Mechanics
Licensed Content Title	An engineering solution for mesh size effects in the simulation of delamination using cohesive zone models
Licensed Content Author	A. Turon,C.G. Dávila,P.P. Camanho,J. Costa
Licensed Content Date	July 2007
Licensed Content Volume	74
Licensed Content Issue	10
Licensed Content Pages	18

Order Details

Type of Use	reuse in a thesis/dissertation
Portion	figures/tables/illustrations
Number of figures/tables/illustrations	1
Format	both print and electronic
Are you the author of this Elsevier article?	No
Will you be translating?	No

About Your Work

Title	EXPERIMENTAL AND NUMERICAL ANALYSIS OF FOAM-FILLED COMPOSITE STRUCTURES SUBJECTED TO AXIAL CRUSHING
Institution name	Boğaziçi University, Institute for Graduate Studies in Science and Engineering
Expected presentation date	Aug 2022

Additional Data

Portions	Figure 2

Figure A.18. Permission for Figure 3.6.

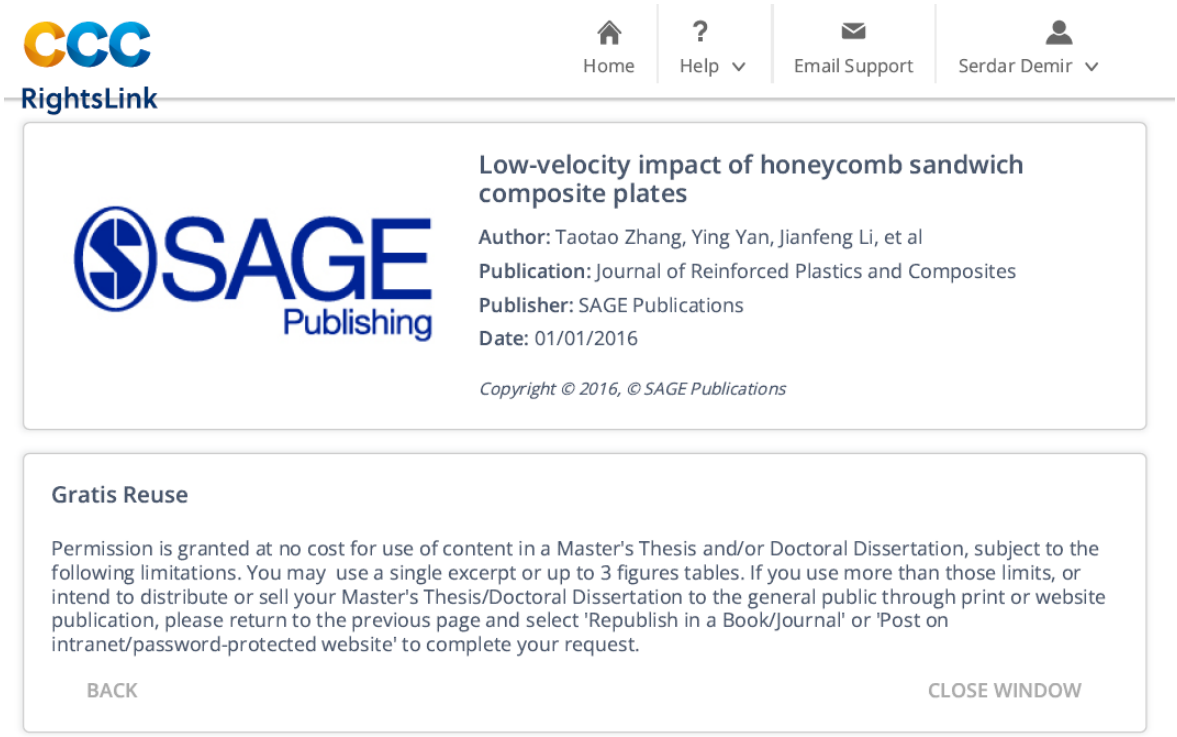

Figure A.19. Permission for Figure 3.7.